The dynamics of an axisymmetric turbulent jet in ambient turbulence interpreted from the passive scalar field statistics

Rana Sahebjam,[1] Khashayar F. Kohan,[1] and Susan Gaskin[1, a)]
Department of Civil Engineering, McGill University, Montréal, Québec, H3A 0C3, Canada

(Dated: 21 December 2021)

The effect of approximately homogeneous isotropic turbulence on the dynamics of an axisymmetric turbulent jet (*Re* = 10600 and 5800) in an ambient with a negligible mean flow is interpreted from the statistics of the passive scalar field. The ambient turbulence is generated by a random jet array and scalar concentrations are measured in orthogonal cross-sections of the jet using planar laser-induced fluorescence. Statistics of the scalar field of the jet in a turbulent ambient are compared to those in a quiescent ambient, using classical Eulerian averages and those conditioned on the jet centroid. A two-region model for the jet structure in ambient turbulence is proposed based on the centroidal statistics. Following the developing region of the jet, the ambient turbulence disrupts the jet structure, due to modulation of the jet interface, meandering of the jet by the large eddies and entrainment of the turbulent ambient fluid, resulting in a faster concentration decay and reduced entrainment compared to the quiescent ambient. Further downstream, once the ambient turbulence has destroyed the jet, only molecular and turbulent diffusion modify the scalar concentrations. The regions' relative lengths depend primarily on the relative turbulence intensity (ξ) between the ambient and the jet, as assessed using the centroidal analysis, which removes the effect of the relative length scale ($\mathscr{L}$) on the jet behavior in the turbulent ambient. The centroidal scalar statistics reveal self-similarity and self-preservation in the mean scalar properties before jet break-up, which occurs abruptly once $\xi > 0.5$. The smaller scales of the ambient turbulence modulate the jet boundary and, when entrained lead to a wider range of centerline concentrations and, also rms concentrations, which are hypothesized to increase local concentration gradients within the jet and reduce the jet mixing.

I. INTRODUCTION

Scalar mixing in turbulent shear flows (jets, plumes, wakes and boundary layers) is of interest in industrial and environmental contexts and has been studied extensively in a quiescent ambient. A jet in a quiescent ambient, after a zone of flow establishment, is self-similar and its mean momentum drives entrainment into the jet with a global entrainment velocity, E_v, that is proportional to a characteristic jet velocity[1] with a constant of proportionality, α, of $O(0.1)$ (e.g. see van Reeuwijk and Craske[2]). Entrainment, the transport of ambient fluid into the turbulent shear flow, occurs by engulfment, a large-scale inviscid process[3,4] and by nibbling at the jet/ambient interface, a small-scale viscous diffusion process.[5,6] The entrainment of ambient fluid results in the outward propagation of the interface between the jet and the ambient fluid at a boundary velocity, E_b.[7]

It has long been assumed (and is still often maintained) that release of a jet into a turbulent ambient flow will increase its rate of dilution through superposition of jet-driven entrainment and turbulent diffusion. This was an expedient approach simplifying modelling in practical applications to predict, for example, air/fuel ratios for combustion or dilution for pollutant dispersion. Despite challenges in producing ambient turbulence for a laboratory study, Gaskin *et al.*[8] demonstrated experimentally that turbulence in the ambient flow serves to disrupt the jet flow resulting in reduced dilution. This was the first experimental evidence in support of Hunt's[9] argument of 1994, that any forcing, such as turbulence in the ambient, tending to break up a jet or plume would reduce entrainment. The reduced entrainment shown experimentally for a shallow jet in a co-flow[8] was confirmed for an axisymmetric jet[10,11] and a buoyant jet.[12]

Break-up of the jet, defined as the condition at which momentum-driven entrainment of the jet stops, is hypothesized to occur once the jet or plume turbulence has decreased to that of the ambient,[9] which has been observed in jets and plumes.[10–15] In experiments, in which a jet issues towards an oscillating grid generated turbulence field, break-up is very rapid due to a simultaneous decrease in jet turbulence as ambient turbulence increases.[13–15] In jets and plumes, the turbulence in the ambient increases the rate of decay of the mean centerline velocity and passive scalar concentration, and increases the root mean square (rms) of the velocity and the concentration. The rate of width growth is increased (but less than the increase in the rate of decay of the mean centerline properties)[8,10–12,16], while the mass flow rate decreases.[11] Similarly, the velocity deficit in a wake decays more quickly[17,18] and its width growth increases once the integral scale of the ambient turbulence is larger than the width of the wake.[19]

The effect of the relative turbulence intensity and the relative length scale between the ambient and the flow was initially observed for boundary layers.[20] In wakes, the ambient turbulence intensity is the dominant factor.[21,22] There is hypothesized to be little effect of the ambient turbulence on the jet or plume flow close to the exit, where it is less intense than the jet turbulence. However, its increasing impact with downstream distance due to an increasing relative turbulence intensity will result, at some point, in the break-up of the jet and destruction of its structure.[9] After the jet structure is destroyed, a passive scalar will then only disperse due to detrain-

[a)]Electronic mail: susan.gaskin@mcgill.ca

ment by turbulent and molecular diffusion.[8,10,11] It should be noted that a maintained jet structure refers to the preservation of the jet mean momentum, and, therefore, its large-scale vorticity structures. These large structures, in turn, induce the global entrainment velocity, E_v.[23]

A jet, whose integral scale (i.e. width) is less than the largest length scale of the ambient turbulence, is advected by the large scales causing its path to meander, while the jet structure/entrainment is affected by the smaller scales.[9,24] Studies of jets and plumes in ambient turbulence, using Eulerian averaging (all to date), include both the effect of the large scales advecting the jet and the effect of the small scales of the ambient turbulence. An increase in jet spreading observed in Eulerian averages of strong jets in a coflow with low levels of ambient turbulence has been interpreted as increased entrainment citing superposition of jet-driven entrainment and ambient turbulent diffusion.[25,26] Jet entrainment (or resulting dilution) is driven by the jet's mean momentum,[1] whereas detrainment by turbulent diffusion is driven by the scalar concentration gradient and facilitated by the ambient turbulence diffusivity. Experimental observations of jets in ambient turbulence have not found self-similarity of first-order properties (Eulerian averages),[10,11] although, in a strong jet in a coflow with very low relative turbulence intensity, self-similarity was observed up to a relative length scale of the ambient to the jet of one.[26]

In real flows, turbulence is generally inhomogeneous and anisotropic. However, the study of shear flows in homogeneous isotropic turbulence (HIT) allows for analysis in a simplified laboratory context. That being said, despite being a simple concept, HIT is challenging to realize in a laboratory due to the necessity of a mean velocity gradient for initial production of turbulent kinetic energy (TKE).[11] Researchers have used different methods to create the closest approximations to HIT, such as oscillating grids,[27] active/passive grids,[28,29] and loudspeakers.[30] However, grid-generated turbulence suffers from large mean flows, and the loud speakers systems can maintain the HIT in only a very small region. Introduction of the random jet array (RJA) enhanced the quality of the turbulence, minimizing the mean flow and increasing the extent of the HIT region.[31–33]

In the current study, the effect of the different intensities of HIT on the evolution and structure of an axisymmetric turbulent jet is investigated through the study of the passive scalar field, building on the work of Khorsandi *et al.*[10] and Pérez-Alvarado[11] (same turbulence properties and jet Reynolds numbers). Scalar statistics of the flow are analyzed using (i) a classical Eulerian average, which is a stationary spatial average, and (ii) an average conditioned on the centroid of the instantaneous jet cross-section, hereafter referred to as Eulerian average and centroidal average, respectively. While the Eulerian average provides information on the spatial dispersion of the scalar concentration relative to the jet axis, the centroidal statistics provide information on the jet dynamics by separating the effect of the larger scales, which advect the jet causing its path to meander, from the smaller scales, which disrupt the jet entrainment and mixing (details in Sec. III).

The experimental set-up of a jet issuing into a HIT with negligible mean flow generated with an RJA is described in Sec. II. The passive scalar field of the jet is experimentally measured using the planar laser induced fluorescence (PLIF) method, as detailed in Sec. II and analyzed using centroidal averages and Eulerian averages, Sec. III. In Sec. IV, the measurement technique is validated. Section V presents the results, and a discussion of the effect of the HIT ambient on the jet dynamics as compared to the jet in a quiescent ambient is provided. Section VI summarizes the conclusions.

II. EXPERIMENTAL METHODS

A turbulent axisymmetric jet was released into a quiescent and a HIT ambient with negligible mean flow. The PLIF method was used to observe the evolution of the passive scalar field in cross-sections of the jet. A detailed description of the experimental facility, the implementation of the PLIF method, and the data acquisition follows. Figure 1 is a schematic view of the experimental apparatus, and examples of instantaneous jet cross-sections in the quiescent and the HIT ambient are shown.

A. Experimental facility

The experiments were carried out in a 1.5 m × 2.4 m × 1 m subsection of a large glass water tank (1.5 m × 6 m × 1 m) open at the top (i.e. the free surface is at ambient pressure). The water in the tank was either quiescent, after being left to settle for sufficient time after slow filling, or turbulent (HIT). An approximately homogeneous and isotropic turbulence with negligible mean flow was generated in the tank by a random jet array (RJA),[31,32] but at a larger scale.[34] The RJA is an array of 6 rows and 10 columns of bilge pumps (Rule 25D, 500 GPH) mounted on a 1 m × 1.5 m vertical sheet of high-density polyethylene. The uniform spacing of the pumps in the horizontal and vertical directions (M = 15 cm, center to center distance), and a reflective boundary condition reduces the occurrence of secondary flows.[32,35]

The turbulence was generated by the RJA using an algorithm to individually turn the jets on and off for periods of time randomly selected from a normal distribution with a $(\mu_{on}, \sigma_{on}) = (12, 4)$ s and $(\mu_{off}, \sigma_{off}) = (108, 36)$ s.[32,34] Thus, 10 % of the pumps operate on average at any given time. Downstream of the RJA, the jets merge and create an approximately HIT ambient. As the intake and discharge of each pump occur simultaneously into the same control volume, there is zero net mass flow rate through each pump, resulting in an overall zero-mean flow in the tank. The random algorithm for the RJA generated a flow that most closely approximated a zero-mean flow HIT as compared to several alternative algorithms.[10,34]

(a)

(b)(c)

FIG. 1. (*a*) Schematic of the PLIF apparatus, and examples of instantaneous jet cross-section in (*b*) the quiescent, and (*c*) the turbulent ambient. The jet/ambient interface is shown with white contours using a threshold value of $\phi_t = 0.15\overline{\phi_c}$, where $\overline{\phi_c}$ is the the mean centerline concentration in the quiescent ambient, and the centroidally averaged concentration in HIT ambient, respectively (Section III). Red cross denotes the jet axis.

B. Jet apparatus

A round turbulent jet with Re = 10600 and 5800 issued into the water tank parallel to the RJA sheet, such that the turbulence level was constant along the jet centerline in the downstream direction. The jet issued from a copper tube with 8.51 mm inner diameter (d), which extended vertically for 1.2 m and, after a 90° bend, extended horizontally for 0.2 m ($\sim 24d$) achieving a fully developed flow at the exit. A constant-head reservoir, located 3 m above the jet, fed the jet flow maintaining a constant flow rate, and thus a constant Reynolds number. The jet was turned on and off with a solenoid valve, while a ball valve was used to adjust the flow rate, measured using a flow meter (Omega FL50002A). The jet measurements were made at orthogonal cross-sections of the jet located at downstream distances of x/d = 20, 30, 40, 50, and 60. The jet was mounted on a traversing mechanism to precisely adjust its position in the streamwise (x) and vertical (z) directions. The jet discharged parallel to the RJA sheet at a transverse distance of 110 cm (i.e. y/M = 7.3), where the turbulent kinetic energy (TKE) of the ambient was k_{RJA} = 4.4 cm^{2}s^{-2}.[10] The experimental parameters are provided in Table I. For more details on the RJA setup and the jet apparatus, the reader is referred to Khorsandi *et al.*,[10] Perez-Alvarado,[11] and Lavertu *et al.*[36]

At this point, it is worth mentioning the range of ratios, of the HIT to the jet, of the length scales ($\mathscr{L}$) and the turbulence intensities (ξ). The relative length scale is approximated by

$$\mathscr{L} = L_{RJA}/b_{\phi,1/2}, \qquad (1)$$

where L_{RJA} is the integral length scale of the HIT ambient at $y/M = 7.3$ and $b_{\phi,1/2}$ is the concentration half-width of the jet in the quiescent background (Sec. IV). In the current study, $L_{RJA} = 11$ cm and is estimated using

$$L_{RJA} = \int_0^\infty \frac{\overline{u_{RJA}(\mathbf{x})\,u_{RJA}(\mathbf{x}+re_x)}}{u^2_{rms,RJA}}\,\mathrm{d}r, \qquad (2)$$

where u_{RJA} is the axial velocity fluctuation of the RJA turbulence and re_x denotes some displacement lag r in the direction of the x-coordinate unit vector.[10] The relative turbulence intensity is defined as

$$\xi = u_{rms,RJA}/u_{rms,jet}, \qquad (3)$$

FIG. 2. Variation of the relative turbulence intensity and the relative length scale at each downstream location of the two jets. Filled symbols: $Re = 10600$, open symbols: $Re = 5800$. $\triangledown$, x/d = 20; $\circ$, x/d = 30, $\triangle$, x/d = 40; $\square$, x/d = 50; $\triangleright$, x/d = 60.

where the velocity information is taken from the study of Khorsandi *et al.*[10] The two selected jet Reynolds numbers allowed us to study the jet behavior above and below the transition Reynolds number, i.e., $Re = 10^4$.[37] Also, it granted a wide range of relative turbulence intensity ($0.16 < \xi < 0.73$) and relative length scale ($2.2 < \mathscr{L} < 6.3$) ratios between the HIT ambient and the jet (Table I). Figure 2 depicts the variation of $\mathscr{L}$ versus ξ at each downstream location for the two jets. The ratios of length scale and turbulence intensity between the HIT ambient and jet approach unity ($\mathscr{L}$ from larger values and ξ from smaller values) as the jet develops downstream, increasingly disrupting the jet structure.[9]

C. PLIF apparatus

The PLIF method was employed to obtain the concentration field of a passive scalar in the jet in orthogonal cross-sections. A small quantity of fluorescent dye (disodium fluorescein, Sc = 2000) was mixed into the jet water supply. A continuous mode 1 W argon-ion laser (Coherent, Innova 90) was used to illuminate the flow cross-section with an excitation wavelength of 514.5 nm. The laser beam was directed into a laser scanning device consisting of (i) a 12.7 mm dielectric mirror (Newport 5151), (ii) a focusing lens with a 1.5 m focal length plano-convex lens (PLCX-25.4-772.6-C), and (iii) a high-speed rotating mirror (Lincoln Laser Company DT-08-236-019). The 8-sided polygonal rotating mirror rotated at 12000 rpm generating a laser sheet with 1600 scans per second of the laser beam over the measurement area. The use of a high speed rotating mirror to generate the light sheet and low dye concentrations, minimized potential sources of PLIF errors, such as photobleaching, thermal blooming and attenuation.[11,38]

Instantaneous fluorescence signals were recorded using a 12 bit CMOS camera (pco.dimax). The camera had a resolution of 2016 $\times$ 2016 pixels, and the acquisition frequency was set to 30 Hz. The incident light first reached a 50 mm diameter 550 nm longpass color filter (ThorLabs FGL550) attached to the camera lens (Pentax 50mm f/1.4) to filter any scattered laser light, and therefore transmitting only the fluorescence signal through the camera lens. An image intensifier (Video Scope VS4-1845) was placed between the camera and the camera lens to increase the light sensitivity of the system. The coupling of the intensifier and the camera reduced the size of the detection area to a central circle with 1601 pixel diameter, covering a circular field of view (FOV) with a diameter of about 64 cm. The rather large FOV was necessary to capture the complete orthogonal spatial extent of the jet subjected to the HIT ambient at large downstream distances. The spatial resolution of the PLIF experiments was about 0.4

TABLE I. Experimental parameters. Note that $Re = U_0 d/\nu$, and $Re_{\lambda,RJA} = \left(\sqrt{150 k_{RJA}}\, L_{RJA}/\nu\right)^{1/2}$. Here $\mathscr{L}_{5800}$ and ξ_{5800} denote the length scale and turbulence intensity ratios of HIT to Re = 5800 jet at the five cross-sections, respectively. Similarly, $\mathscr{L}_{10600}$ and ξ_{10600} are defined for Re = 10600 jet.

Jet Reynolds number	Re	5800, 10600
Schmidt number	Sc	2000
Jet exit velocity	U_0	0.682, 1.245 m s^{-1}
Jet exit inner diameter	d	8.51 mm
Lateral jet position to RJA	y/M (M = 15 cm)	7.3
Ambient TKE (at $y/M = 7.3$)	k_{RJA}	4.4 cm^{2}s^{-2}
Ambient length scale (at $y/M = 7.3$)	L_{RJA}	11 cm
Ambient turbulent Reynolds number	$Re_{\lambda,RJA}$	168
RJA operating algorithm	(μ_{on}, σ_{on}), $(\mu_{off}, \sigma_{off})$	(12, 4) s, (108, 36) s
Axial position of cross-sections	x/d	20, 30, 40, 50, 60
Length scale ratio	$\mathscr{L}_{5800}$	5.8, 4.1, 2.9, 2.5, 2.2
	$\mathscr{L}_{10600}$	6.3, 4.5, 3.1, 2.5, 2.2
Turbulence intensity ratio	ξ_{5800}	0.29, 0.39, 0.52, 0.58, 0.73
	ξ_{10600}	0.16, 0.21, 0.31, 0.34, 0.43
PLIF spatial resolution	-	$4.7\eta - 1.4\eta$, $7.3\eta - 2.2\eta$
Field of view	FOV	64 cm × 64 cm
Sampling frequency	-	30 Hz

mm × 0.4 mm per pixel (Table I). This resolution corresponds to $1.4\eta - 4.7\eta$ for Re = 5800 and $2.2\eta - 7.3\eta$ for Re = 10600, where $\eta = \left(\nu^3/\overline{\varepsilon}\right)^{1/4}$ is the centerline Kolmogorov length scale for the quiescent background case. It is worth noting that the Batchelor microscale is the appropriate length scale for resolving the scalar field at high-Sc flows, which was not attained in the present experimental setup. However, resolution comparable to η has been shown to be sufficient to capture the mean and rms concentration profiles.[39] The lowest resolution occurs at the closest downstream distance ($x/d = 20$) since the turbulent length scales, including η, increase as the jet develops.[40] ν and $\overline{\varepsilon}$ denote the kinematic viscosity ($10^{-6}\,\mathrm{m^2\,s^{-1}}$ for water) and mean centerline dissipation rate, respectively. The latter is calculated using the empirical relation of Friehe, van Atta, and Gibson,[41]

$$\overline{\varepsilon} = 48 \frac{U_0^3}{d} \left(\frac{x - x_0}{d}\right)^{-4}, \quad (4)$$

where U_0 and x_0 denote the nozzle exit velocity and the virtual origin (see Sec. IV), respectively. It should be noted that the estimated values of $\overline{\varepsilon}$ (and therefore η) are only used to calculate the PLIF pixel spacing at each measurement station (Table I).

Although the laser power was constant during the experiments, the laser intensity, defined as the ratio of the laser power to the cross-section of the laser sheet, decayed with the laser sheet expansion (angle of expansion of 45°). Furthermore, the image intensifier caused higher light sensitivity in the central region of the image as compared to the edges. The images were, therefore, calibrated pixel by pixel to convert the light intensity levels to dye concentration values. Over a large range, the relationship between the dye concentration and the emitted light intensity is nonlinear;[42] however, at low concentration levels (as is in the present PLIF experiments), the intensity-concentration relationship is linear. Therefore, a linear curve can be fitted such that $\phi = AI + B$, where I is the light intensity value of the pixel, A and B are the calibration coefficients extracted from the calibration test, and ϕ denotes the concentration value. Details of the calibration and PLIF tests can be found in Perez-Alvarado.[11]

PLIF is prone to measurement errors, including attenuation, photobleaching, trapping, thermal blooming and inertial effects. Attenuation of the laser beam occurs when (a part of) the laser energy is absorbed by the fluorescent dye when the laser beam crosses through non-negligible volumes of dyed fluid before it reaches the measurement location. Photobleaching is the reduction in fluorescence intensity due to constant laser irradiation. Trapping occurs if the emitted fluorescence light at the measurement section is absorbed by dye at some other location, e.g. at the space between the laser sheet and the camera. Thermal blooming describes the condition in which the laser beam diverges due to fluid density variation because of heating of the dyed medium by the laser. Variation in fluid temperature and/or density would also cause buoyancy and inertial effects.

A series of tests were conducted by Lavertu[38] and Perez-Alvarado[11] on a similar experimental apparatus (the latter having the same PLIF setup) to evaluate and minimize the above errors using technical and theoretical measures. According to Perez-Alvarado[11], the maximum attenuation of the laser beam for a 10 cm spanwise shift of the dyed fluid (for concentrations within the calibrated range) towards the beam source was less than one percent. Estimating the attenuation across the jet profile results in an error of less than 1% (this is due to the very low concentrations of dye used in experiments). Photobleaching and thermal blooming were reduced to negligible values by using a high-rev rotating mirror, at which the residence time of a single beam in the volume covered by each camera pixel was approximately 2 μs, while 200 μs was required for the fluorescence signal to reduce by 2% due to constant irradiation of the dyed fluid.[38] It should be noted that Lavertu[38] used punctual LIF, which is subject to much higher possibility of constant irradiation of the dyed fluid compared to the present PLIF measurements. Trapping of the laser light was shown to be less than one percent for the calibrated range of the concentration values.[11] Furthermore, the inertial effects were negligible during the experiments because of the use of very low concentrations of disodium fluorescein (maximum 7.66×10^{-7} $\mathrm{mol\,L^{-1}}$) having a molecular mass of 376.3 $\mathrm{g\,mol^{-1}}$, which introduces a density variation of less than 2.8×10^{-5} % between the jet fluid and the ambient water. Therefore, common errors in the PLIF measurements are minimal in the present study.

III. DATA PROCESSING

The passive scalar field of the two jets with Re = 10600 and 5800 issuing into the turbulent ambient are compared to those in a quiescent ambient. The PLIF images were obtained at axial distances of x/d = 20, 30, 40, 50, and 60. In order to achieve first- and second-order scalar concentration convergence at these axial positions in the quiescent ambient case, data sets over a period of 27 s, 45 s, 63 s, 81 s, and 100 s resulting in a total of 789, 1315, 1841, 2367, and 2893 PLIF images were obtained, respectively. While in the HIT ambient case, five sets of PLIF experiments, each obtained for 170 seconds containing 4997 images, were taken for each axial position. Custom MATLAB codes were employed to obtain scalar concentration statistics of the jet cross-section in the turbulent and the quiescent ambient cases.

Instantaneous images of the jet cross-section show greater irregularity when the jet is released into a turbulent ambient. The jet is also displaced laterally by the large eddies of the ambient turbulence (see Fig. 1*c*). The isocontours of the joint probability density function (JPDF) of the position of the jet centroid for the jet in the HIT ambient for Re = 10600 and 5800 jets are presented in Fig. 3. The mean radius of the jet in the quiescent ambient is approximately $r/x = \sqrt{y^2+z^2}/x =$ 0.2 centered at zero (not shown for brevity). The jet centroid in the HIT ambient is displaced over an area greater than that occupied by the jet in the quiescent ambient.

The standard deviation of the position of the jet centroid in the quiescent and HIT ambient is depicted against the axial position in Fig. 4. In the quiescent ambient, the standard deviations range between $0.004 < \sigma/x < 0.010$ and $0.005 < \sigma/x < 0.011$ for the Re = 10600 and Re = 5800 jets, respectively, while in the turbulent ambient, the standard deviations increase to $0.11 < \sigma/x < 0.15$ and $0.17 < \sigma/x < 0.22$ for the Re = 10600 and Re = 5800 jets, respectively. Therefore, in the quiescent ambient, the jet is almost always centered on the jet axis, while in the turbulent ambient, the position of the jet centroid varies significantly, which is more noticeable in the low-Re jet (higher ξ). Large standard deviations of the position of the jet centroid indicate a meandering path of the jet in the turbulent ambient (schematic view in Fig. 5), while the jet path in the quiescent ambient is almost a straight line. The meandering path of the jet is due to lateral advection of the jet by the large ambient eddies, and is more noticeable closer to the jet exit, where $\mathscr{L} \gg 1$. As the jet grows in the downstream direction, the relative length scale between the ambient and the jet decreases, and hence the large eddies of the HIT ambient are less able to advect the jet. This is evident in the generally decreasing standard deviation of the jet centroid position with the axial distance in Fig. 4. Particularly, beyond $x/d = 40$ for both jets where $\mathscr{L} \approx 3.0$, the role of the large-scale ambient eddies on the jet motion is less dominant. However, at x/d = 20 of Re = 10600 jet, the standard deviation has a local minimum due to the strong structure of the jet that resists the external forcing advecting the jet path. Similar meandering due to the turbulence in the ambient was observed in wakes.[22] It should be noted that in the present study, the only apparent role of the relative length scale ($\mathscr{L}$) on the jet behavior in the HIT ambient is to cause the jet path to meander, which is effectively removed in the centroidal analysis of the data. Therefore, in the following sections only the effect of the turbulence intensity ratio on the jet behavior in HIT ambient is discussed.

The time averaged characteristics of the jet are obtained from Eulerian averages and centroidal averages of the instantaneous images. The Eulerian average provides the ensemble averaged concentration at a particular location (geometric position) relative to the jet axis, which includes the composite effects of the large- and small-scales of the ambient turbulence on the jet at a particular location in space. The second approach, by being conditioned on the centroid of the jet cross-section, excludes the effect of the larger scales translating the jet laterally, and includes primarily the influence of the smaller scales of the ambient turbulence, which modify the internal jet structure and dynamics.[9,24] However, it should be noted that at high levels of turbulence intensity, the effect of the large scale eddies are not fully removed due to the meandering of the jet resulting in a discontinuity in the jet structure. The analyses are carried out on a profile equidistant from the RJA plane, passing through the centerline or the centroid, which is subjected to an approximately constant level of ambient turbulence at any given downstream position. A similar approach was previously adopted in axisymmetric[43] and line[44] plumes in order to eliminate the effect of large-scale meandering by considering the flow characteristics in the plume coordinates, i.e., following the instantaneous turbulent/non-turbulent interface (TNTI) of the plume. It is worth noting that the centroidal origin ($r = 0$) in the current study is positioned on the mass center of the bulk of the flow within the FOV, whereas the origin of the plume coordinates in the aforementioned studies is the middle point of the left and right TNTI at each downstream distance. We note that although the FOV is fairly large, the calculation of the centroid position is affected to a small extent by the amount of dye going out of the FOV due to meandering of the jet path. A sensitivity analysis is carried out in Appendix A to quantify the dependence of the mean centroid location on scalar concentrations above a range of thresholds.

FIG. 3. Isocontour of the JPDF of the jet centroid position in the HIT ambient. The red cross shows the jet axis, while the red circle denotes the mean position of the jet centroid in the turbulent ambient. For Re = 10600 jet at (a) x/d = 20, (b) 30, (c) 40, (d) 50, and (e) 60. Similarly, for Re = 5800 jet at (f) to (j) for x/d = 20 to 60. Note that the RJA acts on the right side of the images. The colorbars are logarithmic.

FIG. 4. Standard deviation of the jet centroid with the axial distance in the quiescent and in the turbulent ambient. Symbols: ○, Re = 10600 quiescent; ● Re = 10600 HIT; ▽, Re = 5800 quiescent; ▼, Re = 5800 HIT.

FIG. 5. Schematic of the jet structure in the ambient turbulence, showing the jet axis (dotted line), and the jet centroid (dashed line). Large scale eddies of the HIT ambient cause the jet to meander.

IV. MEASUREMENT VALIDATION

Measurements of the scalar field of the jet in a quiescent ambient show a self-similar behavior in the mean and rms concentration profiles,[45] similar to those in the velocity field (e.g. see Hussein *et al.*[46]). The scalar concentration measurements of the jet issued into a quiescent ambient of the current work are validated by a comparison to those reported in the literature using different experimental methods: Mie scattering,[47] Rayleigh scattering,[48] PLIF,[49–52] and by direct numerical simulation (DNS) of a turbulent jet.[53]

The downstream evolution of the mean centerline concentration, $\overline{\phi_c}$, normalized by the jet exit concentration, ϕ_0, for the jet in a quiescent ambient is shown in Fig. 6(a). Along the jet centerline, $\overline{\phi_c}$ varies inversely with the downstream distance as $\overline{\phi_c} = \kappa\phi_0(\frac{x-x_0}{d})^{-1}$, where κ is the decay constant, and the position of the virtual origin, x_0, is 2.4d in the present work. The current work shows a power law decay of x^{-1} as predicted theoretically and previously observed.[48,49,53,54] The decay constant, κ, depends slightly on Reynolds number and on the initial conditions,[55] and its value here ($\kappa = 5.4$) lies within the reported range of $4.48 < \kappa < 5.59$ in Dowling and Dimotakis.[48] A comprehensive review of the asymptotic behavior of κ is presented in Table 1 of Mi *et al.*[55]

The downstream evolution of the concentration half-width, $b_{\phi,1/2}$, defined as the radial position at which the concentration reduces to half of its centerline value, is shown in Fig. 6(b). In a quiescent ambient in the self-similar region of the jet, $b_{\phi,1/2}$ is a linear function of the downstream distance, $b_{\phi,1/2}(x) = S(x-x_0)$, where S is the spreading rate of the scalar field in the jet. Experimental data show that S is independent of Reynolds number, and varies between $0.101 < S < 0.156$.[45] In the present work, S is about 0.112.

The radial profiles of the mean concentration normalized by their respective centerline value are shown in Fig. 7(a). The analytical solution for the mean concentration profile of a round jet is given by $\overline{\phi}/\overline{\phi_c} = \{1+a(r/x)^2\}^{-2}$, where a is a constant, $a = (\sqrt{2}-1)/S^2$.[54] The analytical solution and a Gaussian fit to the experimental data are also shown in Fig. 7(a). The profiles at x/d = 20 and 40 show a good agreement with the previous experimental results,[48,51] a DNS study,[53] and the Gaussian fit. The profiles at x/d = 30, 50, and 60 also show a good agreement and are not included here for brevity. It is noted that the analytical solution overestimates the concentration values near the edges of the jet[54] as a constant turbulent diffusivity is assumed across the flow, while it is, in fact, lower near the edges due to external intermittency.

The radial profiles of rms concentration fluctuations normalized by their respective centerline values at x/d = 20 and 40, are also shown in Fig. 7(b). The profiles are self-similar and behave similarly to those reported in the literature.[47,48] The rms profiles at x/d = 30, 50, and 60 also show a good agreement.

V. RESULTS AND DISCUSSION

The effect of the ambient turbulence on the jet characteristics is determined by the relative magnitudes of the turbulence intensity, ξ, and the integral length scales, $\mathscr{L}$, between the the HIT ambient and the jet.[8,9] While in the present study $\mathscr{L} > 1$ and $\xi < 1$ at all measurement stations (see Table I), they both approach unity at the furthest downstream locations and become $O(1)$. This is the condition at which the ambient turbulence affects the jet structure and changes the entrainment process and the subsequent scalar mixing. Note that it is mainly the intense smaller eddies of the ambient that alter the jet structure, while the larger eddies serve to advect the jet, resulting in a meandering path.[9] Also, it should be noted that once $\mathscr{L}$ and ξ become $\mathscr{O}(1)$, the effect of ξ has a dominant effect on the jet behavior, causing the jet to break up at a critical axial distance. For example, Kankanwadi & Buxton[22] recently showed the predominance of ξ as compared to $\mathscr{L}$ in the context of entrainment into a cylinder wake in a homogeneous turbulent ambient. Therefore, the following discussion of the results covers only the effect of ξ on the jet behavior in HIT ambient (note that the role of $\mathscr{L}$ is to cause the jet path to meander, and its effect has been essentially removed in the

(a)(b)

FIG. 6. Downstream evolution of the (*a*) mean centerline concentration, and (*b*) concentration half-width of an axisymmetric jet at Re = 5800 issued into a quiescent ambient.

(a)(b)

FIG. 7. Radial profiles of (*a*) mean concentration, and (*b*) rms concentration fluctuations of an axisymmetric jet at Re = 5800 issuing into a quiescent ambient. The solid line and the dashed line in (*a*) show the Gaussian fit and the analytical solution of the round jet, respectively.

centroidal data analysis.)

The growth, structure and statistics of the passive scalar field of an axisymmetric turbulent jet issuing into a turbulent ambient are presented and compared to those of the jet in a quiescent ambient. The TKE of the ambient turbulence is k_{RJA} = 4.44 cm^{2}s^{-2}, and the jet Reynolds numbers are Re = 10600 and 5800. Five orthogonal cross-sections in the self-similar zone of the jet in a quiescent ambient have been studied (x/d = [20, 30, 40, 50, 60]). Variation of ξ and $\mathscr{L}$ for each downstream location of the two jets results in ten different case studies, as depicted in Fig. 2. To present the results, first, the evolution and structure of the jet will be discussed in terms of the mean concentration, the concentration half-width, and the rms concentration. Then, the self-similarity of the scalar field will be studied. Finally, statistics of the scalar mixing will be presented using the intermittency factor, probability density functions (PDFs) and the cumulative distribution functions (CDFs) of the centerline concentration. It should be noted that the variation between the centroidal and the Eulerian analyses in the quiescent ambient was negligible for the mean profiles (less than 1%), and was less than 4% and 7% for the PDFs and the rms profiles, respectively. Therefore, in the following figures, only the centroidal analysis of the jet in a quiescent ambient is provided.

A. Evolution and structure of the jet

The turbulent jet issuing into HIT ambient is subject to an increasing impact from the intensity of the ambient turbulence (i.e. increasing ξ) and a decreasing impact from the length scale of the ambient turbulence (i.e. decreasing $\mathscr{L}$) as its own turbulence intensity decreases and length scale increases, while those of the ambient turbulence are constant with downstream distance. In ambient turbulence, jet entrainment is reduced as the jet flow is progressively disrupted. Two regions of behavior of the jet are identified, based on the jet statistics conditioned on the jet centroid, which allow the jet structure to be assessed. The regions reflect the increasing impact of the ambient turbulence intensity and are characterized by 1) a perturbed jet structure, downstream of the developing jet region, and, further downstream, 2) a destroyed jet structure. The relative lengths of these regions depends on the relative turbulence intensity between the ambient and the jet. In this study, region 1 is observed in the Re = 10600 jet, while regions 1 and 2 are observed in the Re = 5800 jet, for x/d = 20 to 60.

The downstream evolution of the mean jet centerline concentration ($\overline{\phi_c}/\phi_0$) of the jet issuing into a turbulent ambient results in lower concentrations and a faster decay as compared to the jet in a quiescent ambient. Hereafter, $\overline{\phi_c}$ denotes the mean concentration of the geometric centerline (i.e. jet axis) in the Eulerian averaging method, while it represents the ensemble average of the instantaneous centroid scalar concentration values in the centroidal averaging procedure. The concentration decay initially follows a power-law for both the centroidal and Eulerian averages of the jet in a turbulent ambient, as shown in Fig. 8. The decay exponents are, $\overline{\phi_c}/\phi_0 \propto x^{-1.1}$ for both jets for the centroidal average and $\overline{\phi_c}/\phi_0 \propto x^{-1.6}$ and x^{-2} for Re = 10600 and 5800 jets, respectively for the Eulerian average. The uncertainty in the measurements is three orders of magnitude smaller than the mean values due either to the low variance (in quiescent ambient) or due to the high number of samples (in HIT ambient). The power-law region is the perturbed jet region in the two-region jet model. The effect of the ambient turbulence is greater at larger values of relative turbulence intensity (ξ), which is inversely proportional to Re, i.e. $\xi_{5800} > \xi_{10600}$ at each downstream distance. This is evident in the relative lengths of the power-law regions of the jets, which is up to x/d = 60 for Re = 10600 (the jet was observed to break up at x/d = 70 for the Eulerian average in Pérez-Alvarado[11]), while in the Re = 5800 jet, it is only valid up to x/d = 40, beyond which the concentration decay accelerates, and where it is later shown that the jet structure has been destroyed. The Eulerian averaging shows a faster concentration decay as compared to the centroidal averaging because the effect of the jet meandering, causing low concentrations to appear at the geometric axis, is included in the Eulerian average. The power-law region of the jet (i.e. first region) starts following the developing region of the jet. If the power-law behavior of the jet is extrapolated backwards, it predicts that $\overline{\phi}_c/\phi_0 = 1$ at $x/d \approx 7$ and 6 for the centroidal analysis of the Re = 10600 jet in a quiescent and HIT ambient, respectively. Similarly, $x/d \approx 7$ and 2 is predicted for the Re = 5800 jet. This suggests that the length of the developing region of the jet is reduced in the HIT ambient, but this requires further experiments for verification. It appears that although both jet Reynolds numbers are affected, the effect is greater for the jet with higher relative turbulence intensity (i.e. Re = 5800). Similarly, the length of the recirculating region of a wake is reduced in an isotropic turbulent ambient.[18,56] Table II provides the decay exponents for the mean centerline concentration in the power-law regions of the Re = 10600 and 5800 jets (as well as those for the concentration half-width and the rms

(a)(b)

FIG. 8. The effect of ambient turbulence on the downstream evolution of the mean centerline concentration. (*a*) Re = 10600, and (*b*) Re = 5800. Symbols: ○, quiescent ambient; □ centroidal, and ▽ Eulerian averaging in HIT ambient. Figures are in log-log coordinates.

TABLE II. Power law exponents for the jet in quiescent and HIT ambient.

Background condition	Averaging method	Re = 10600			Re = 5800		
		$\overline{\phi_c}/\phi_0$	$b_{\phi,1/2}/d$	$\phi_{rms,c}/\phi_0$	$\overline{\phi_c}/\phi_0$	$b_{\phi,1/2}/d$	$\phi_{rms,c}/\phi_0$
Quiescent	Centroidal	x^{-1}	x^{1}	$x^{-0.7}$	x^{-1}	x^{1}	$x^{-0.7}$
Turbulent	Centroidal	$x^{-1.1}$	$x^{1.1}$	$x^{-0.94}$	$x^{-1.1}$ $(x/d \leqslant 40)$	$x^{1.1}$ $(x/d \leqslant 40)$	$x^{-0.92}$ $(x/d \leqslant 40)$
	Eulerian	$x^{-1.6}$	$x^{1.2}$	$x^{-0.73}$	x^{-2} $(x/d \leqslant 40)$	$x^{1.5}$ $(x/d \leqslant 40)$	$x^{-0.83}$ $(x/d \leqslant 40)$

concentration, discussed below).

The mean scalar concentration profiles of the Re = 10600 and Re = 5800 jets issuing into a quiescent and into a turbulent ambient are close to Gaussian in shape, as shown in Fig. 9. As observed for the centerline concentrations, turbulence in the ambient results in faster concentration decay leading to lower concentrations in the profiles, except in the tails, i.e. $|r/x| >$ 0.2 (for all tails but those of x/d > 40 for Re = 5800 jet). The higher concentrations in the tails are due to the greater width of the profile in the HIT ambient, and, for the Eulerian average, the inclusion of the jet meandering. In the HIT ambient, the centroidal average concentration profiles for both jet Reynolds numbers are lower and slightly wider than those of the quiescent ambient for the perturbed jet region (x/d = 20 to 60 for the Re = 10600 jet and x/d = 20 to 40 for the Re = 5800 jet, for which all $\xi < 0.5$). For the Re = 5800 jet, beyond x/d = 40 (where $\xi > 0.5$), the profiles narrow indicating a greatly reduced entrainment and, therefore, the destruction of the jet structure. The Eulerian average profiles are generally lower than those of the centroidal average due to the inclusion of the jet meandering. However, the maximums of the Eulerian profiles for Re = 10600 up to x/d = 30 and for Re = 5800 at x/d = 20 are higher than those of the centroidal profiles because, although the extent of the jet boundary is relatively stationary, the position of passive scalar centroid is affected by the ambient turbulence. The Eulerian average observations of mean centerline concentration confirm those of Pérez-Alvarado.[11]

The concentration half-width, $b_{\phi,1/2}$, is a characteristic length scale of the scalar field, and its downstream evolution is shown in Fig. 10. In the quiescent ambient, the concentration half-width grows linearly with the axial distance, x, as predicted by dimensional analysis. In the turbulent ambient, the half-width is greater than in the quiescent ambient and its rate of growth is faster ($b_{\phi,1/2} \propto x^{1.1}$) for both jet Reynolds numbers in the perturbed jet region for the centroidal average. The width growth ceases for $x/d > 40$ for the Re = 5800 jet indicating that the time-averaged entrainment into the jet has stopped (as discussed below), which implies that the jet structure has been destroyed, meeting the criteria of jet break-up. Jet break-up is, therefore, identified to occur at $x/d > 40$ for the Re = 5800 jet, and the region beyond it (where $\xi > 0.5$) is the destroyed jet region, which is only subject to turbulent and molecular diffusion (the Re = 10600 jet is destroyed at x/d = 70).[11] It is relevant to note that the scalar width of a round jet subjected to volumetric heating also ceases to grow upon disruption of the large-scale vortical structures of the jet.[57,58] The Eulerian average data obscure the change in behavior of the Re = 5800 jet due to the inclusion of the meandering of the jet, which also results in a much higher rate of width growth ($b_{\phi,1/2} \propto x^{1.2}$ and $b_{\phi,1/2} \propto x^{1.5}$ for the Re = 10600 and Re = 5800 jets, respectively). This is consistent with the growth rates (from Eulerian average data) of the concentration half-width of jets,[11] the velocity half-width of momentum-driven[10] and buoyant jets,[12] and of wakes (e.g. see Eames *et al.*[19] and Legendre *et al.*[17]) in a HIT ambient.

The effect of the HIT ambient on the entrainment into the jet can be deduced from the integral volume flux, Q, momentum flux, M, and scalar flux, F, defined as

$$Q \equiv 2\pi \int_0^\infty \overline{u} r \,\mathrm{d}r, \quad M \equiv 2\pi \int_0^\infty \overline{u}^2 r \,\mathrm{d}r, \quad F \equiv 2\pi \int_0^\infty \overline{u}\overline{\phi} r \,\mathrm{d}r, \tag{5}$$

where $\overline{u}$ is the mean streamwise velocity of the jet. The entrainment hypothesis[1] states that the entrainment into a jet in a quiescent ambient is a function of the entrainment velocity, E_v, which is proportional to a characteristic jet velocity, usually the mean axial velocity, i.e. $E_v \propto \overline{u}_c$. With continuous entrainment of the ambient fluid at the jet interface, the mass flow rate of the jet ($m = 2\pi\rho \int_0^\infty \overline{u} r \,\mathrm{d}r$) increases linearly with downstream distance. In the HIT ambient, it is expected that the mass flow rate of the jet is decreased due to lower mean axial velocities compared to the quiescent ambient.[10] Also, one can expect that the mass flow rate of the jet does not increase beyond the jet break-up, because the mean axial velocity becomes negligible. A reduction in mass flow rate in the HIT ambient is observed for the $Re = 10600$ jet,[10] whose rate of increase decreases by $x/d = 70-80$. A second-order integral model has also been proposed predicting a reduced volume flux ($Q = m/\rho$) in the HIT ambient that reaches a plateau at a critical downstream distance.[12] A lower mass flow rate (and lower volume flux) of the jet in the HIT ambient indicates a lower entrainment into the jet compared to the quiescent ambient. The asymptotic behavior of m/m_0 and Q/Q_0 (m_0 and Q_0 denoting the jet exit mass flow rate and volume flux, respectively) indicates the cessation of the entrainment into the jet beyond the jet break-up.[10,12]

FIG. 9. Radial profiles of the mean concentration. For *Re* = 10600 jet at (*a*) x/d = 20, (*b*) 30, (*c*) 40, (*d*) 50, and (*e*) 60. Similarly, for *Re* = 5800 jet at (*f*) to (*j*) for x/d = 20 to 60. Symbols: ○, quiescent ambient; □ centroidal, and ▽ Eulerian averaging in HIT ambient. Dashed magenta curves are Gaussian fit to the profiles.

FIG. 10. The effect of the ambient turbulence on the downstream evolution of the concentration half-width. (*a*) *Re* = 10600, and (*b*) *Re* = 5800. Symbols: ○, quiescent ambient; □ centroidal, and ▽ Eulerian averaging in HIT ambient. Figures are in log-log coordinates. A dash-dotted line in (*b*) denotes the unchanged concentration half-width in the second region.

FIG. 11. The effect of the ambient turbulence on the downstream evolution the mean scalar flux of the jet. Symbols: ○, *Re* = 10600 quiescent; • *Re* = 10600 HIT; □, *Re* = 5800 quiescent; ■, *Re* = 5800 HIT. Dashed lines are power-law fits to the data. Solid lines show the prediction by Lai *et al.*'s[12] exponential model for the scalar flux of the jet in the HIT ambient.

Furthermore, the mean momentum flux and the mean scalar flux are indicators of the jet entrainment. For the jet in a quiescent ambient, both M/M_0 and F/F_0 are conserved ($M/M_0 \approx 1, F/F_0 \approx 1$) and the mean momentum flux and the mean scalar flux contribute almost 90% and 92% of the jet exit momentum, M_0, and the jet exit scalar flux, F_0, respectively.[16,46] For the jet in a turbulent ambient, however, M/M_0 and F/F_0 are less than one and increasingly so with the downstream distance[11] as the contribution of the mean fluxes decreases due to the increasing effect of the disruption of the jet structure (Fig. 11), while the second-order fluxes become more important.[10–12] Lai *et al.*[12] argued that the conservation of the total momentum of the jet in the HIT ambient can be demonstrated only if the second-order momentum flux is included. The scalar flux is calculated using the present concentration data and the velocity data from Khorsandi *et al.*[10] It is noted as only the spatially-averaged velocity data (up to $x/d = 50$) were available, the spatially-averaged concentrations were used to calculate the scalar flux. The mean momentum flux[11] and the mean scalar flux (Fig. 11) are lower for the $Re = 5800$ jet and decrease faster compared to the $Re = 10600$ jet in the HIT ambient. This reflects the larger ratio of the turbulence intensity of the HIT to the jet, ξ, for the $Re = 5800$ jet at any given downstream position. Both M/M_0 and F/F_0 are approaching zero by $\xi = 0.58$ (i.e. $x/d = 50$ for the $Re = 5800$ jet), which is found within the destroyed jet region. Lai *et al.*'s exponential model[12] has also been used to reproduce the scalar flux of the current jet in the HIT ambient in Fig. 11, which shows good agreement with the experimental data.

In the second region of the jet in the HIT ambient ($\xi > 0.5$) the centroidal scalar half-width stops growing (Fig. 10*b*, $x/d > 40$ for the $Re = 5800$ jet), which indicates the cessation of the entrainment into the jet. To further investigate the entrainment in the second region, we have defined the top-hat width, b_m, and velocity, u_m, of the jet

$$b_m \equiv \frac{Q}{\sqrt{M}}, \quad u_m \equiv \frac{M}{Q}. \tag{6}$$

The rate of change of the volume flux in the streamwise direction is evaluated as,

$$\frac{\mathrm{d}Q}{\mathrm{d}x} = \underbrace{b_m^2 \frac{\partial u_m}{\partial x}}_{Q^- < 0} + \underbrace{2 b_m u_m \frac{\partial b_m}{\partial x}}_{Q^+ > 0}. \tag{7}$$

For a jet in quiescent background, $Q^+ = 2|Q^-|$ due to the conservation of momentum, meaning that the jet is entraining ambient fluid on average. In a HIT ambient, however, the lack of growth of the centroidal scalar half-width in the second region (Fig. 10*b*, $Re = 5800$ jet) implies that the rate of increase of the integral jet width with downstream distance is zero. This leads to the second term of the right hand side of Eq. 7 to be zero, and, thus,

$$\frac{\mathrm{d}Q}{\mathrm{d}x} \approx b_m^2 \frac{\partial u_m}{\partial x} \leqslant 0, \tag{8}$$

since the characteristic velocity is decaying.[10] Therefore, the change in the integral volume flux with distance, which is interpreted as the time-averaged entrainment rate, has ceased in the second region. A similar claim can be made for the integral momentum flux in this region, that is,

$$\frac{\mathrm{d}M}{\mathrm{d}x} \approx 2 u_m b_m^2 \frac{\partial u_m}{\partial x} \leqslant 0, \tag{9}$$

meaning that the mean momentum flux, M, has no means of increasing. According to Morton, Taylor, and Turner,[1] the lack of global entrainment in the second region implies the absence of a mean velocity to drive the entrainment process, and this in turn demonstrates that a jet no longer exists beyond $\xi > 0.5$.

(a)(b)

FIG. 12. The effect of ambient turbulence on the downstream evolution of the centerline rms concentration. (*a*) *Re* = 10600, and (*b*) *Re* = 5800. Symbols: ○, quiescent ambient; □ centroidal, and ▽ Eulerian averaging in HIT ambient. Figures are in log-log coordinates.

Higher rms concentration values, ϕ_{rms}, occur in the jet in the turbulent ambient as compared to the quiescent ambient, as shown in Fig. 12. Previously, Pal & Sarkar[21] also reported an increased turbulence level (or equivalently an increased turbulent kinetic energy) in towed wakes subjected to isotropic turbulence, due to entrainment of background fluctuations. The rate of decay of the rms centreline concentration in the turbulent ambient of the centroidal average data is more rapid (at a rate of $\phi_{rms,c} \propto x^{-0.94}$ and $x^{-0.92}$ for the *Re* = 10600 and 5800 jets, respectively) than that in the quiescent ambient (at a rate of $\phi_{rms,c} \propto x^{-0.7}$). Due to the inclusion of the jet meandering in addition to the changes in rms concentration in the jet, the rms of the Eulerian average data is higher than that of the centroidal average data and has a slower rate of decay (at $\phi_{rms,c} \propto x^{-0.73}$ and $x^{-0.83}$ for the *Re* = 10600 and 5800 jets, respectively). Note that once the jet is destroyed (beyond $x/d = 40$ in the *Re* = 5800 jet), the rate of decay of the Eulerian average is more rapid than in the power-law region (perturbed jet region), as there is no longer a contribution to the scalar fluctuations from the jet structure, but only from the advection of the scalar by the HIT ambient.

The rms concentration profiles are shown in Fig. 13. The double peaked shape of the rms profiles in the quiescent ambient show the location of the shear layer between the jet flow and the ambient. The shear layer in the jet is preserved but weakening in the turbulent ambient for the *Re* = 10600 jet as shown by the double peaked centroidal average profiles with maximum ϕ_{rms} at $r/x \approx \pm\, 0.1$, similarly to the jet in a quiescent ambient. By $x/d = 60$, the maximum rms concentration is observed at the centreline, implying a change in the small-scale structure of the jet, while the first order statistic of mean concentration is still in the power-law region. For the *Re* = 5800 jet, on which the ambient turbulence has a greater impact, i.e. $\xi_{5800} > \xi_{10600}$, the shape of the profiles at $x/d = 20$ is two-stepped, with the first step at $r/x \approx \pm\, 0.2$ corresponding to the center of the shear layer between the jet and the ambient, while the second step at $r/x \approx \pm\, 0.4$ may be an indication of the effect of the ambient eddies modulating the jet/ambient interface. By $x/d = 30$, the first step is still visible and demonstrates the relatively strong jet structure despite the impact of the ambient turbulence. The width of the profile starts to decrease from $x/d = 40$, reducing to that of the quiescent case by $x/d = 60$, again indicating a decaying jet structure. The Eulerian averaging obscures the detail of the jet structure and the rms concentration profiles are single peaked for both jet Reynolds numbers (beyond $x/d = 30$ for the *Re* = 10600 jet) and become super Gaussian with downstream distance, the effect being stronger in the *Re* = 5800 jet, confirming the results of Pérez-Alvarado.[11]

To summarize, two regions of jet behavior are identified in the jet in a HIT ambient. In the first region, the perturbed jet region (which is the main focus of this study), the ambient turbulence disrupts the jet structure due to meandering of the jet and entrainment of the turbulent ambient fluid resulting in a faster decay of the jet and a lower entrainment rate than in the quiescent ambient. This region follows the developing region of the jet, and the first- and second-order properties of the scalar field show power-law behavior. In the second region, the destroyed jet region, the ambient turbulence is comparable to the jet turbulence ($\xi > 0.5$), and the jet has been broken up and destroyed. Beyond the break-up position, the jet momentum-driven mechanism of scalar transport is replaced by molecular and turbulent diffusion by the ambient eddies. The transition between the two regions is determined by the relative turbulence intensity, ξ, and the second (destroyed) region occurs for $\xi > 0.5$.

The observations of the evolution and structure of the jet in the turbulent ambient, conditioning the average data on the jet centroid, show that the ambient turbulence serves to reduce the mean concentration, while increasing the rms concentration, and to increase the concentration half-width up to the point where the jet structure breaks up. The mean concentration profiles maintain their Gaussian shape for both jet Reynolds numbers (up to the limit of observations), despite the external forcing. The shear layer between the jet and the ambient is found to be well preserved in the perturbed jet region before break-up. The rate of decay of the mean concentration and the growth rate of the concentration half-width are the same for both jet Reynolds numbers in the perturbed jet region. Beyond jet break-up, identified as where the relative turbulence intensity, $\xi > 0.5$, the mean concentration decays more rapidly and the half-width stops increasing. The lack of growth of the concentration half-width indicates that the jet-driven entrainment is no longer occurring, implying that the jet has been destroyed, and only molecular and turbulent diffusion is occurring.[8] We hypothesize that when accounting for the large-scale meandering (i.e. using centroidal averaging), the evolution of the scalar field in axisymmetric jets is universal in the HIT ambient, provided the jet structure is not destroyed. Additional data over a broader range of Reynolds numbers and downstream distances (i.e. a wider range of ξ and $\mathscr{L}$) would allow us to confirm this conjecture.

B. Self-similarity and self-preservation

Self preservation of the velocity field of an axisymmetric jet in a quiescent ambient requires that the product of the normalized mean centerline velocity, $\overline{u}_c/U_0$, and the normalized velocity half-width, $b_{u,1/2}/d$, scales to a constant (e.g. see Hussein *et al.*[46]). The (first-order) self-preservation also holds for the normalized scalar concentration, $\overline{\phi_c}/\phi_0$ and the concentration half-width, $b_{\phi,1/2}/d$, in a quiescent ambient, that is, $\overline{\phi_c}/\phi_0 \times b_{\phi,1/2}/d \propto x^0$. The jet issuing into a turbulent am-

FIG. 13. Radial profiles of the rms concentration fluctuations. For *Re* = 10600 jet at (*a*) x/d = 20, (*b*) 30, (*c*) 40, (*d*) 50, and (*e*) 60. Similarly, for *Re* = 5800 jet at (*f*) to (*j*) for x/d = 20 to 60. Symbols: ○, quiescent ambient; □ centroidal, and ▽ Eulerian averaging in HIT ambient.

FIG. 14. Mean concentration profiles normalized by their centerline value. Radial distance is normalized by corresponding characteristic axial length scale, $\hat{x} = (x-x_0)^n/d^{n-1}$, where n is the growth exponent of the concentration half-width in the turbulent ambient. (*a*) *Re* = 10600 centroidal (n = 1.1), (*b*) *Re* = 10600 Eulerian (n = 1.2), (*c*) *Re* = 5800 centroidal (n = 1.1), and (*d*) *Re* = 5800 Eulerian (n = 1.5). Symbols: ∗, x/d = 20; ○, x/d = 30; ▽, x/d = 40; △, x/d = 50; □, x/d = 60.

bient is self-preserving in the power-law region where the jet is perturbed by the ambient turbulence ($\xi < 0.5$ and before jet break-up, $\mathscr{L} = 2.2$ - 6.3 for *Re* = 10600 and $\mathscr{L} = 2.9$ - 5.8 for *Re* = 5800), as $\overline{\phi_c}/\phi_0 \propto x^{-1.1}$ and $b_{\phi,1/2}/d \propto x^{1.1}$ for both jet Reynolds numbers (so that $\overline{\phi_c}/\phi_0 \times b_{\phi,1/2}/d \propto x^0$), when the average is conditional on the jet centroid (see Table II). Therefore, in this region, the jet maintains its evolution almost akin to the jet in a quiescent ambient, although with lower concentrations and a slightly greater spreading rate, i.e. $S = 0.14$ and $S = 0.16$ in the HIT ambient for *Re* = 10600 and *Re* = 5800 jets, respectively, as compared to that in a quiescent ambient, $S = 0.112$.

Support for the self-similarity of the mean scalar field of the jet in a turbulent ambient, in the first or perturbed jet region, is provided by the collapse onto a single curve of the mean concentration profiles (centroidal and Eulerian averages) seen in Fig. 14 (for all x/ds for the $Re = 10600$ jet and up to jet break-up at $x/d = 40$ for the $Re = 5800$ jet), when the concentration is normalized by the mean centerline concentration, $\overline{\phi_c}$ and the radial distance by the characteristic axial length scale,[59] $\hat{x} = (x-x_0)^n/d^{n-1}$, where n is the growth exponent of the concentration half-width in the turbulent ambient, see Table II. However, the mean scalar concentration is not self-similar in the second or destroyed jet region as seen in the centroidally averaged data [see Fig.13(c)]. Only the region $r/\hat{x} \geqslant 0$ is shown due to symmetry. In a similar HIT ambient generated by the RJA ($k_{RJA} = 4.4\,\text{cm}^2\text{s}^{-2}$), the Eulerian velocity profiles of Khorsandi *et al.*[10] were reported to reveal no self-similarity of the jet flow, unlike the Eulerian concentration profiles of this study. A recent study of round jets in a turbulent coflow with very weak external turbulence (relative turbulence intensities of ξ = 0.03 to 0.23 for x/d = 45 to 105 for the case of low $k_{RJA} = 0.04$ cm^{2}s^{-2} and high $k_{RJA} =$ 0.12 cm^{2}s^{-2}), reported self-similarity in the Eulerian averaged profiles when $\mathscr{L} \approx 1$.[26] The rms concentration profiles of both Reynolds number jets in HIT ambient of the current study were not self-similar, reflecting the greater vulnerability of higher statistics of the velocity and scalar fields to external forcing.

C. Statistics of the passive scalar mixing

The statistics of the passive scalar mixing are investigated in terms of the intermittency, and the PDFs (and CDFs) of the scalar concentration at the jet centreline. The intermittency of a jet describes the probability of the jet being present at a given location, (allowing the structure of the jet to be deduced), and is defined as $\gamma = prob(\phi(r,x) > \phi_t)$, where ϕ_t is the scalar threshold used to define the jet/ambient interface; that is, the turbulent/non-turbulent interface (TNTI) in the quiescent ambient and the turbulent/turbulent interface (TTI) in the turbulent ambient. The interface between the inner turbulent flow and the outer ambient is usually detected by applying a suitable threshold to a flow variable, e.g., enstrophy,[60,61] spanwise vorticity,[62] streamwise velocity,[63,64] TKE,[65,66] standard deviation of the velocity[67] and velocity fluctuation,[68] and scalar concentration.[39,69] Recently, several machine learning tools have also been utilized to detect the TNTI and the TTI.[70–72] In high Schmidt number flows, momentum diffusivity, ν, is much greater than scalar diffusivity, $\mathscr{D}$, resulting in a sharp interface with a distinct concentration jump, also in a turbulent ambient (e.g. see Kankanwadi & Buxton[22] for axisymmetric wakes in a homogeneous turbulent ambient). Furthermore, the interface detected using moderate and high Schmidt passive scalars coincides with that of the enstrophy and spanwise vorticity, and, thus, reliably demarcates the turbulent flow and the ambient.[73] The threshold value of $\phi_t = 0.15\overline{\phi_c}$ was selected empirically from the range of $0.13\overline{\phi_c}$ to $0.17\overline{\phi_c}$, for which the TNTI and TTI have only small variations (see Appendix B). In a similar experimental flow, $\phi_t = 0.13\overline{\phi_c}$ was the threshold selected for the TNTI outline detection using a conditional pixel-averaged concentration method.[39]

In a quiescent ambient, the intermittency profile of the jet (a)(b)(c)

(d)(e)

(f)(g)(h)

(i)(j)

FIG. 15. Radial profiles of the intermittency. For Re = 10600 jet at (a) x/d = 20, (b) 30, (c) 40, (d) 50, and (e) 60. Similarly, for Re = 5800 jet at (f) to (j) for x/d = 20 to 60. Symbols: ○, quiescent ambient; □ centroidal, and ▽ Eulerian averaging in HIT ambient. The solid orange line in (d) shows the intermittency profile in Kohan & Gaskin,[39] calculated using the cumulative distribution of the TNTI radial position.

FIG. 16. Examples of instantaneous concentration field of the jet in the quiescent (top) and the HIT (bottom) ambient for x/d = 20 - 60, Re = 5800. Each concentration field is normalized by its ϕ_{max}, as seen in the colorbar. The red cross denotes the jet axis. In the turbulent ambient, the interface is longer and more tortuous due to the interaction of small-scale eddies of the ambient on the jet interface. Note the increasing presence of very low concentrations in the jet in the HIT ambient, more noticeable beyond the jet break-up at $x/d > 40$. At x/d = 60 the core has decayed significantly.

indicates a coherent core ($\gamma = 1$) with a width of $|r/x| <$ 0.1 and a sharply defined TNTI, whose position varies over $|r/x| = [0.1 - 0.2]$, as shown in Fig. 15 for jet Reynolds numbers of $Re = 10600$ and 5800. The quiescent profile at $x/d =$ 50 for $Re = 10600$ jet is in good agreement with a profile calculated using the cumulative distribution of the TNTI radial position.[5,39] In the turbulent ambient, before jet break-up, the extent of the jet core is very similar to that in the quiescent ambient (when the data are centroidal averages), although the edge of the core is less distinct (γ reduces gradually to 0.9 over $|r/x| \approx [0.08 - 0.13]$). After jet break-up ($x/d > 40$ for Re = 5800), the remains of the jet core region becomes less coherent, as γ decreases rapidly with downstream distance (γ_{max} = 0.9 at x/d = 50, γ_{max} = 0.6 at x/d = 60), indicating destruction of the jet structure as ambient fluid is often found in the core region. In the turbulent ambient, the jet interface (TTI) position relative to the centroid varies over a greater radial distance of $|r/x| \approx$[0.1 - 0.4] in the power-law region (i.e. the perturbed jet region before jet break-up at $x/d > 60$ for Re = 10600 and $x/d > 40$ for Re = 5800 jets). There is a low likelihood of interface excursions (increasing slightly with axial distance) between $|r/x| = [0.4 - 0.6]$ seen as the tails of the intermittency profiles. The greater range of possible radial distances of the jet/ambient interface indicates an interface that is modulated by the eddies of the ambient turbulence. The modulation results in a longer and more tortuous interface than in the quiescent ambient as seen in the flow visualization (Figs. 1 and 16). This increases the surface area of the interface over which nibbling can occur, however, as entrainment decreases in the turbulent ambient, we can reason that the local entrainment velocity is greatly reduced. Local entrainment velocity is the normal component of the relative velocity between the boundary propagation rate (E_b) and the local fluid velocity at the interface, and is often used to quantify the strength of the nibbling mechanism.[74–76] As jet break-up approaches, the radial position over which the interface is located increases slightly, before decreasing rapidly after jet break-up (at x/d = 40 for Re = 5800 the radial position of the interface has narrowed to $|r/x| = [0 - 0.2]$). The intermittency profiles obtained with an Eulerian average include the effect of the jet meandering, obscuring the evidence of the jet structure, shown by the intermittency values of less than one in the jet core region and by the triangular shaped profiles.

Further understanding of the jet dynamics in a HIT ambient is obtained from the analysis of the PDFs and corresponding CDFs of the jet centerline concentrations. In the quiescent ambient, the PDFs of the centerline concentration are almost Gaussian with the lowest concentration non-zero and decreasing with axial distance, as seen in Fig. 17 for the Re = 10600 and 5800 jets. By comparison, in the power-law region of the jet (x/d = 20 - 60 at Re = 10600 and x/d = 20 - 40 at Re = 5800), turbulence in the ambient results in a greater occurrence of lower concentrations as expected from the lower mean centerline concentrations (observed from the centroidal average). The PDFs become skewed towards the lower concentrations, with lower maximums and a minimum of zero. The maximum concentrations (defined by the 98^{th} percentile of the CDF) are reduced compared to the quiescent case by 10 - 25% and 25 - 35% for the Re = 10600 and Re = 5800 jets, respectively. The wider PDFs, in general, suggest a lower scalar mixing compared to the quiescent ambient (as argued in Nedic and Tavoularis[77]). The probability of concentrations below the threshold increases with downstream distance and are due to discontinuities in the jet due to its lateral advection by large eddies in the ambient leaving isolated islands of the scalar. After jet break-up ($x/d > 40$ for Re = 5800 jet), there are an increased number of lower concentrations and a sharply increasing occurrence of below threshold concentrations (12% at x/d = 50 and 40% at x/d = 60 for the centroidal average of the Re = 5800 jet). The PDFs and CDFs obtained from the Eulerian averaging again obscure the detail of the jet structure, but do indicate a greater frequency of lower concentrations, while the greatly increased likelihood of below threshold or zero concentrations is due to the inclusion of the effect of jet meandering on the analysis.

We hypothesize that greater local scalar concentration gra-

FIG. 17. PDF of centerline concentration. For *Re* = 10600 jet at (*a*) x/d = 20, (*b*) 30, (*c*) 40, (*d*) 50, and (*e*) 60. Similarly, for *Re* = 5800 jet at (*f*) to (*j*) for x/d = 20 to 60. Symbols: ○, quiescent ambient; □ centroidal, and ▽ Eulerian averaging in HIT ambient. The solid, dashed and dashed-dotted lines show the corresponding threshold values, ϕ_t/ϕ_0, in the quiescent ambient, and the Eulerian and centroidal averaging methods in HIT ambient, respectively. The insets depict the corresponding CDF values in the quiescent and in the HIT ambient.

dients occur within the boundary of the jet in the HIT ambient, as compared to the quiescent case, due to entrainment of the small-scale turbulence of the ambient (see Fig. 16 for instantaneous concentration fields). This is plausible due to the increased rms concentrations in the jet and the increased range of the centerline concentration seen in the PDFs. The presence of increased local scalar gradients is corroborated by the greater differential diffusion observed for a jet in a turbulent ambient as compared to a quiescent ambient[38] (jet *Re* = 10600 and same HIT). This hypothesis could be validated by directly calculating the local instantaneous concentration gradients within the jet boundary, however, lack of sufficient spatial resolution prevents us from capturing the Batchelor microscale ($\eta_B = \eta Sc^{-1/2}$), which in turn greatly underestimates the calculation of the scalar gradients.

The time-averaged net entrainment into the jet in a HIT ambient is decreased compared to the quiescent case due to the lower characteristic jet velocity driving the entrainment[10] and due to greater detrainment induced by the background turbulence.[22] The increased detrainment is due to the frequent and extreme outward flux of detached jet fluid into the ambient as a result of the advection of the jet by large-scale ambient eddies and due to increased turbulent diffusion at the jet/ambient interface, TTI. In the quiescent ambient, the detached scalar patches are re-entrained into the jet within an eddy turnover time,[78] while in the turbulent ambient, re-entrainment is much weaker and the detached patches diffuse into the ambient (as seen by visualization, Fig. 16). After the jet breaks up, it is no longer self-similar and its intermittency increases. The decreased width of the intermittency profile post break-up confirms that jet-driven entrainment is no longer occurring, and only turbulent and molecular diffusion is transporting the scalar. This is consistent with Hunt's hypothesis[9] that forcing of a jet disrupts the jet structure, and with previous experimental observations.[8,10–12]

D. Summary of the experimental observations

All the observations support a two-region model for the behavior of the jet in the HIT ambient, in which the regions are defined based on the ratio of the turbulence intensity between the ambient and the jet, ξ. In this study, for $\xi \leqslant 0.5$, the jet is perturbed by the HIT ambient, showing a faster decay of the centroidal mean concentration and a faster growth of the centroidal concentration half-width (both following power-laws) compared to the quiescent case. Despite the external forcing, the core of the jet is well preserved and the jet maintains its self-similarity and self-preservation in this region ($\xi \leqslant 0.5$). For $\xi > 0.5$, however, the decay of the mean concentration and the growth of the concentration half-width deviate from their power-law behaviors. The centroidally-averaged concentration half-width stops growing, which (according to the entrainment theory) indicates that the jet-driven entrainment into the jet has stopped. The "no entrainment" status implies that the mean centerline velocity $\overline{u}_c$ and hence the global entrainment velocity, $E_v = \alpha \overline{u}_c$, are zero. This means that no "jet" exists beyond $\xi > 0.5$, and that the jet structure has been destroyed by the ambient turbulence. The destroyed jet structure for $\xi > 0.5$ is reflected in the scalar profiles in Fig. 14*c* no longer being self-similar, in the decayed jet core in the centroidal intermittency profiles (Fig. 15*i, j*), and in the increasing presence of the ambient fluid at the jet centroid in the centroidal CDFs (Fig. 17*i, j*). All the above discussions support the proposal of the two-region model for the jet in the HIT ambient, a sketch of which is illustrated in Fig. 18.

In fact, the two-region model is a refinement of the discussions from previous observations for the jet in a HIT ambient, stating that the behavior of the jet (as well as the entrainment process and subsequent scalar mixing) is different before and after the jet break-up.[10–12] In the present study, the centroidally-averaged data allowed for the separation of the effect of the HIT ambient on the jet entrainment from the effect of the HIT causing the jet path to meander. Using this method, the structure of the jet is more apparent, and it is clearly visible that beyond $\xi = 0.5$ the jet has been destroyed by the ambient turbulence eddies and no longer exists. In Eulerian averages (of above studies), the evolution and structure of the jet are partially obscured due to the inclusion of the jet meandering.

VI. CONCLUSION

The effect of an approximately homogeneous and isotropic turbulence with a negligible mean flow on the evolution of the structure and the dynamics of an axisymmetric turbulent jet, with *Re* = 10600 and *Re* = 5800 was investigated by analyz-

FIG. 18. Schematic of the scalar field characteristics of a jet subjected to HIT ambient using the available data. The important properties of the two-region model is delineated with a centroidal averaging method. The jet axis and its centroid are shown with the dotted line and dashed line, respectively.

ing the passive scalar field. Planar laser-induced fluorescence was used to visualize the jet and the measured scalar statistics were compared to those of the jet issuing into a quiescent ambient. The scalar statistics were conditioned on the jet centroid to separate the effects of the larger and smaller scale ambient eddies on the jet dynamics, which were also compared to classical Eulerian statistics.

Turbulence in the ambient reduces jet entrainment and results in a rapid jet break-up. it This is due to disruption of the jet structure by external forcing as hypothesized by Hunt,[9] contrary to the long-held intuitive assumption that jet dilution and turbulent diffusion can be superimposed.

A two-region model for the jet evolution and structure, when released into the turbulent ambient, is proposed based on averages conditioned on the jet centroid (Fig. 18). In the first region, following the developing jet region, the ambient turbulence disrupts the jet structure, due to modulation of the jet interface, meandering of the jet by the large eddies and entrainment of the turbulent ambient fluid, resulting in a faster decay of the jet and decreased entrainment. In the second region, identified as where the relative turbulence intensity $\xi >$ 0.5, the ambient turbulence has destroyed the jet structure. Although scalar remains, as there is no momentum to drive the entrainment, the momentum-driven mechanism for scalar transport is replaced by turbulent/molecular diffusion by the ambient eddies. The relative lengths of the two regions depend primarily on the relative turbulence intensity, ξ, between the ambient and the jet, as assessed by the centroidal analysis, which removes the effect of the relative length scale ($\mathscr{L}$) on the jet behavior in the HIT ambient.

The first region (the perturbed jet region) is of particular interest as the jet structure is present, but its dynamics are modified by the ambient turbulence. The mean properties of the scalar remain self-similar and self-preserved when conditioned on the jet centroid (i.e. following the meandering jet path), but have greater concentration decay ($\overline{\phi_c}$) and half-width growth rate ($b_{\phi,1/2}$). The ambient turbulence increases the modulation of the jet/ambient interface. The entrainment of the ambient turbulence increases the rms concentrations and is hypothesized to increase local concentration gradients within the jet. The same power-law behavior in the perturbed jet region for the decay of the mean centroidal concentration, concentration rms, and width growth for both jet Reynolds numbers, indicates the universality of the evolution of the scalar statistics in HIT ambient, provided the jet structure is preserved. To further investigate the effect of the ambient turbulence on the scalar mixing in jets, a larger range of Reynolds numbers and ambient turbulence conditions (ξ and $\mathscr{L}$), as well as simultaneous velocity and scalar measurements are recommended.

ACKNOWLEDGMENTS

The authors acknowledge the assistance of Amirhossein Afrooz in conducting our experimental campaign. This study was supported by the Natural Sciences and Engineering Research Council (NSERC) of Canada Discovery Grant (RGPIN 2016-04473).

Appendix A: Effect of the threshold value on the position of the centroid

The mean location of the centroids exhibited by red circle markers in Fig. 3 are the ensemble average of the instantaneous centroids, calculated from the bulk of the flow without applying a threshold to the scalar fields. Regions characterized by intense values of passive scalar often control the position of the centroid, as evident from its definition in Eq. A1. However, large-scale meandering of the jet in the presence of HIT ambient often results in non-trivial values of passive scalar being pushed out of the FOV. Thus, in order to check the validity of the centroidal analysis presented throughout the manuscript, we investigate the relationship between the average location of the centroid and a wide range of scalar thresholds. The radial position, R_C, and orientation, θ_C, of the centroids calculated for regions where the local concentration is larger than the threshold value are expressed in Eq. A1 and Eq. A2, respectively,

$$R_C = \frac{\int (r\,\mathrm{d}\phi)\,|_{\phi>\phi_t}}{\int \mathrm{d}\phi|_{\phi>\phi_t}}, \tag{A1}$$

$$\theta_C = -\tan^{-1}\left(\frac{z_C}{y_C}\right), \tag{A2}$$

where y_C and z_C denote the coordinates of the instantaneous centroids calculated from thresholded scalar fields, i.e., $R_C^2 = y_C^2 + z_C^2$.

Figure 19 shows the ensemble averaged radial location, $\overline{R_C}$, and orientation, $\overline{\theta_C}$, of the centroids for the worst case scenario, that is, Re = 5800 jet at $x/d = 60$ against a range of thresholds. As can be seen, the orientation is quite insensitive to the threshold value. More importantly, one can observe only slight changes in the radial location of the centroid with increasing values of the scalar threshold. Specifically, by applying $\phi_t/\overline{\phi_c} = 0.15$, which is the threshold for detecting the jet region (Sec. V C), the radial position changes by 5% relative to the unthresholded value. Furthermore, thresholding the scalar fields results in centroids being closer to the jet axis, implying the existence of intense concentration values near the geometrical centerline even in the presence of extreme meandering. Overall, we deduce that the position of the centroids are well-defined.

FIG. 19. Variation of $\overline{R_C}$ and $\overline{\theta_C}$ versus $\phi_t/\overline{\phi_c}$ normalized by their respective un-thresholded values. Data for Re = 5800 at x/d = 60. Symbols: $\bullet$, $\overline{R_C}$; $\blacktriangledown$, $\overline{\theta_C}$.

FIG. 20. Variation of intermittency profiles versus ϕ_t. Data for Re = 5800 at x/d = 60. Symbols: $\square$, $\phi_t/\overline{\phi_c}$ = 0.13; $\triangle$, $\phi_t/\overline{\phi_c}$ = 0.15; $\circ$, $\phi_t/\overline{\phi_c}$ = 0.17. Black, blue, and red marker colors correspond to quiescent, centroidal turbulent, and Eulerian turbulent backgrounds, respectively.

Appendix B: Effect of threshold value on the intermittency profiles

The location of the outer boundary demarcating the high-Sc flows and the ambient shows small sensitivity to the chosen threshold due to the weak diffusive nature of the passive scalar (e.g. see Westerweel *et al.*[69]). However, this may not be the case in turbulent backgrounds due to the presence of appreciable amounts of passive scalar (close to the threshold concentration value) in the ambient. Here, we investigate the effect of varying the scalar threshold on the intermittency profiles presented in Fig. 15. To this end, we employ thresholds in the range of $\phi_t/\overline{\phi_c} = 0.15 \pm 13\%$ and recalculate the intermittency profiles in the quiescent and the turbulent background cases. Figure 20 shows the intermittency profiles for the worst case scenario, i.e., x/d = 60 at Re = 5800 jet. Indeed, there are only slight changes in the detected jet regions for different values of the scalar threshold, as made evident by the approximate collapse of the intermittency profiles. Therefore, we conclude the robustness of the present criterion for detecting the jet interface even when the jet is subjected to HIT ambient, independent of the averaging method, that is, Eulerian or centroidal.

DATA AVAILABILITY

The data that supports the findings of this study are available from the corresponding author upon reasonable request.

[1] B. R. Morton, G. I. Taylor, and J. Turner, "Turbulent gravitational convection from maintained and instantaneous sources," Proc. R. Soc. Lond. A **234**, 1–23 (1956).
[2] M. van Reeuwijk and J. Craske, "Energy-consistent entrainment relations for jets and plumes," J. Fluid Mech. **782**, 333–355 (2015).
[3] A. A. Townsend, "The mechanism of entrainment in free turbulent flows," J. Fluid Mech. **26**, 689–715 (1966).
[4] W. A. Dahm and P. E. Dimotakis, "Measurements of entrainment and mixing in turbulent jets," AIAA J. **25**, 1216–1223 (1987).
[5] S. Corrsin and A. L. Kistler, "Free-stream boundaries of turbulent flows," NACA Tech. Rep. **1244**, 1033 (1955).
[6] J. Mathew and A. Basu, "Some characteristics of entrainment at a cylindrical turbulence boundary," Phys. Fluids **14**, 2065–2072 (2002).
[7] C. B. da Silva, J. C. R. Hunt, I. Eames, and J. Westerweel, "Interfacial layers between regions of different turbulence intensity," Annu. Rev. Fluid Mech. **46**, 567–590 (2014).
[8] S. Gaskin, M. McKernan, and F. Xue, "The effect of background turbulence on jet entrainment: an experimental study of a plane jet in a shallow coflow," J. Hydraulic Res. **42**, 533–542 (2004).
[9] J. C. R. Hunt, "Atmospheric jets and plumes," In Recent Research Advances in the Fluid Mechanics of Turbulent Jets and Plumes **255**, 309–334 (1994).
[10] B. Khorsandi, S. Gaskin, and L. Mydlarski, "Effect of background turbulence on an axisymmetric turbulent jet," J. Fluid Mech. **736**, 250–286 (2013).
[11] A. Perez-Alvarado, *Effect of background turbulence on the scalar field of a turbulent jet*, PhD dissertation, McGill University, Department of Mechanical Engineering (2016).
[12] A. C. Lai, A. W. K. Law, and E. E. Adams, "A second-order integral model for buoyant jets with background homogeneous and isotropic turbulence," J. Fluid Mech. **871**, 271–304 (2019).
[13] C. Y. Ching, H. J. S. Fernando, and A. Robles, "Breakdown of line plumes in turbulent environments," J. Geophys. Res.: Oceans **100**, 4707–4713 (1995).
[14] Y. Guo, D. Malcangio, P. A. Davies, and H. J. Fernando, "A laboratory investigation into the influence of a localized region of turbulence on the evolution of a round turbulent jet," Fluid Dyn. Res. **36**, 78–89 (2005).
[15] A. J. Cuthbertson, D. Malcangio, P. A. Davies, and M. Mossa, "The influence of a localised region of turbulence on the structural development of a turbulent, round, buoyant jet," Fluid Dyn. Res. **38**, 683–698 (2006).
[16] H. Wang and A. W. Law, "Second-order integral model for a round turbulent buoyant jet," J. Fluid Mech. **459**, 397–428 (2002).
[17] D. Legendre, A. Merle, and J. Magnaudet, "Wake of a spherical bubble or a solid sphere set fixed in a turbulent environment," Phys. Fluids **18**, 048102 (2006).
[18] Z. Amoura, V. Roig, F. Risso, and A. M. Billet, "Attenuation of the wake of a sphere in an intense incident turbulence with large length scales," Phys. Fluids **22**, 055105 (2010).
[19] I. Eames, C. Jonsson, and P. B. Johnson, "The growth of a cylinder wake in turbulent flow," J. Turbulence **12**, N39 (2011).
[20] P. E. Hancock and P. Bradshaw, "Turbulence structure of a boundary layer beneath a turbulent free stream," J. Fluid Mech. **205**, 45–76 (1989).
[21] A. Pal and S. Sarkar, "Effect of external turbulence on the evolution of a wake in stratified and unstratified environments," J. Fluid Mech. **772**, 361–385 (2015).
[22] K. S. Kankanwadi and O. R. Buxton, "Turbulent entrainment into a cylinder wake from a turbulent background," J. Fluid Mech. **905**, A35 (2020).
[23] J. Philip and I. Marusic, "Large-scale eddies and their role in entrainment in turbulent jets and wakes," Phys. Fluids **24**, 055108 (2012).
[24] S. Gaskin, A. Perez-Alvarado, and L. Mydlarski, "Impact of relative turbulence scales on the effect of background turbulence on jet flows," 4th International Symposium of Shallow Flows (2017).
[25] S. J. Wright, "The effect of ambient turbulence on jet mixing," In Recent Research Advances in the Fluid Mechanics of Turbulent Jets and Plumes **255**, 13–27 (1994).
[26] M. Moeini, B. Khorsandi, and L. Mydlarski, "Effect of coflow turbulence on the dynamics and mixing of a non-buoyant turbulent jet," J. Hydraulic Eng. **147**, 04020088 (2020).
[27] I. P. D. De Silva and H. J. S. Fernando, "Oscillating grids as a source of nearly isotropic turbulence," Phys. Fluids **6**, 2455–2464 (1994).
[28] L. Mydlarski and Z. Warhaft, "On the onset of high-reynolds-number grid-generated wind tunnel turbulence," J. Fluid Mech. **320**, 331–368 (1996).
[29] P. Lavoie, L. Djenidi, and R. Antonia, "Effects of initial conditions in decaying turbulence generated by passive grids," J. Fluid Mech. **585**, 395–420 (2007).
[30] D. Webster and A. Brathwaite, "A novel laboratory apparatus for simulating isotropic oceanic turbulence at low Reynolds number," Limnology and Oceanography: Methods **2**, 1–12 (2004).
[31] E. A. Variano and E. A. Cowen, "A random-jet-stirred turbulence tank," J. Fluid Mech. **604**, 1–32 (2004).
[32] E. A. Variano, E. Bodenschatz, and E. A. Cowen, "A random synthetic jet array driven turbulence tank," Exp. Fluids **37**, 613–615 (2008).
[33] D. Carter, A. Petersen, O. Amili, and F. Coletti, "Generating and controlling homogeneous air turbulence using random jet arrays," Exp. Fluids **57**, 1–15 (2016).
[34] A. Perez-Alvarado, L. Mydlarski, and S. Gaskin, "Effect of the driving algorithm on the turbulence generated by a random jet array," Exp. Fluids **57**, 20 (2016).
[35] H. J. S. Fernando and I. P. D. De Silva, "Note on secondary flows in oscillating-grid, mixing-box experiments," Phys. Fluids **5**, 1849–1851

(1993).
[36]T. M. Lavertu, L. Mydlarski, and S. Gaskin, "Differential diffusion of high-schmidt-number passive scalars in a turbulent jet," J. Fluid Mech. **612**, 439–475 (2008).
[37]P. E. Dimotakis, "The mixing transition in turbulent flows," J. Fluid Mech. **409**, 69–98 (2000).
[38]T. M. Lavertu, *Differential diffusion in a turbulent jet*, PhD dissertation, McGill University, Department of Mechanical Engineering (2006).
[39]K. F. Kohan and S. Gaskin, "The effect of the geometric features of the turbulent/non-turbulent interface on the entrainment of a passive scalar into a jet," Phys. Fluids **32**, 095114 (2020).
[40]M. van Reeuwijk and M. Holzner, "The turbulence boundary of a temporal jet," J. Fluid Mech. **739**, 254–275 (2014).
[41]C. A. Friehe, C. W. van Atta, and C. H. Gibson, "Jet turbulence: dissipation rate measurements and correlations," NATO Advisory Group for Aerospace Research and Development (1971).
[42]G. G. Guilbault, *Practical Fluorescence: Theory, Methods, and Techniques* (Marcel Dekker, 1973).
[43]H. C. Burridge, D. A. Parker, E. Kruger, J. Partridge, and P. Linden, "Conditional sampling of a high péclet number turbulent plume and the implications for entrainment," J. Fluid Mech. **823**, 26–56 (2017).
[44]D. A. Parker, H. C. Burridge, J. Partridge, and P. Linden, "A comparison of entrainment in turbulent line plumes adjacent to and distant from a vertical wall," J. Fluid Mech. **882**, A4 (2019).
[45]H. B. Fischer, J. E. List, C. R. Koh, J. Imberger, and N. H. Brooks, *Mixing in Inland and Coastal Waters* (Academic press, 1979).
[46]H. J. Hussein, S. P. Capp, and W. K. George, "Velocity measurements in a high-reynolds-number, momentum-conserving, axisymmetric, turbulent jet," J. Fluid Mech. **258**, 31–75 (1994).
[47]H. A. Becker, H. C. Hottel, and G. C. Williams, "The nozzle fluid concentration field of the round turbulent jet," J. Fluid Mech. **30**, 285–303 (1967).
[48]D. R. Dowling and P. E. Dimotakis, "Similarity of the concentration field of gas-phase turbulent jets," J. Fluid Mech. **218**, 109–141 (1990).
[49]A. W. K. Law and H. Wang, "Measurement of mixing processes with combined digital particle image velocimetry and planar laser induced fluorescence," Exp. Thermal and Fluid Sci. **22**, 213–229 (2000).
[50]D. R. Webster, P. J. Roberts, and L. Ra'ad, "Simultaneous DPTV-PLIF measurements of a turbulent jet," Exp. in Fluids **30**, 65–72 (2001).
[51]E. A. Cowen, K. A. Chang, and Q. Liao, "A single-camera coupled PTV-LIF technique," Exp. Thermal and Fluid Sci. **22**, 213–229 (2000).
[52]C. Fukushima, L. Aanen, and J. Westerweel, "Investigation of the mixing process in an axisymmetric turbulent jet using PIV and LIF," In laser techniques for fluid mechanics , 339–356 (2002).
[53]C. L. Lubbers, G. Brethouwer, and B. J. Boersma, "Simulation of the mixing of a passive scalar in a round turbulent jet," Fluid Dyn. Res. **28**, 189 (2002).
[54]S. B. Pope, *Turbulent Flows* (Cambridge University Press, 2000).
[55]J. Mi, D. Nobes, and G. Nathan, "Influence of jet exit conditions on the passive scalar field of an axisymmetric free jet," J. Fluid Mech. **432**, 91–125 (2001).
[56]P. Bagchi and S. Balachandar, "Response of the wake of an isolated particle to an isotropic turbulent flow," J. Fluid Mech. **518**, 95 (2004).
[57]G. S. Bhat and R. Narasimha, "A volumetrically heated jet: large-eddy structure and entrainment characteristics," J. Fluid Mech. **325**, 303–330 (1996).
[58]A. Agrawal and A. K. Prasad, "Evolution of a turbulent jet subjected to volumetric heating," J. Fluid Mech. **511**, 95–123 (2004).
[59]J. C. LaRue and P. A. Libby, "Temperature fluctuations in the plane turbulent wake," Phys. Fluids **17**, 1956–1967 (1974).
[60]D. K. Bisset, J. C. R. Hunt, and M. M. Rogers, "The turbulent/non-turbulent interface bounding a far wake," J. Fluid Mech. **451**, 383–410 (2002).
[61]M. Wolf, B. Luthi, M. Holzner, D. Krug, W. Kinzelbach, and A. Tsinober, "Investigations on the local entrainment velocity in a turbulent jet," Phys. Fluids **24**, 105110 (2012).
[62]G. Balamurugan, A. Rodda, J. Philip, and A. C. Mandal, "Characteristics of the turbulent/non-turbulent interface in a spatially evolving turbulent mixing layer," J. Fluid Mech. **894**, A4 (2020).
[63]M. Khashehchi, A. Ooi, J. Soria, and I. Marusic, "Evolution of the turbulent/non-turbulent interface of an axisymmetric turbulent jet," Exp. Fluids **54**, 1449 (2013).
[64]M. van Reeuwijk, J. C. Vassilicos, and J. Craske, "Unified description of turbulent entrainment," J. Fluid Mech. **908**, A12 (2020).
[65]K. Chauhan, J. Philip, and I. Marusic, "Scaling of the turbulent/non-turbulent interface in boundary layers," J. Fluid Mech. **751**, 298–328 (2014).
[66]K. U. Kim, G. S. Elliot, and J. C. Dutton, "Compressibility effects on large structures and entrainment length scales in mixing layers," AIAA Journal **58**, 12 (2020).
[67]N. Reuther and C. J. Kahler, "Evaluation of large-scale turbulent/non-turbulent interface detection methods for wall-bounded flows," Exp. Fluids **59**, 121 (2018).
[68]Y. Long, D. Wu, and J. Wang, "A novel and robust method for the turbulent/non-turbulent interface detection," Exp. Fluids **62**, 138 (2021).
[69]J. Westerweel, C. Fukushima, J. M. Pedersen, and J. C. R. Hunt, "Momentum and scalar transport at the turbulent/non-turbulent interface of a jet," J. Fluid Mech. **631**, 199 (2009).
[70]Z. Wu, J. Lee, C. Meneveau, and T. Zaki, "Application of a self-organizing map to identify the turbulent-boundary-layer interface in a transitional flow," Phys. Rev. Fluids **4**, 023902 (2019).
[71]B. Li, Z. Yang, X. Zhang, G. He, B. Deng, and L. Shen, "Using machine learning to detect the turbulent region in flow past a circular cylinder," J. Fluid Mech. **905**, A10 (2020).
[72]K. Younes, B. Gibeau, S. Ghasemi, and J. Hickey, "A fuzzy cluster method for turbulent/non-turbulent interface detection," Exp. Fluids **62**, 73 (2021).
[73]T. Watanabe, X. Zhang, and K. Nagata, "Turbulent/non-turbulent interfaces detected in dns of incompressible turbulent boundary layers," Phys. Fluids **30**, 035102 (2018).
[74]M. Holzner and B. Lüthi, "Laminar superlayer at the turbulence boundary." Phys. Rev. Lett. **106**, 134503 (2011).
[75]D. Mistry, J. Philip, J. R. Dawson, and I. Marusic, "Entrainment at multi-scales across the turbulent/non-turbulent interface in an axisymmetric jet," J. Fluid Mech. **802**, 690–725 (2016).
[76]R. Jahanbakhshi, "Mechanisms of entrainment in a turbulent boundary layer," Phys. Fluids **33**, 035105 (2021).
[77]J. Nedić and S. Tavoularis, "Measurements of passive scalar diffusion downstream of regular and fractal grids." J. Fluid Mech. **800**, 358–386 (2016).
[78]A. K. M. F. Hussain and A. R. Clark, "On the coherent structure of the axisymmetric mixing layer: a flow-visualization study," J. Fluid Mech. **104**, 263–294 (1981).

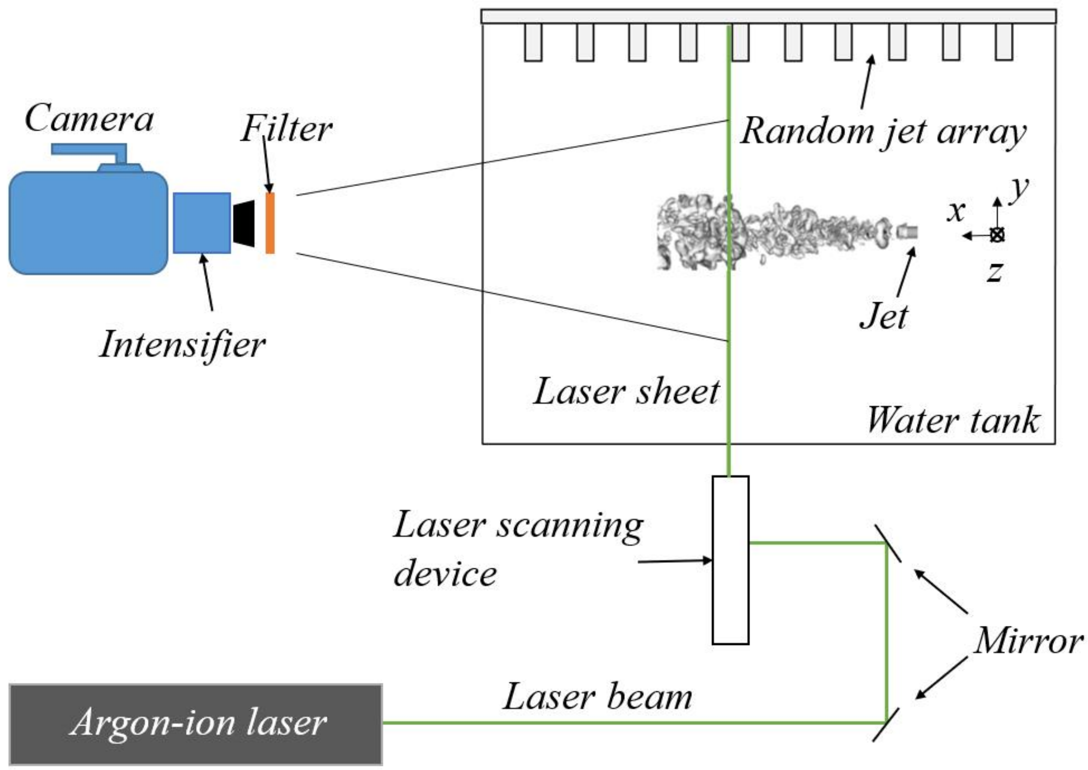
Camera
Filter
Random jet array
Intensifier
Jet
x
y
z
Laser sheet
Water tank
Laser scanning device
Mirror
Laser beam
Argon-ion laser

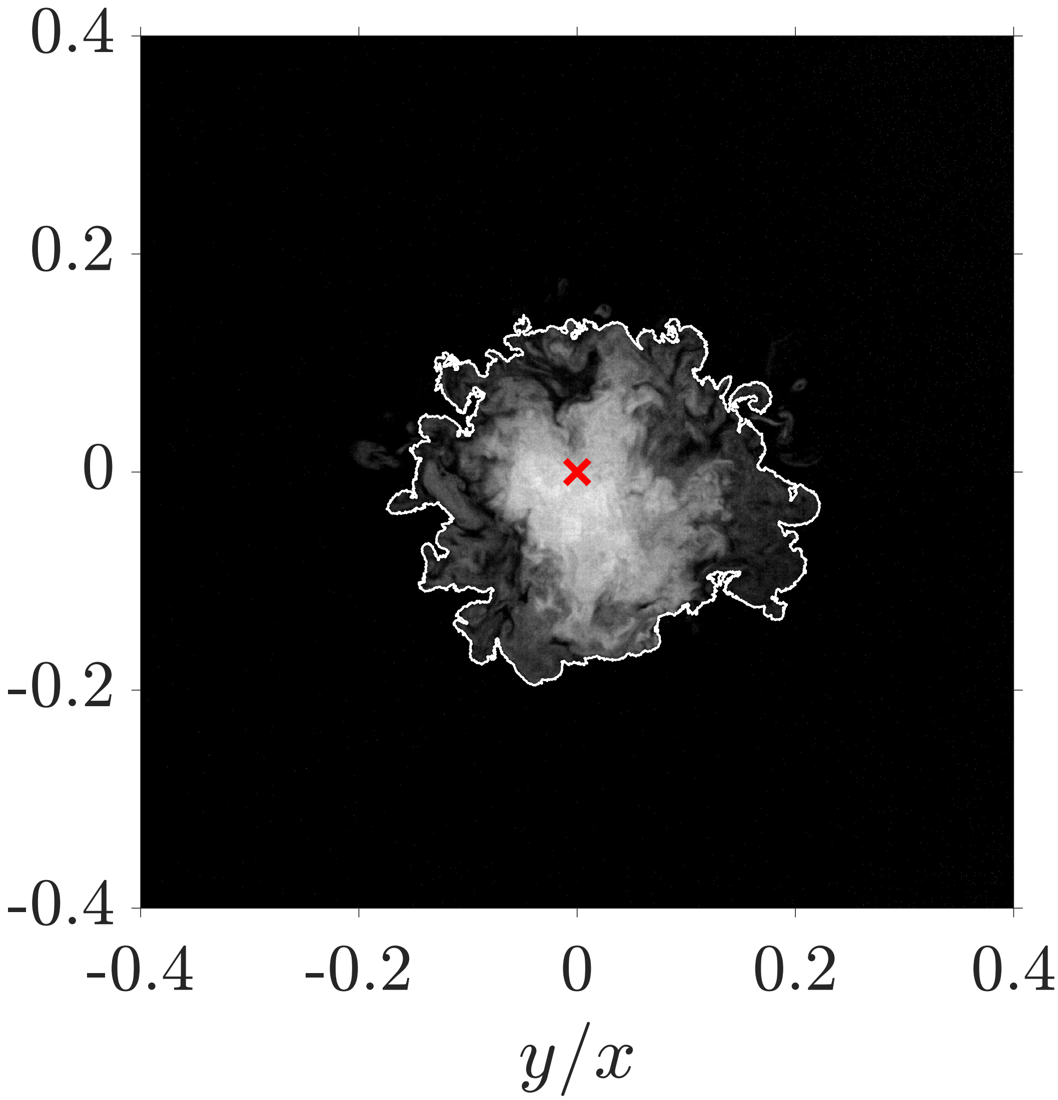
0.4
0.2
0
-0.2
-0.4
z/x
-0.4
-0.2
0
0.2
0.4
y/x

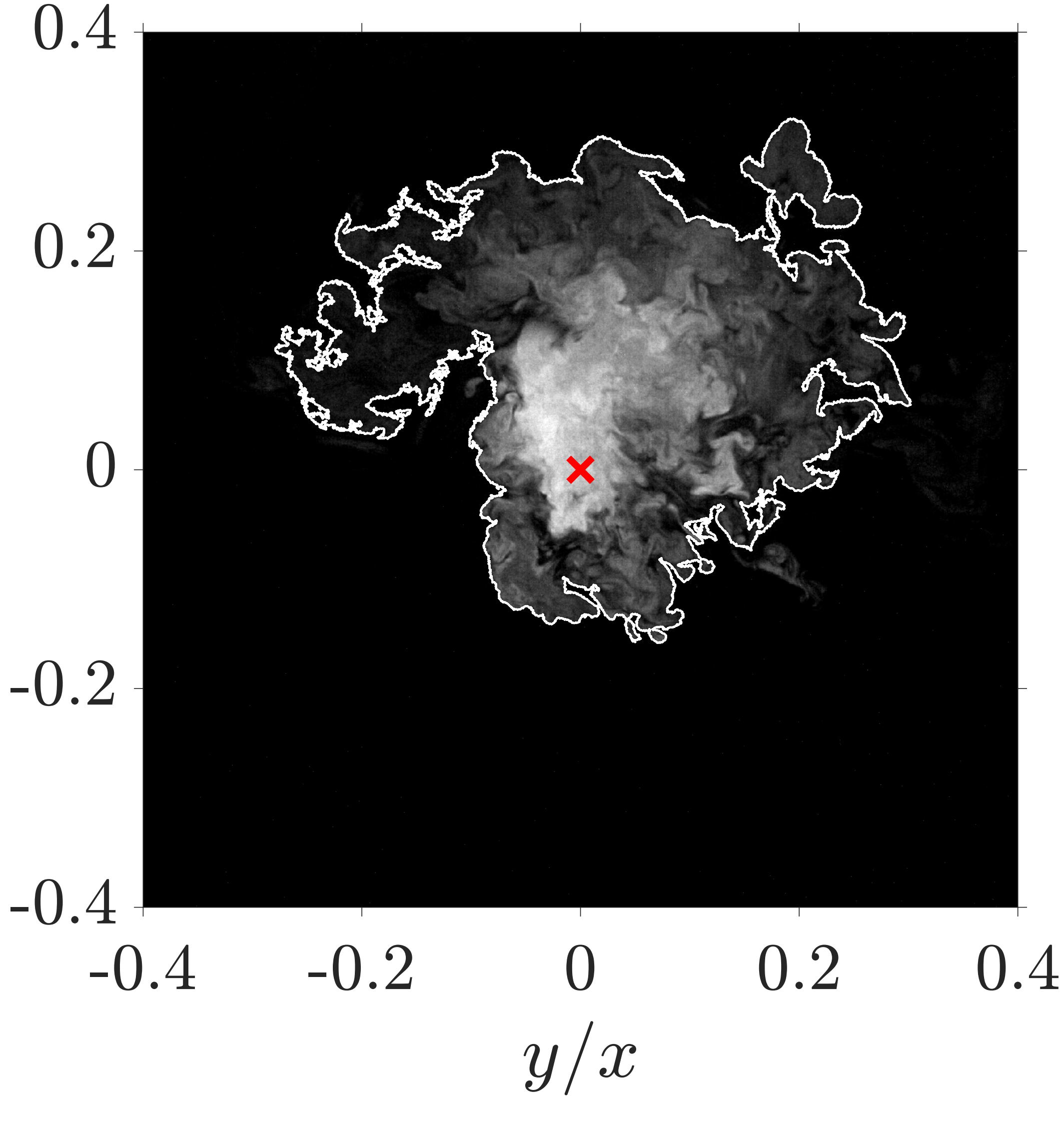
0.4
0.2
0
-0.2
-0.4
-0.4
-0.2
0
0.2
0.4
y/x

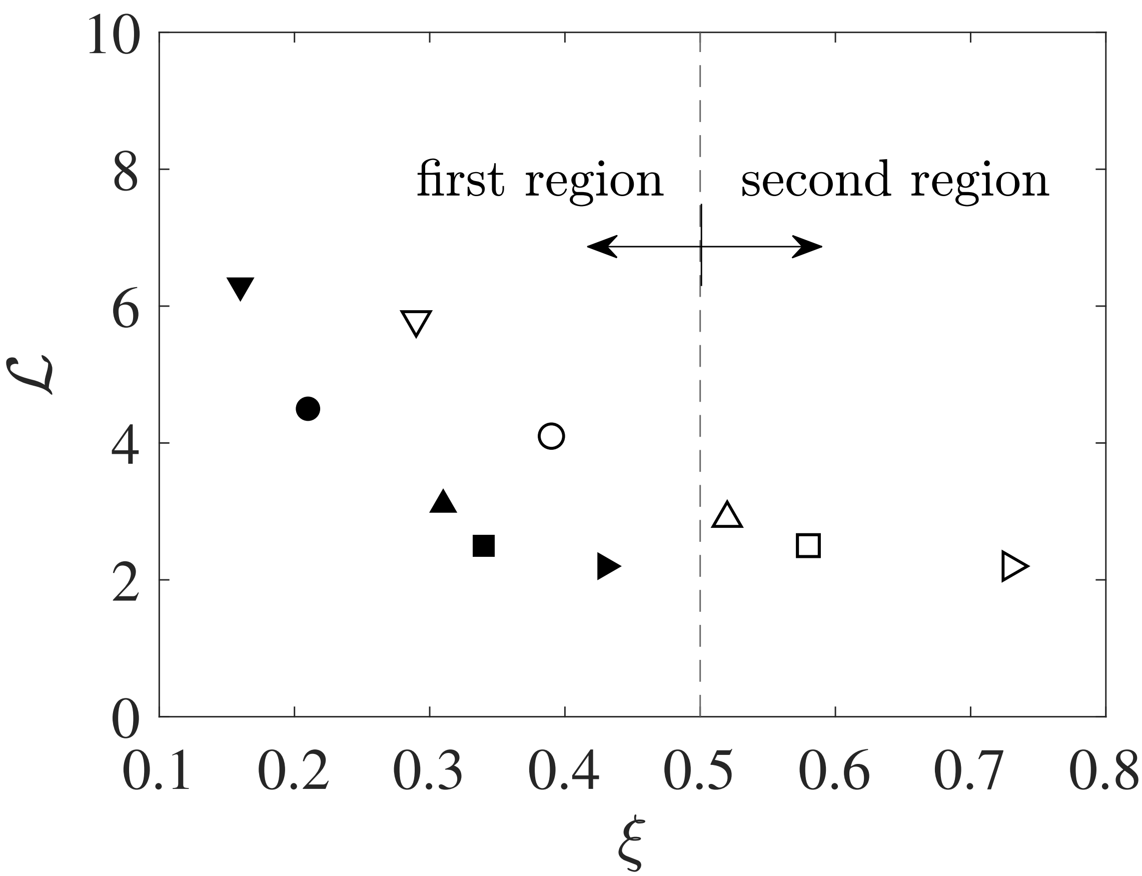
first region
second region
$\mathcal{L}$
ξ
0
2
4
6
8
10
0.1
0.2
0.3
0.4
0.5
0.6
0.7
0.8

PLEASE CITE THIS ARTICLE AS DOI: 10.1063/5.0071023

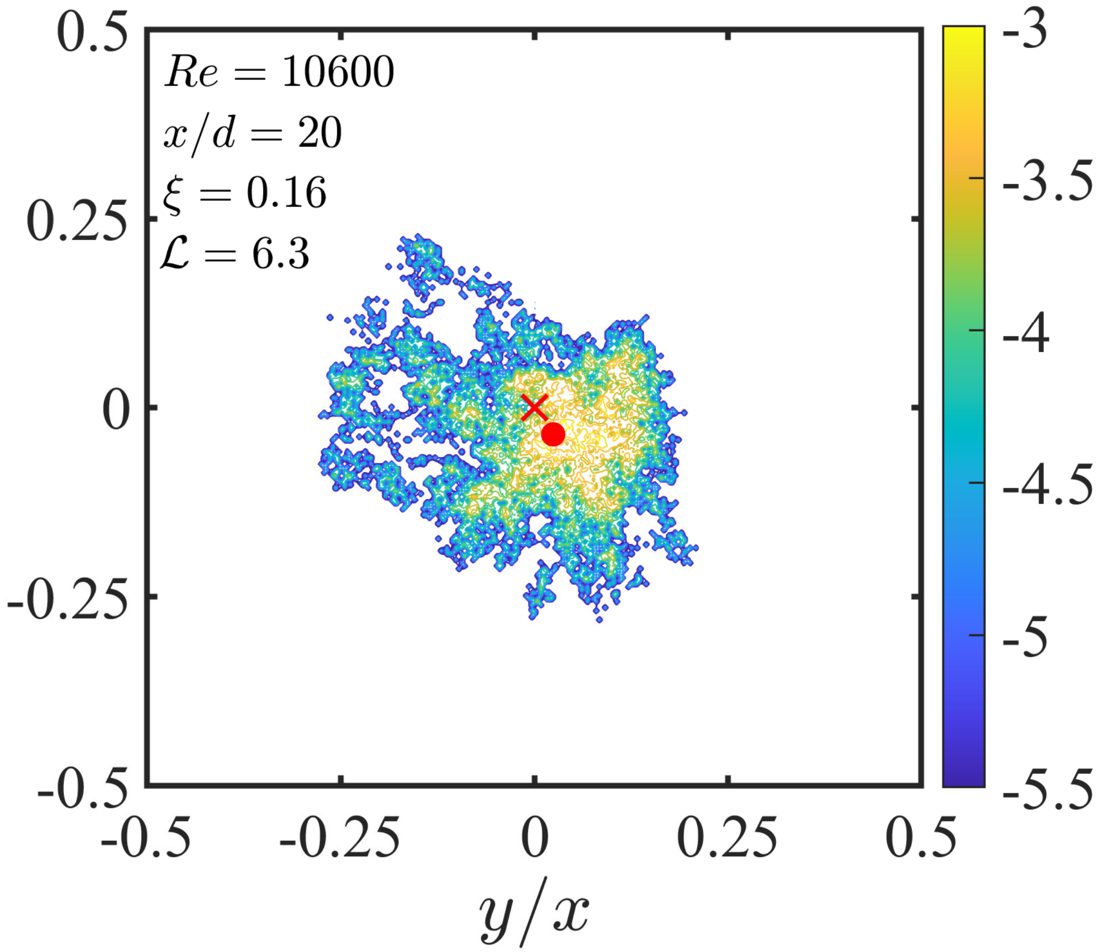

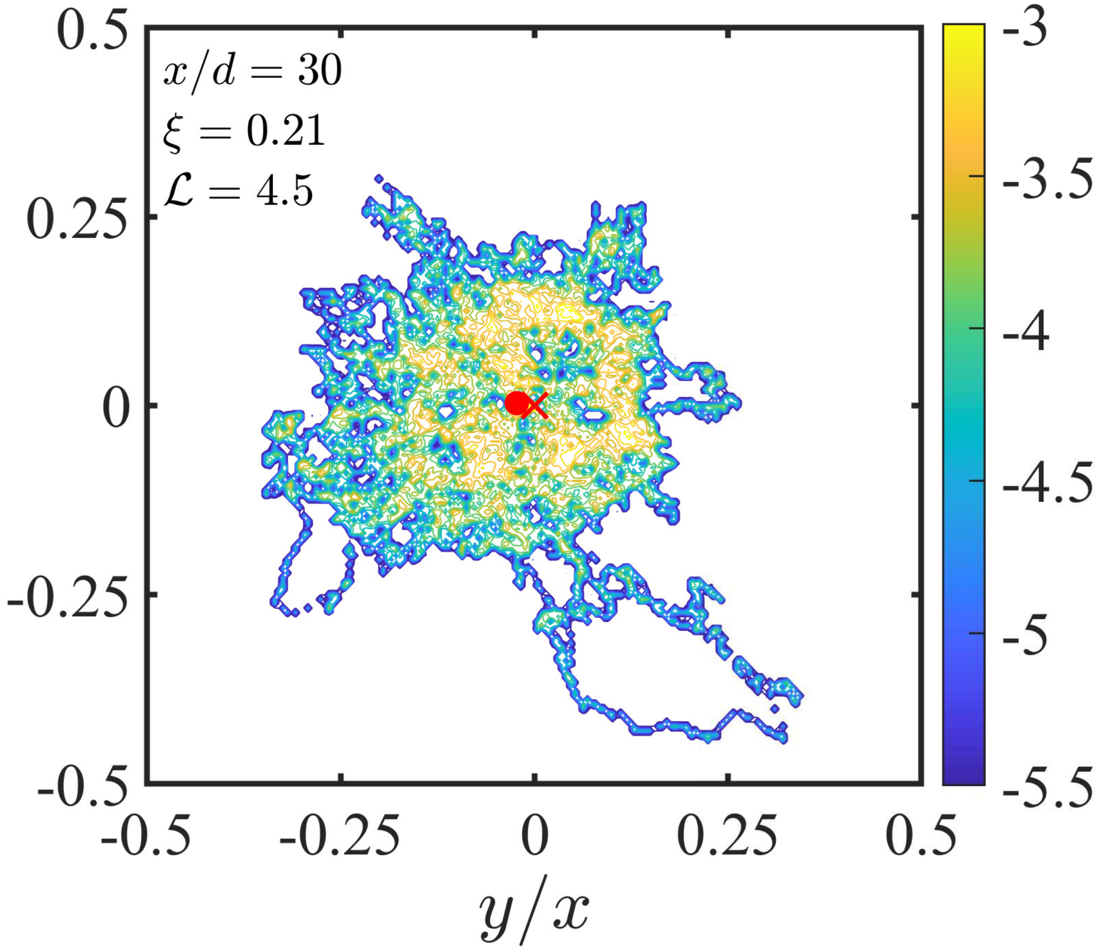
$x/d = 30$
$\xi = 0.21$
$\mathcal{L} = 4.5$
0.5
0.25
0
-0.25
-0.5
-0.5
-0.25
0
0.25
0.5
y/x
-3
-3.5
-4
-4.5
-5
-5.5

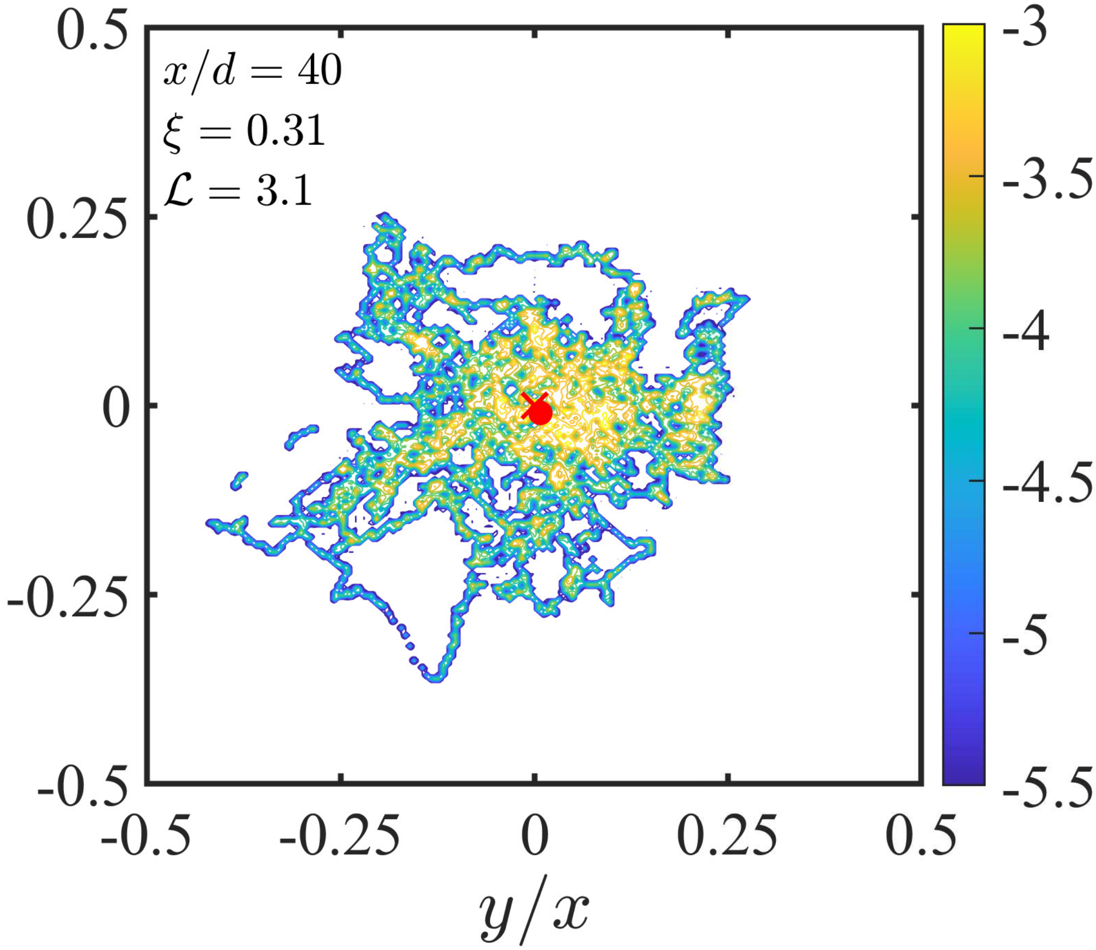
$x/d = 40$
$\xi = 0.31$
$\mathcal{L} = 3.1$
0.5
0.25
0
-0.25
-0.5
-0.5
-0.25
0
0.25
0.5
y/x
-3
-3.5
-4
-4.5
-5
-5.5

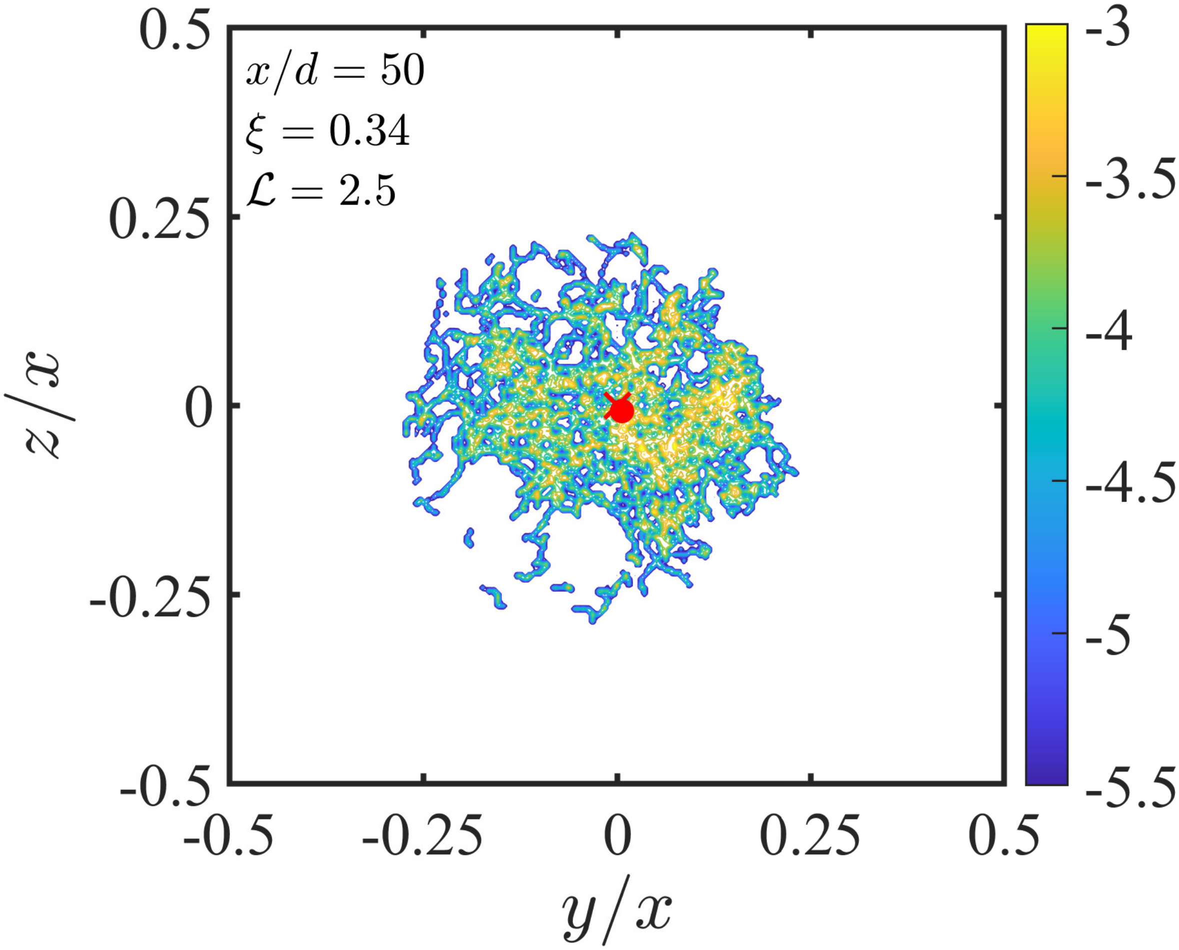
$x/d = 50$
$\xi = 0.34$
$\mathcal{L} = 2.5$
0.5
0.25
0
-0.25
-0.5
z/x
-0.5
-0.25
0
0.25
0.5
y/x
-3
-3.5
-4
-4.5
-5
-5.5

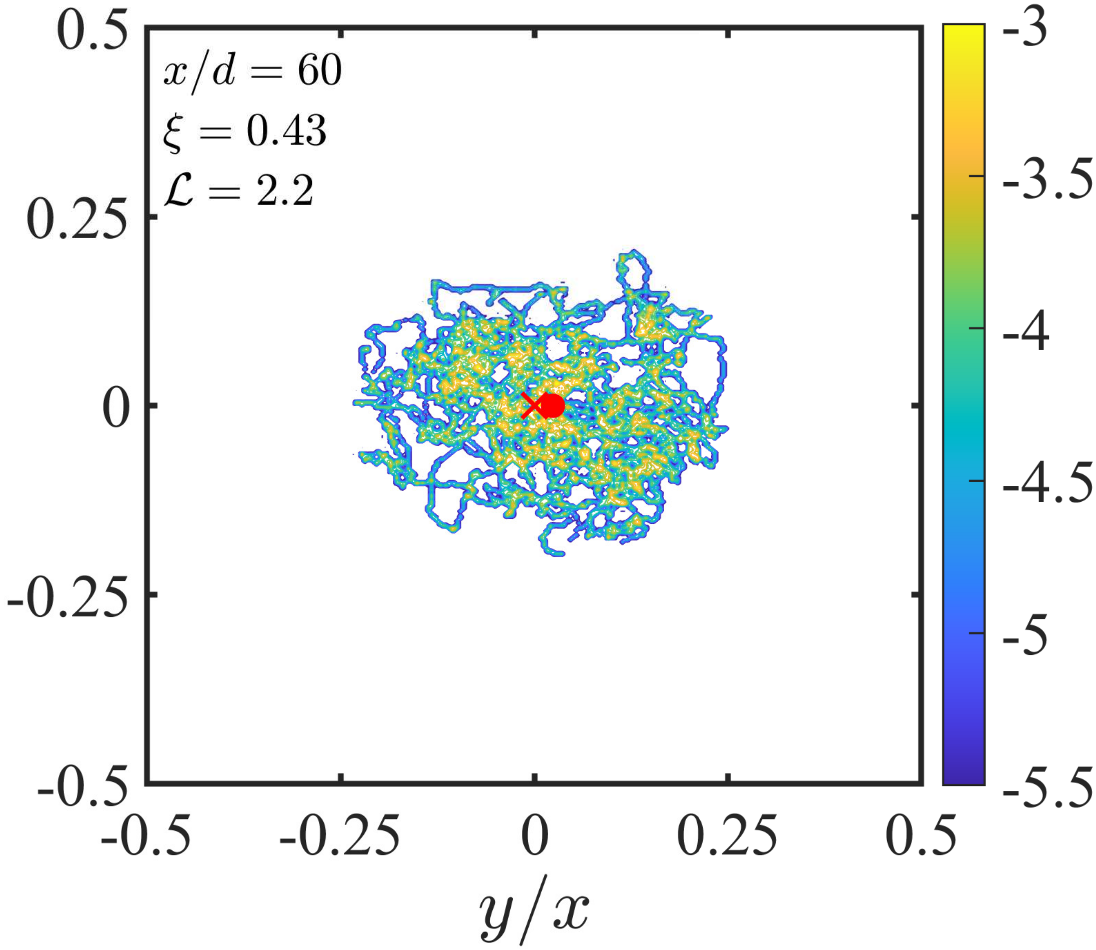
$x/d = 60$
$\xi = 0.43$
$\mathcal{L} = 2.2$
0.5
0.25
0
-0.25
-0.5
-0.5
-0.25
0
0.25
0.5
y/x
-3
-3.5
-4
-4.5
-5
-5.5

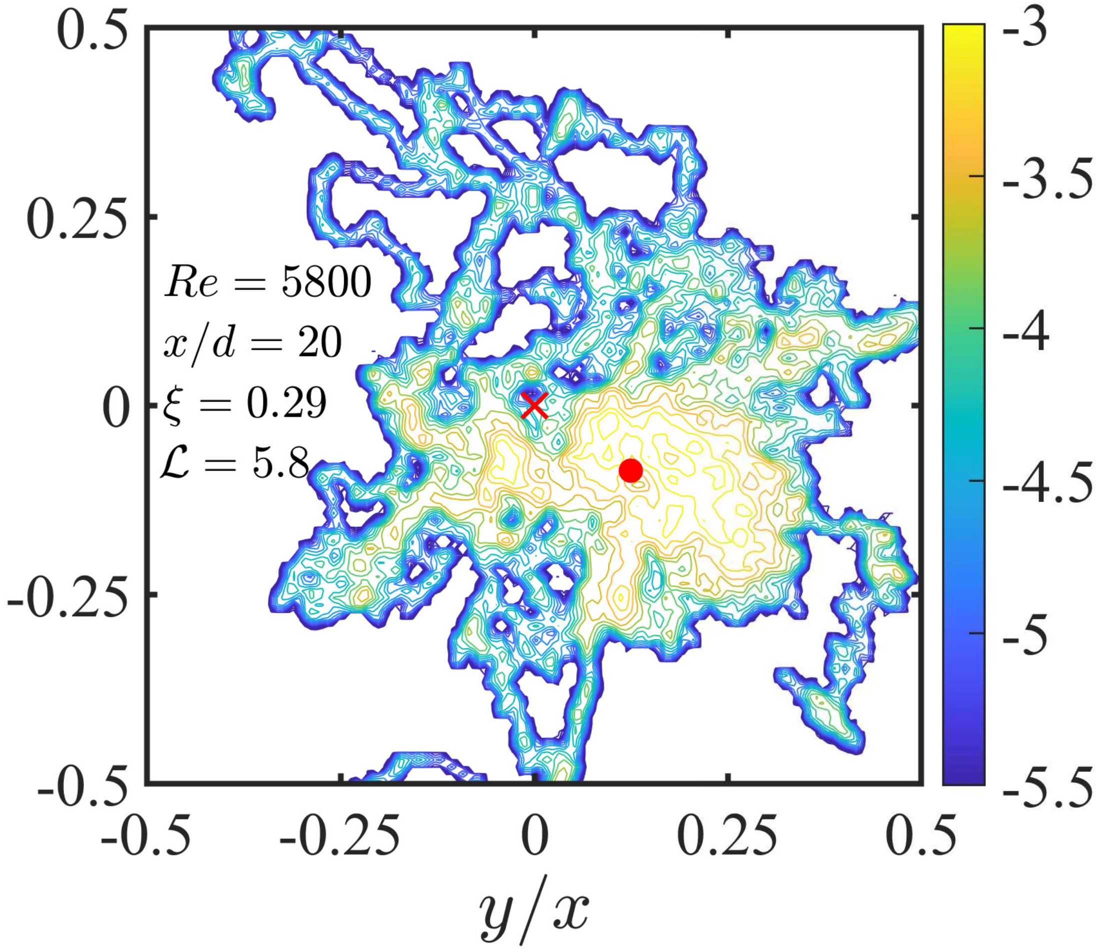
0.5
0.25
0
-0.25
-0.5
z/x
$Re = 5800$
$x/d = 20$
$\xi = 0.29$
$\mathcal{L} = 5.8$
-0.5
-0.25
0
0.25
0.5
y/x
-3
-3.5
-4
-4.5
-5
-5.5

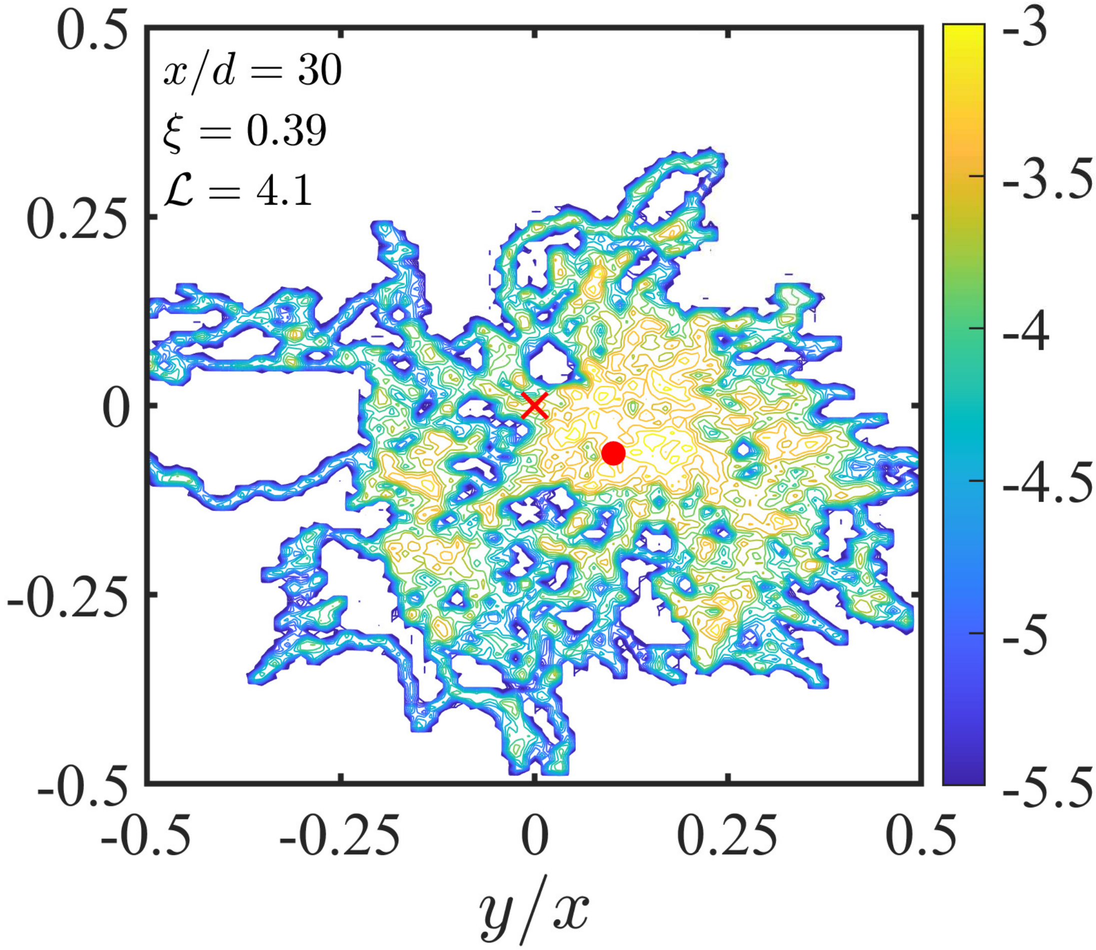
$x/d = 30$
$\xi = 0.39$
$\mathcal{L} = 4.1$
0.5
0.25
0
-0.25
-0.5
-0.5
-0.25
0
0.25
0.5
y/x
-3
-3.5
-4
-4.5
-5
-5.5

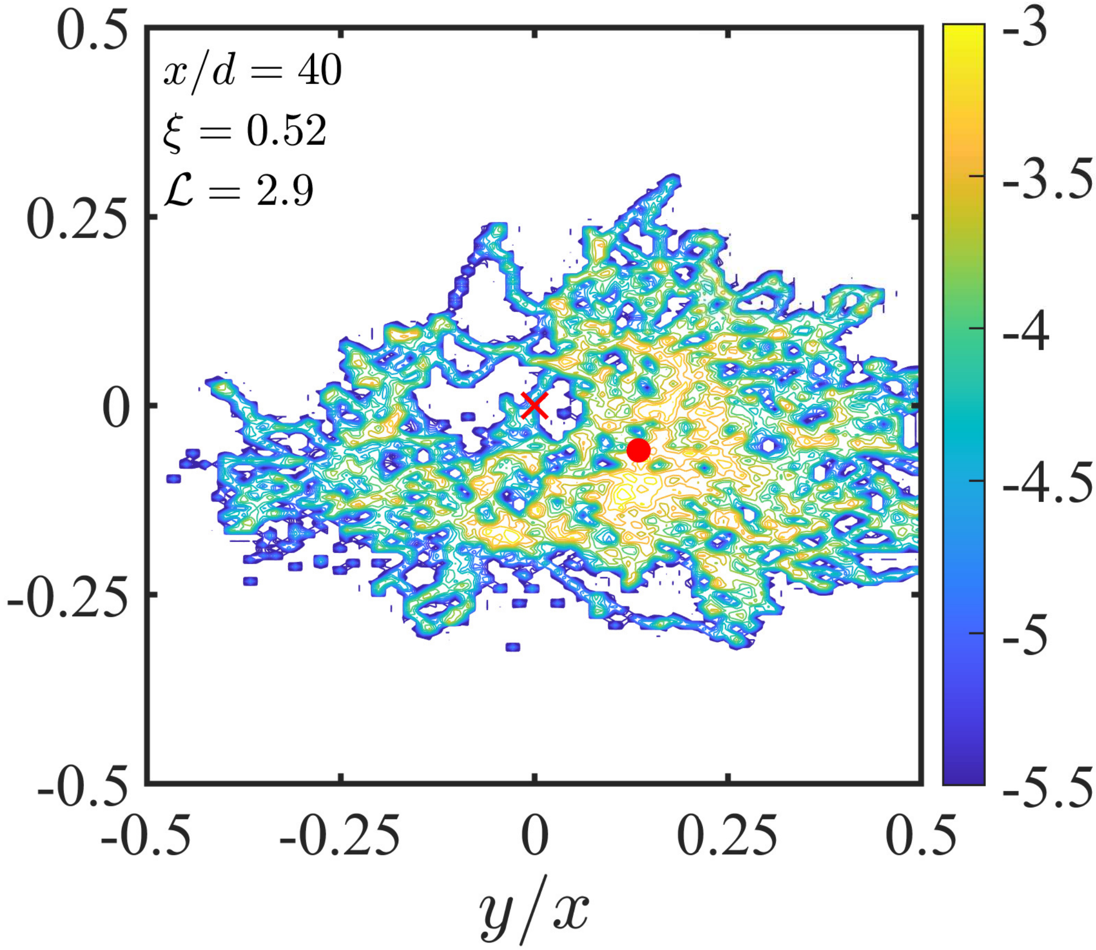
$x/d = 40$
$\xi = 0.52$
$\mathcal{L} = 2.9$
0.5
0.25
0
-0.25
-0.5
-0.5
-0.25
0
0.25
0.5
y/x
-3
-3.5
-4
-4.5
-5
-5.5

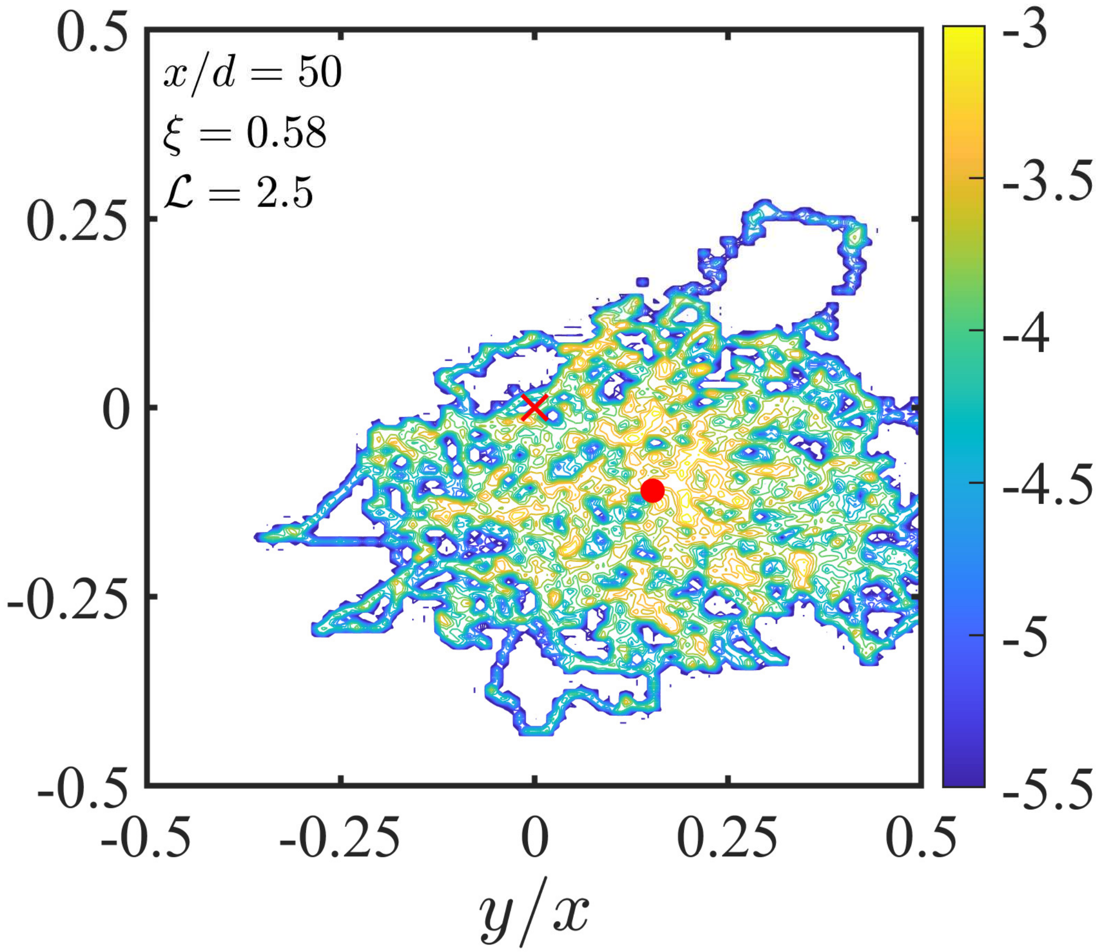
$x/d = 50$
$\xi = 0.58$
$\mathcal{L} = 2.5$
z/x
y/x
0.5
0.25
0
-0.25
-0.5
-0.5
-0.25
0
0.25
0.5
-3
-3.5
-4
-4.5
-5
-5.5

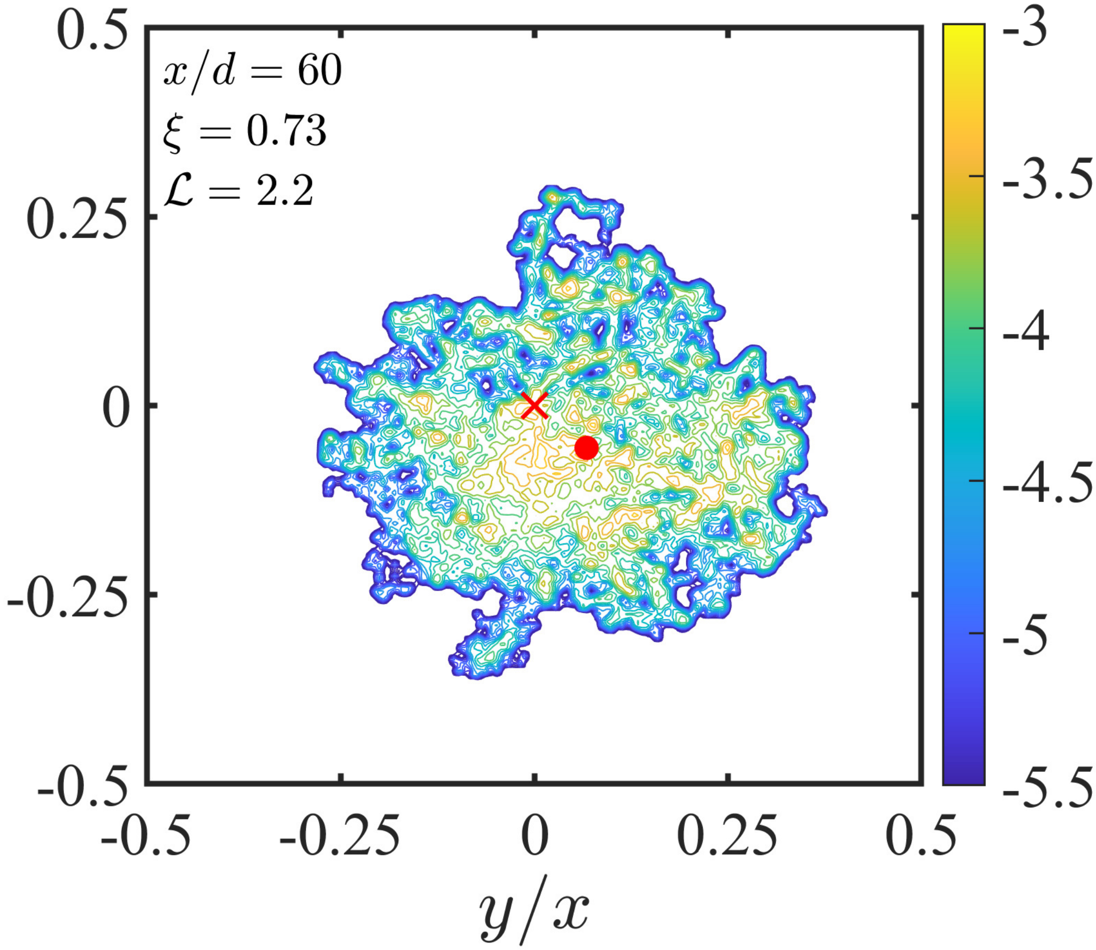
$x/d = 60$
$\xi = 0.73$
$\mathcal{L} = 2.2$
0.5
0.25
0
-0.25
-0.5
-0.5
-0.25
0
0.25
0.5
y/x
-3
-3.5
-4
-4.5
-5
-5.5

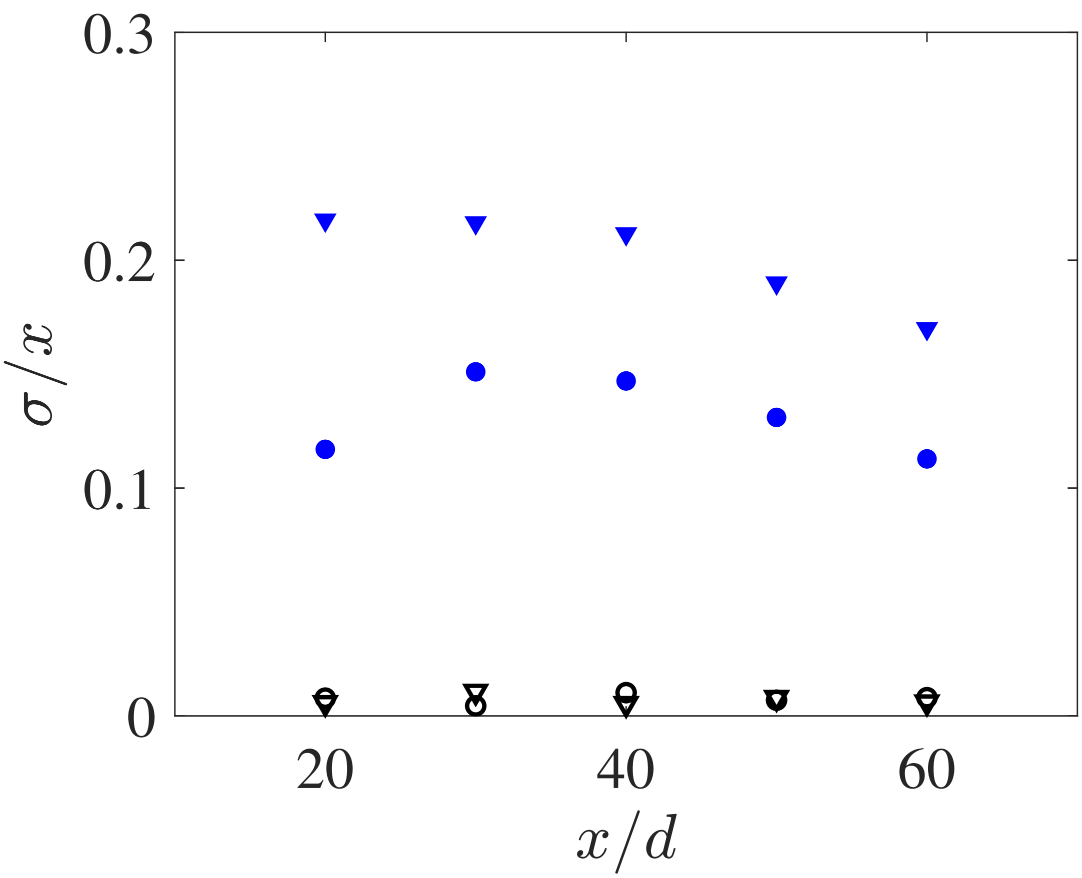
0.3
0.2
0.1
0
σ/x
20
40
60
x/d

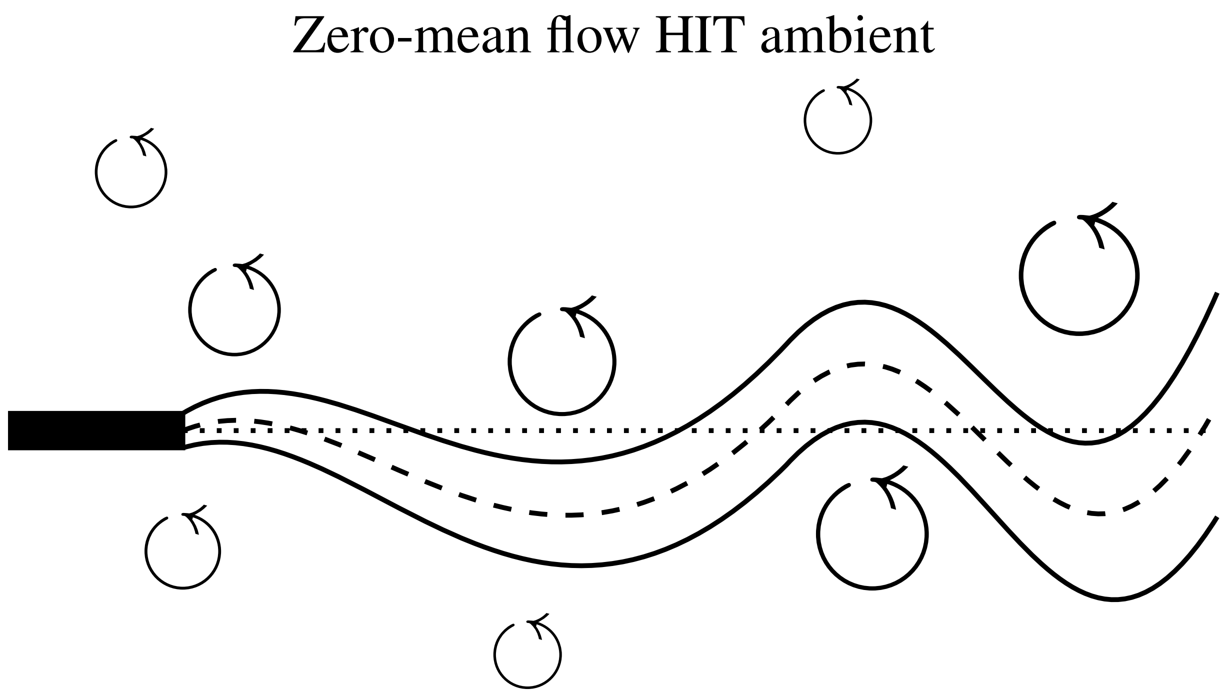
Zero-mean flow HIT ambient

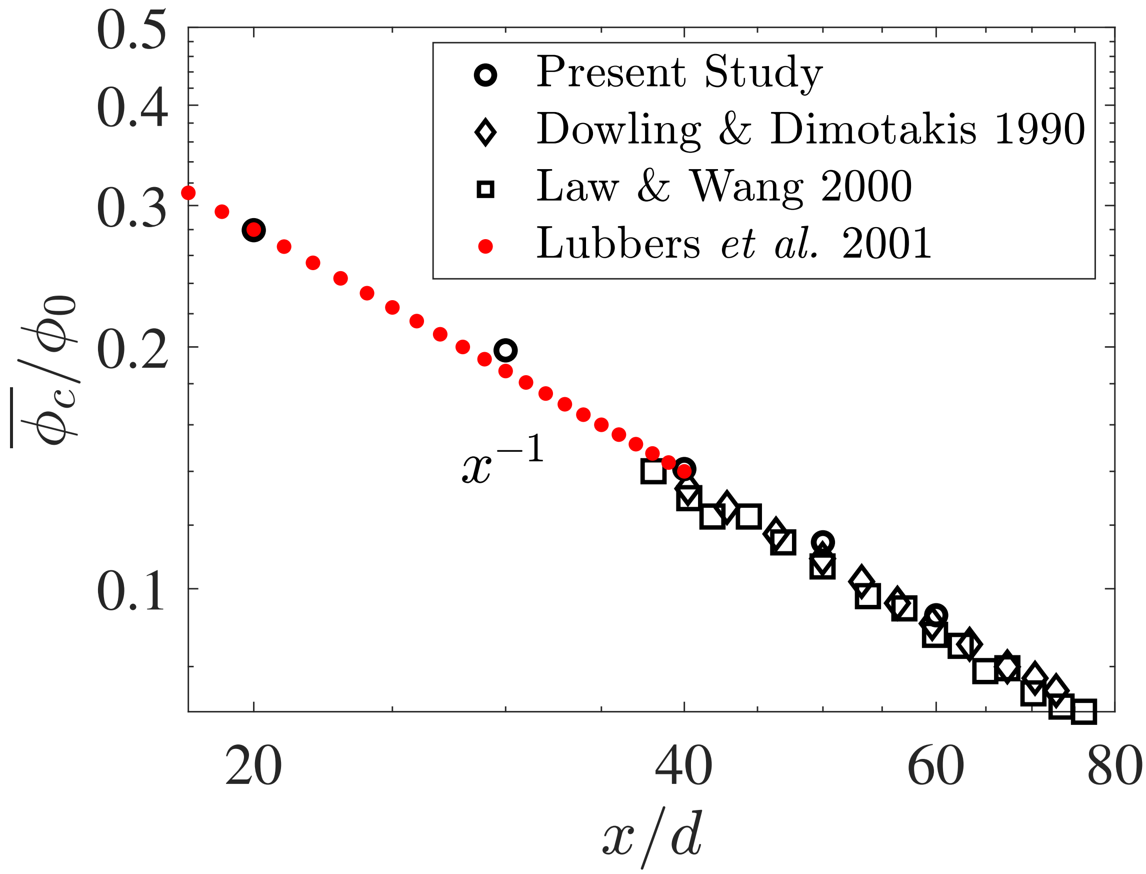
0.5
0.4
0.3
0.2
0.1
$\overline{\phi_c}/\phi_0$
Present Study
Dowling & Dimotakis 1990
Law & Wang 2000
Lubbers *et al.* 2001
x^{-1}
20
40
60
80
x/d

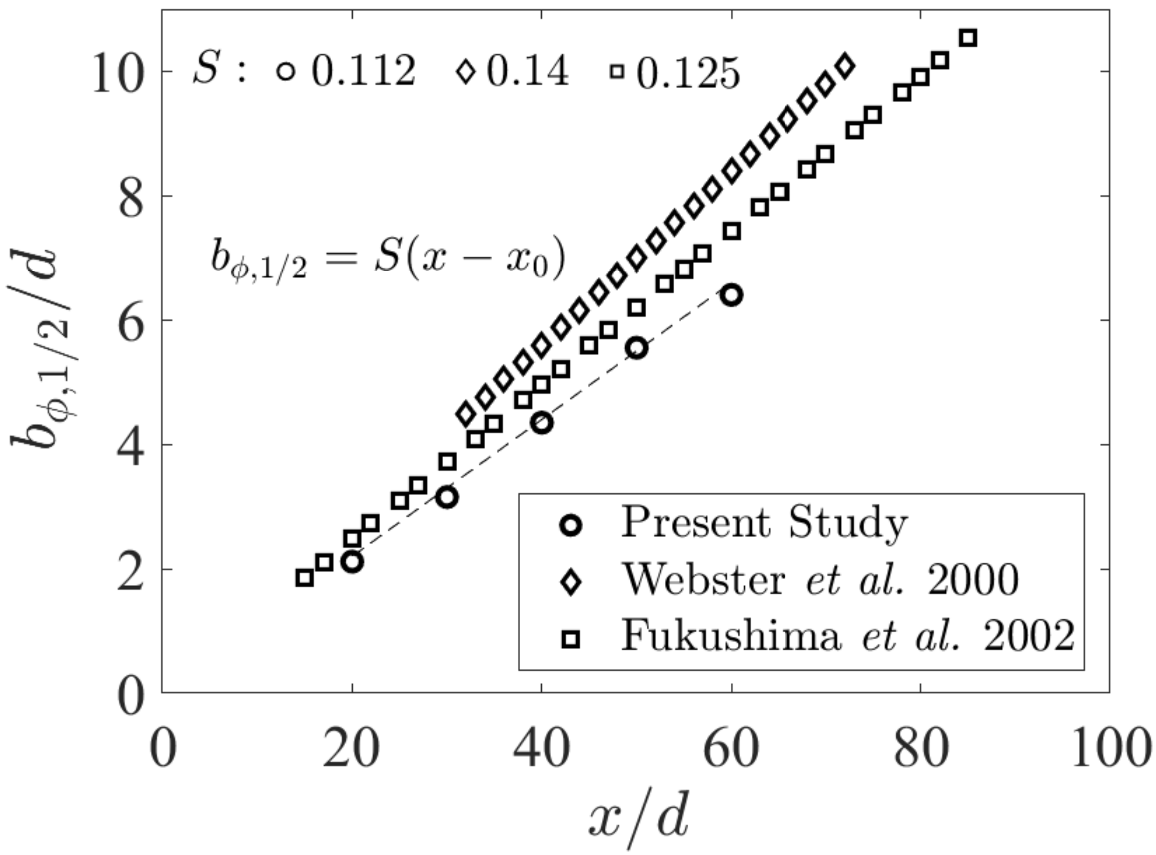
S : ○ 0.112 ◇ 0.14 □ 0.125
$b_{\phi,1/2} = S(x - x_0)$
Present Study
Webster *et al.* 2000
Fukushima *et al.* 2002
$b_{\phi,1/2}/d$
x/d
0
2
4
6
8
10
0
20
40
60
80
100

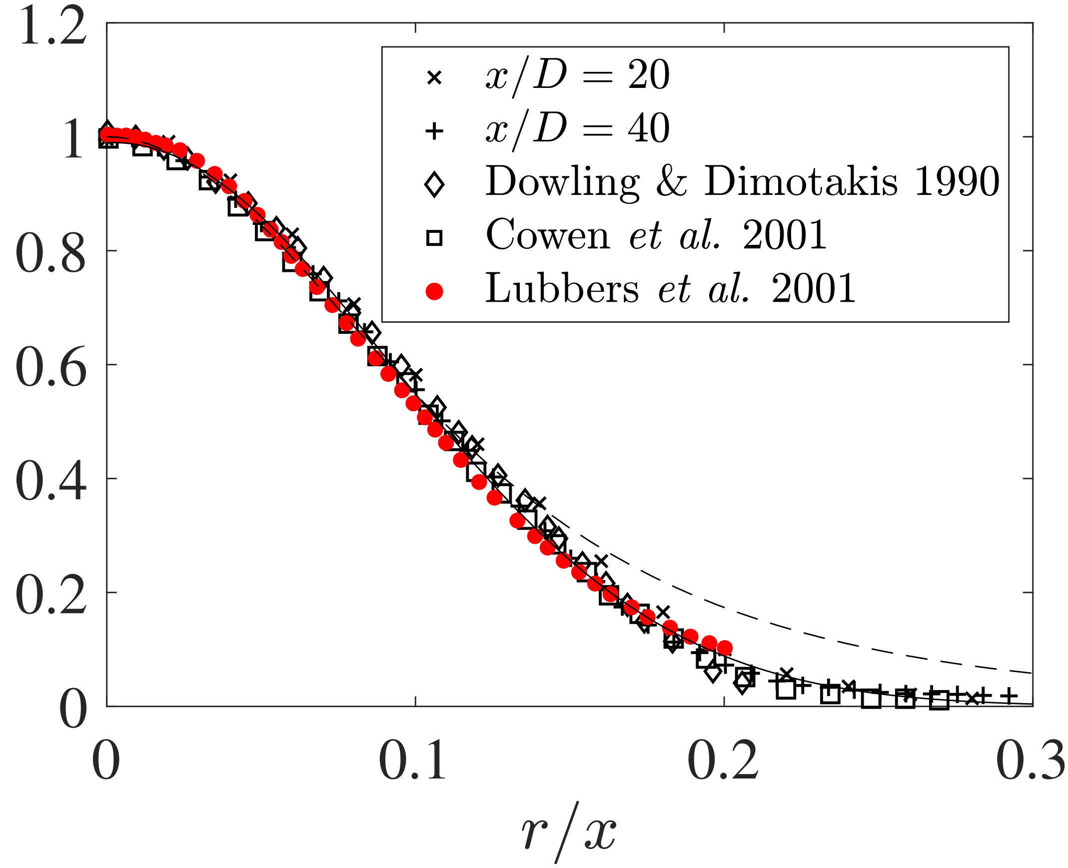

$x/D = 20$
$x/D = 40$
Dowling & Dimotakis 1990
Cowen *et al.* 2001
Lubbers *et al.* 2001
$\overline{\phi}/\overline{\phi_c}$
r/x
0
0.2
0.4
0.6
0.8
1
1.2
0.1
0.2
0.3

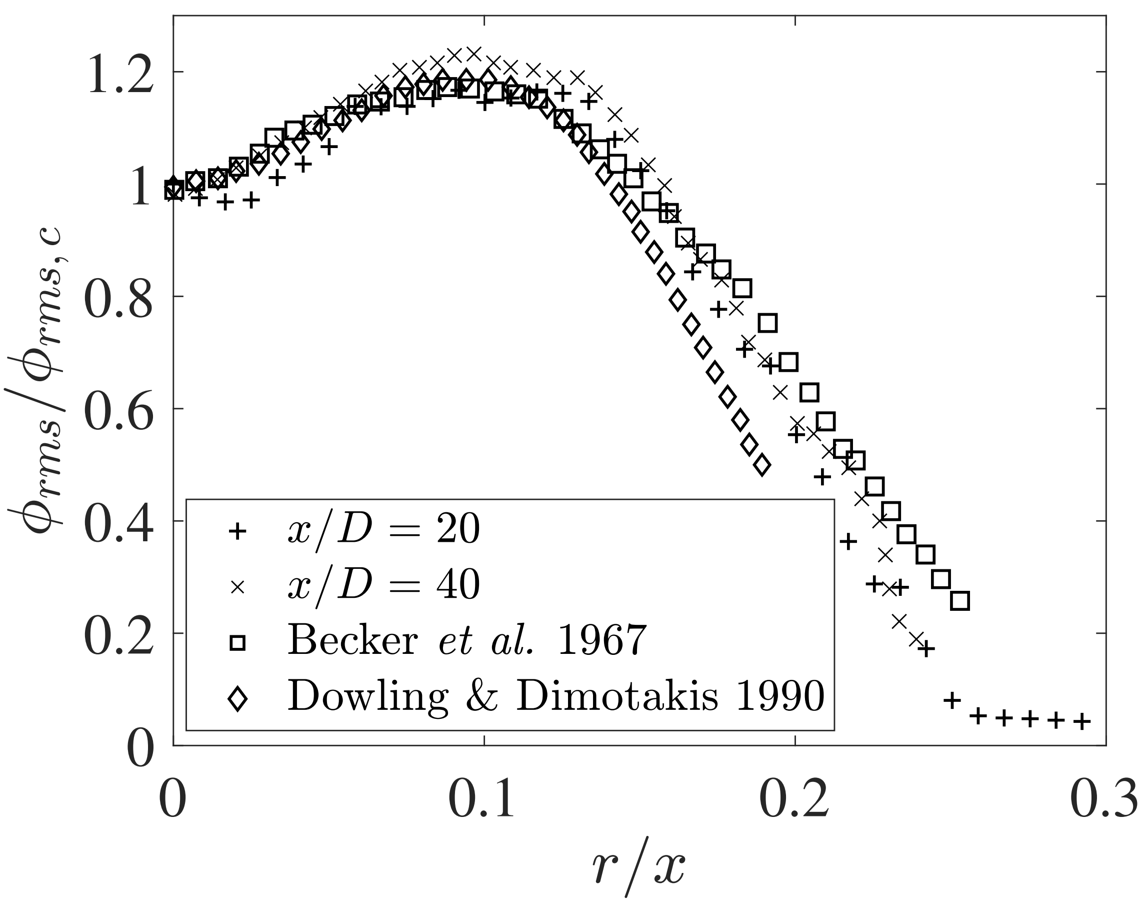
$\phi_{rms}/\phi_{rms,c}$
r/x
0
0.2
0.4
0.6
0.8
1
1.2
0
0.1
0.2
0.3
$x/D = 20$
$x/D = 40$
Becker *et al.* 1967
Dowling & Dimotakis 1990

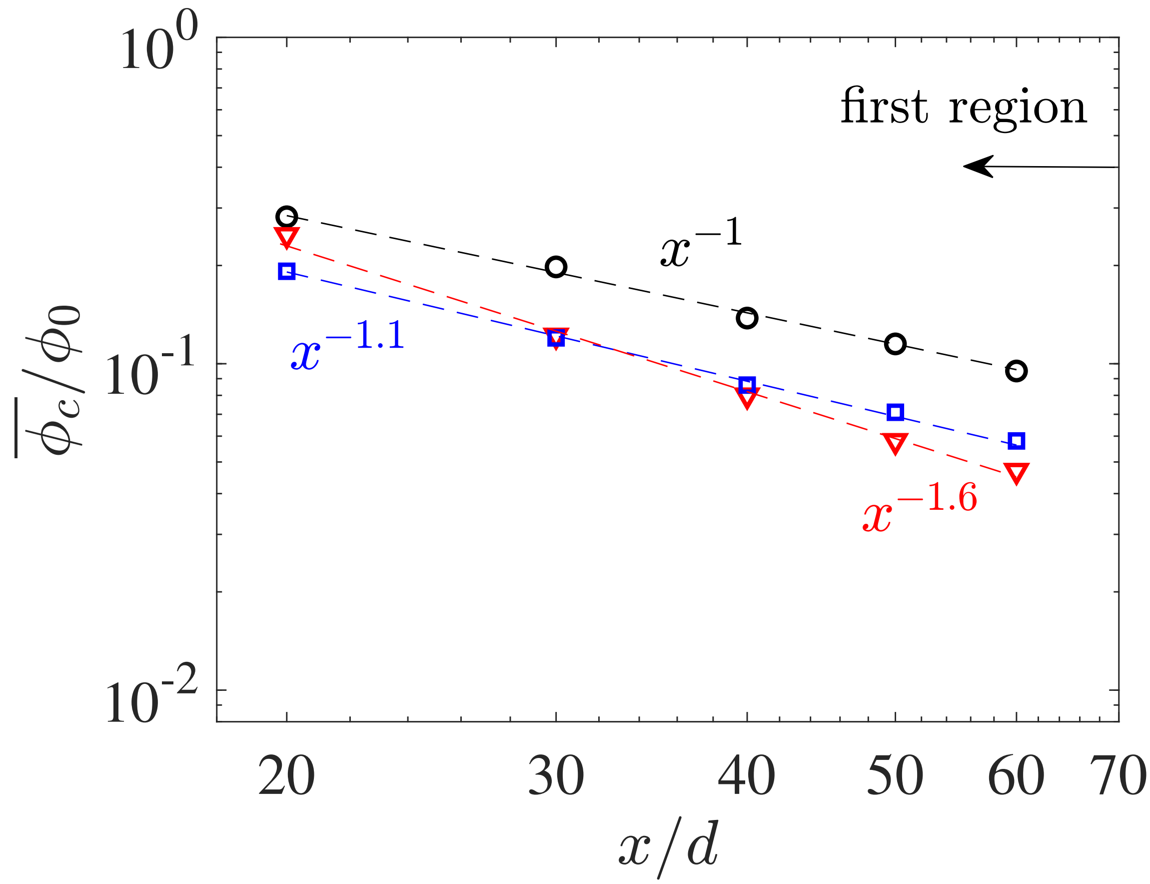
10^0
10^{-1}
10^{-2}
$\overline{\phi_c}/\phi_0$
first region
x^{-1}
$x^{-1.1}$
$x^{-1.6}$
20
30
40
50
60
70
x/d

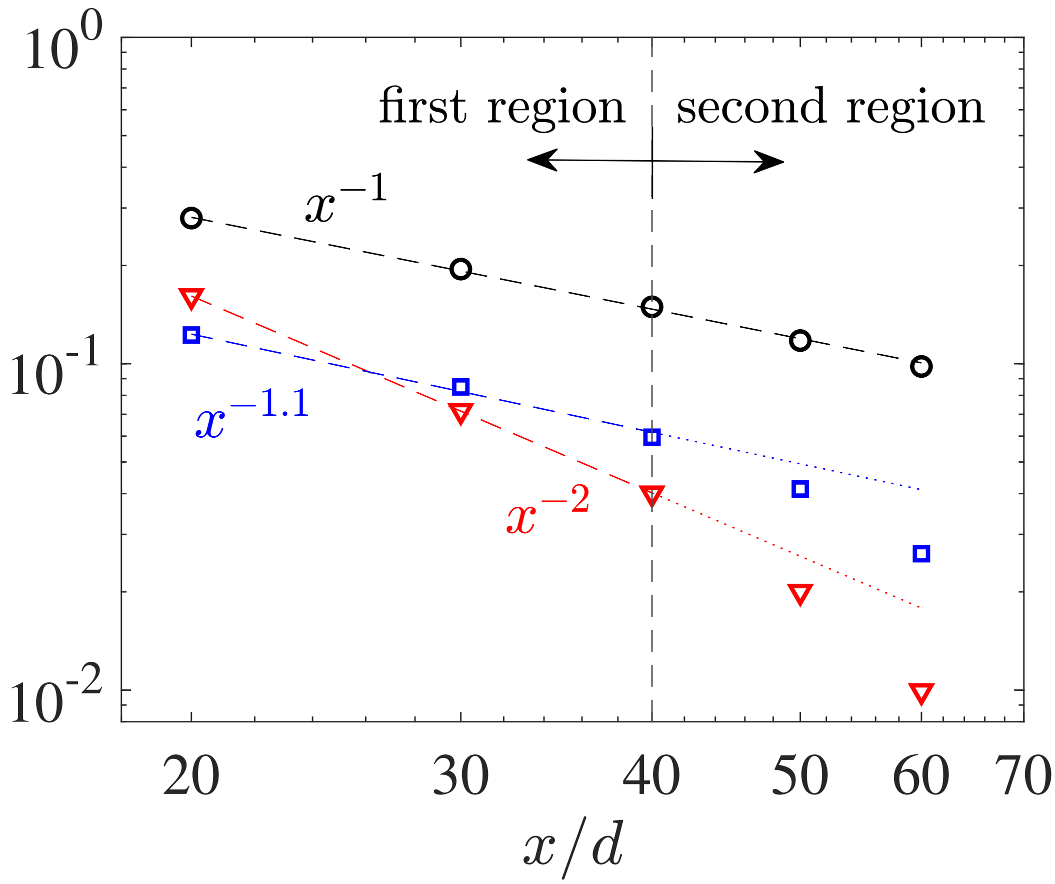
first region
second region
x^{-1}
$x^{-1.1}$
x^{-2}
10^0
10^{-1}
10^{-2}
20
30
40
50
60
70
x/d

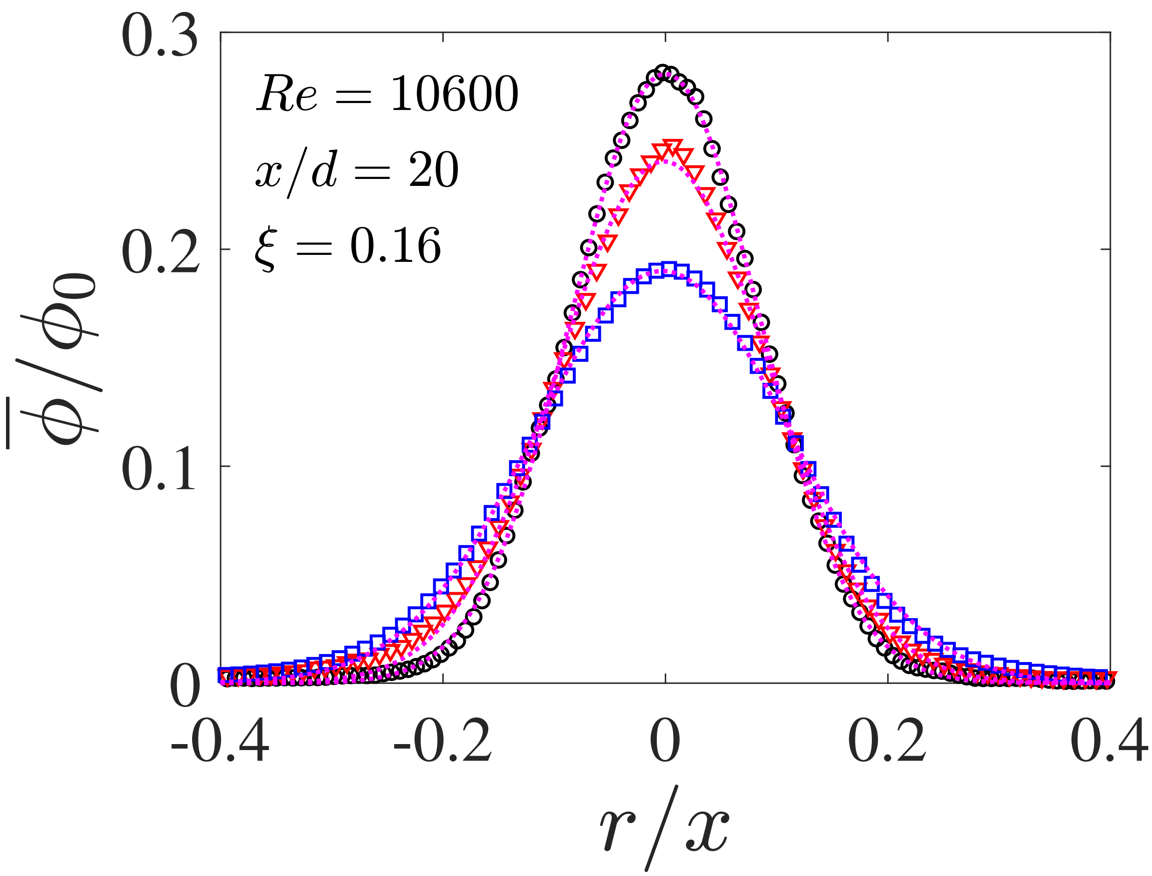
0.3
0.2
0.1
0
-0.4
-0.2
0
0.2
0.4
$Re = 10600$
$x/d = 20$
$\xi = 0.16$
$\overline{\phi}/\phi_0$
r/x

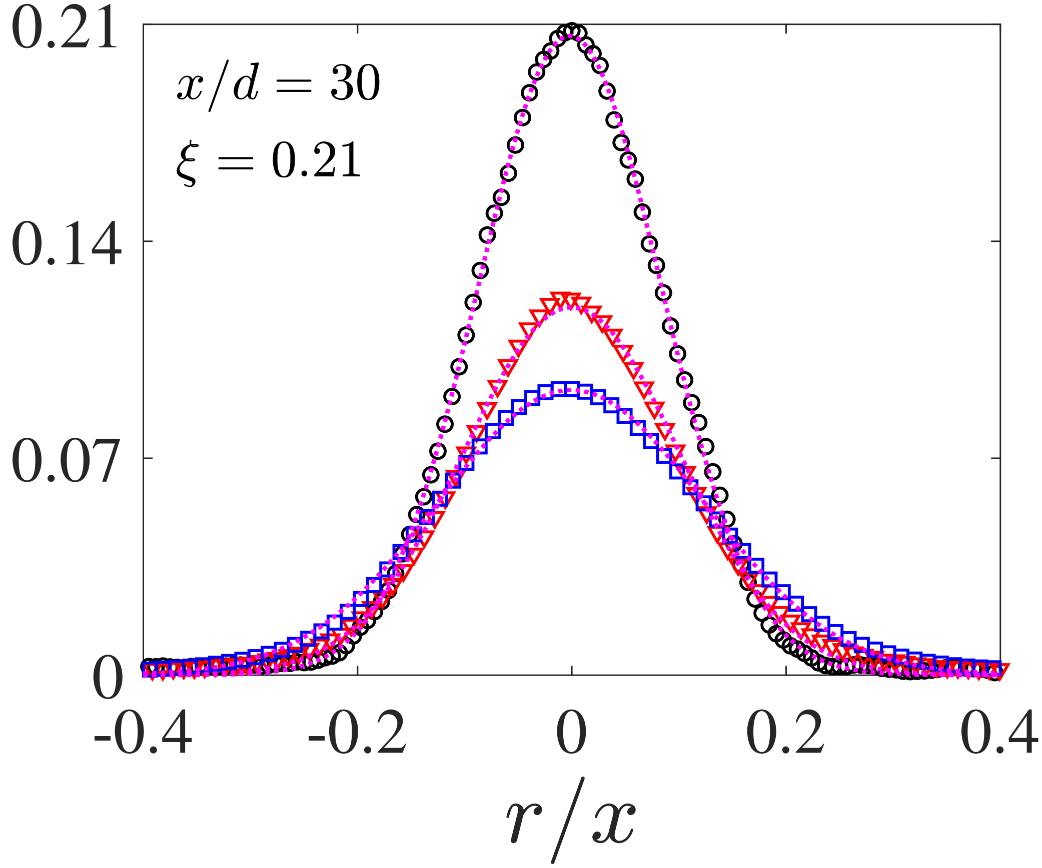
0.21
0.14
0.07
0
$x/d = 30$
$\xi = 0.21$
-0.4
-0.2
0
0.2
0.4
r/x

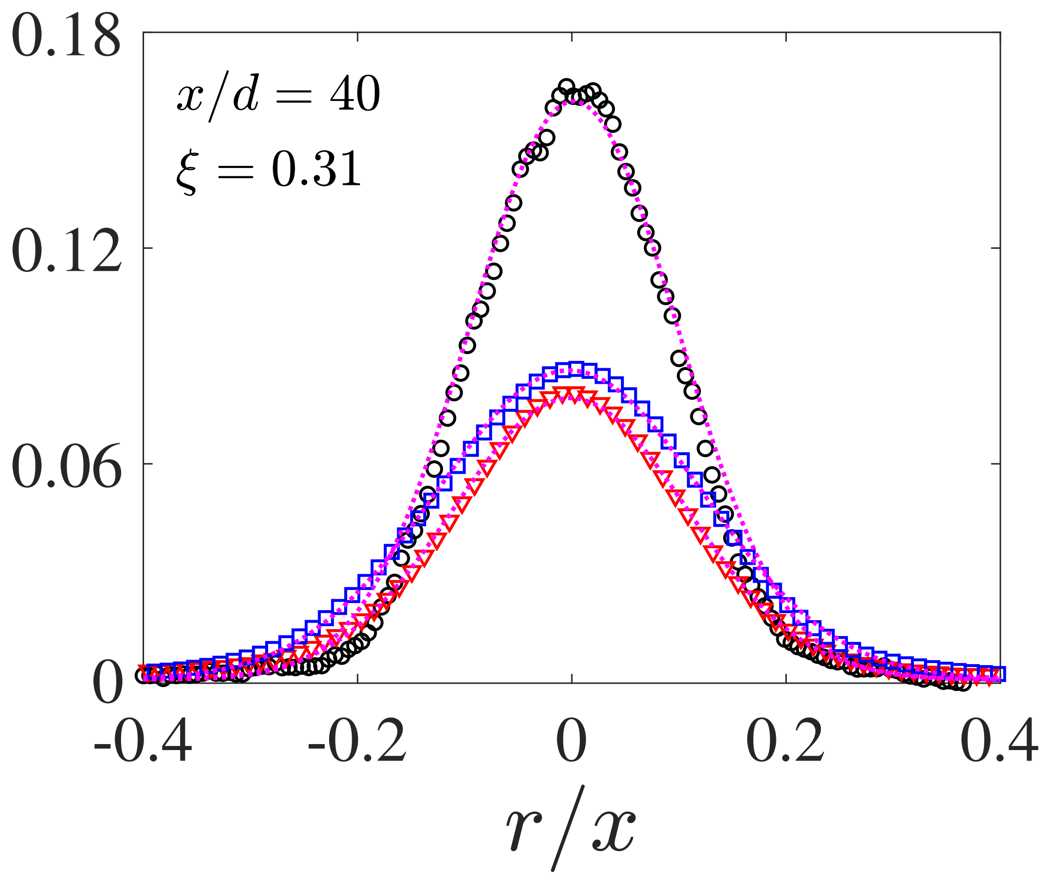
0.18
0.12
0.06
0
-0.4
-0.2
0
0.2
0.4
$x/d = 40$
$\xi = 0.31$
r/x

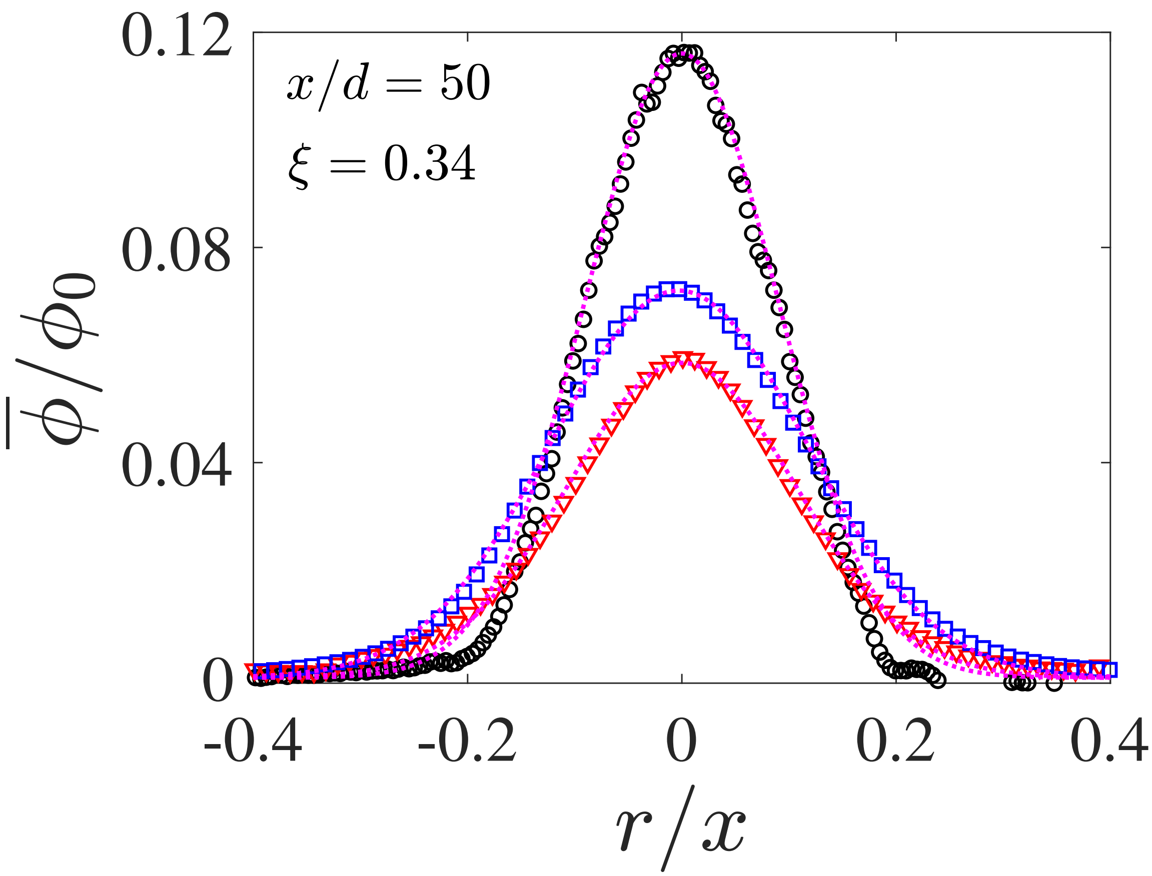
$x/d = 50$
$\xi = 0.34$
$\overline{\phi}/\phi_0$
0.12
0.08
0.04
0
-0.4
-0.2
0
0.2
0.4
r/x

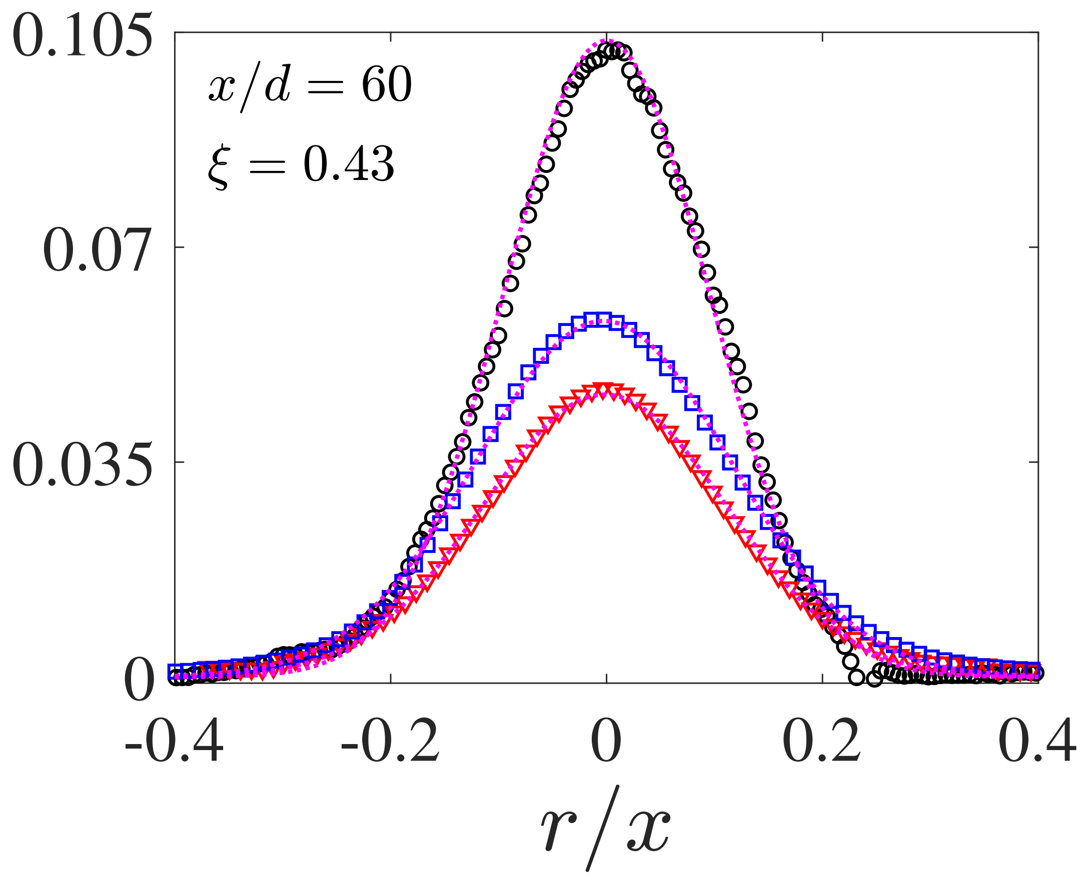
$x/d = 60$
$\xi = 0.43$
0.105
0.07
0.035
0
-0.4
-0.2
0
0.2
0.4
r/x

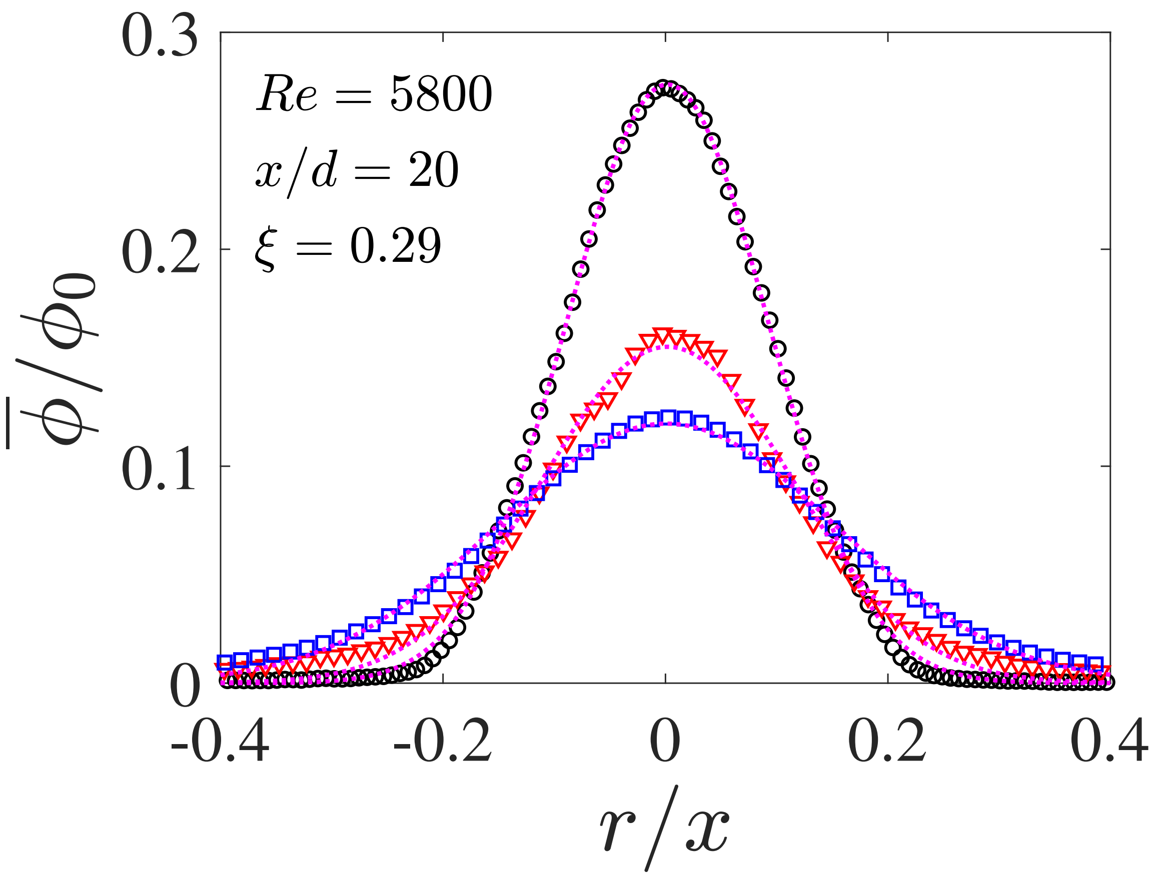
$Re = 5800$
$x/d = 20$
$\xi = 0.29$
$\overline{\phi}/\phi_0$
r/x
0.3
0.2
0.1
0
-0.4
-0.2
0
0.2
0.4

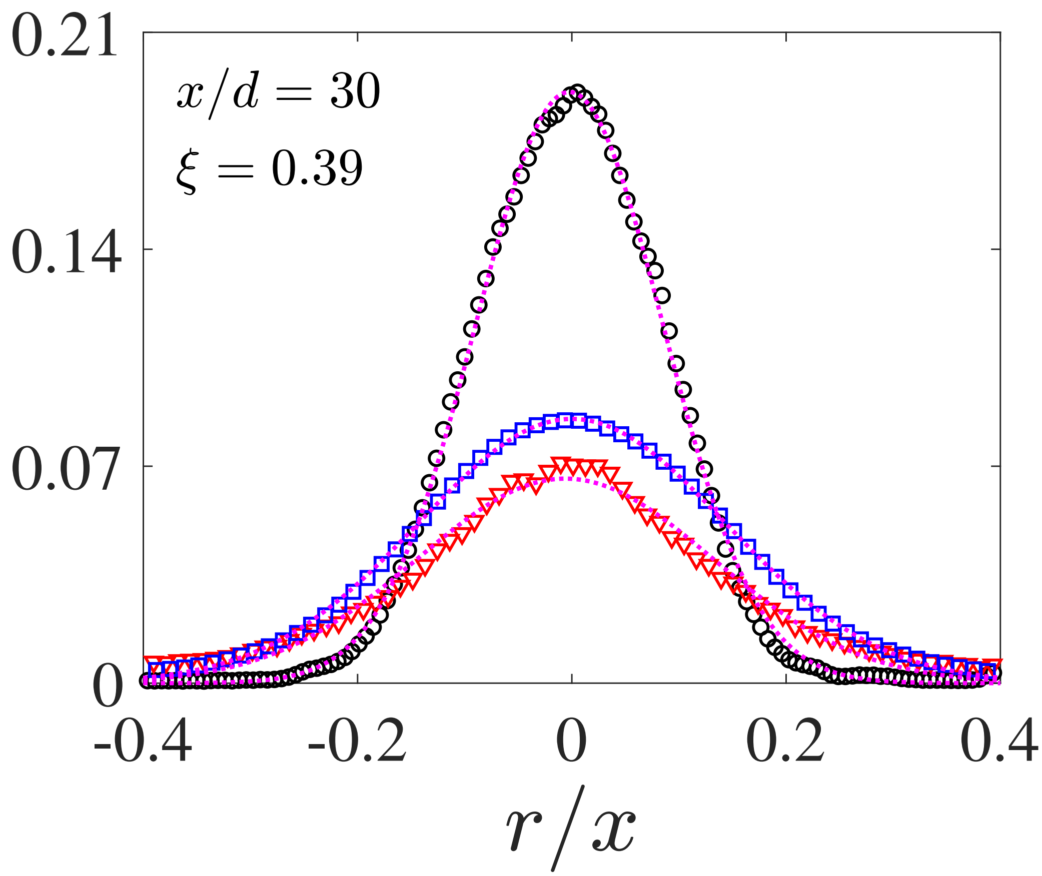
0.21
0.14
0.07
0
-0.4
-0.2
0
0.2
0.4
r/x
$x/d = 30$
$\xi = 0.39$

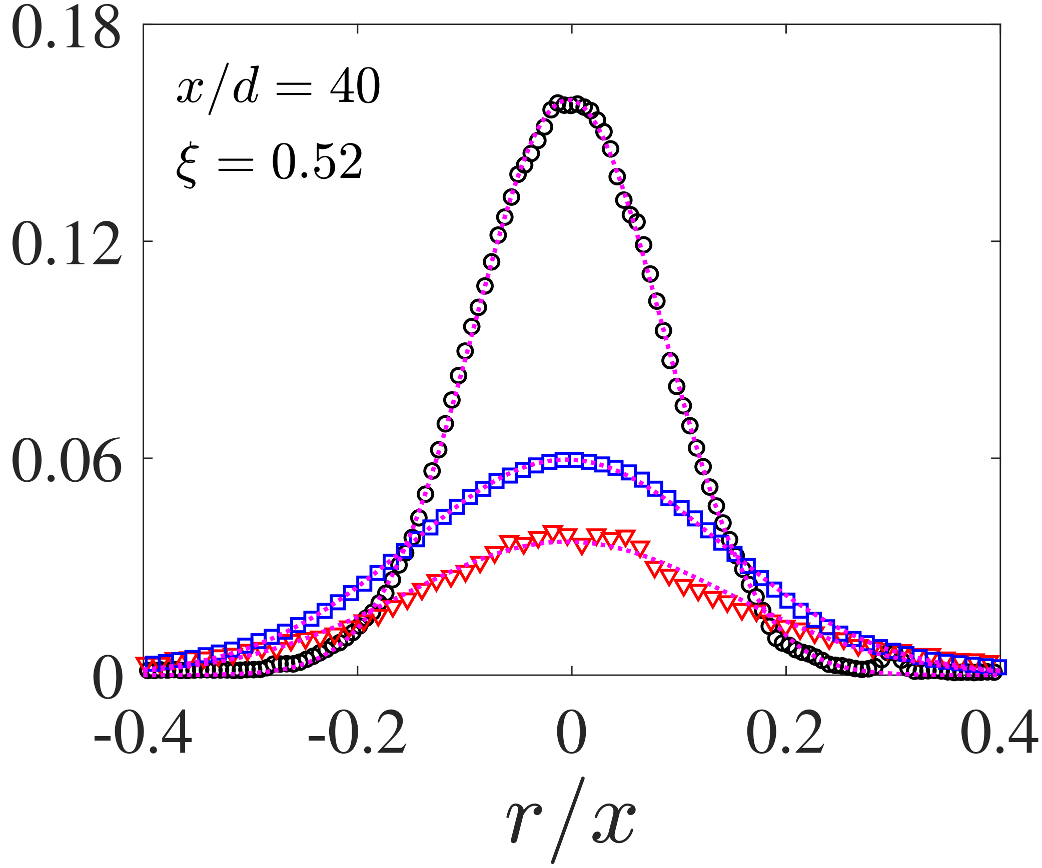
0.18
0.12
0.06
0
$x/d = 40$
$\xi = 0.52$
-0.4
-0.2
0
0.2
0.4
r/x

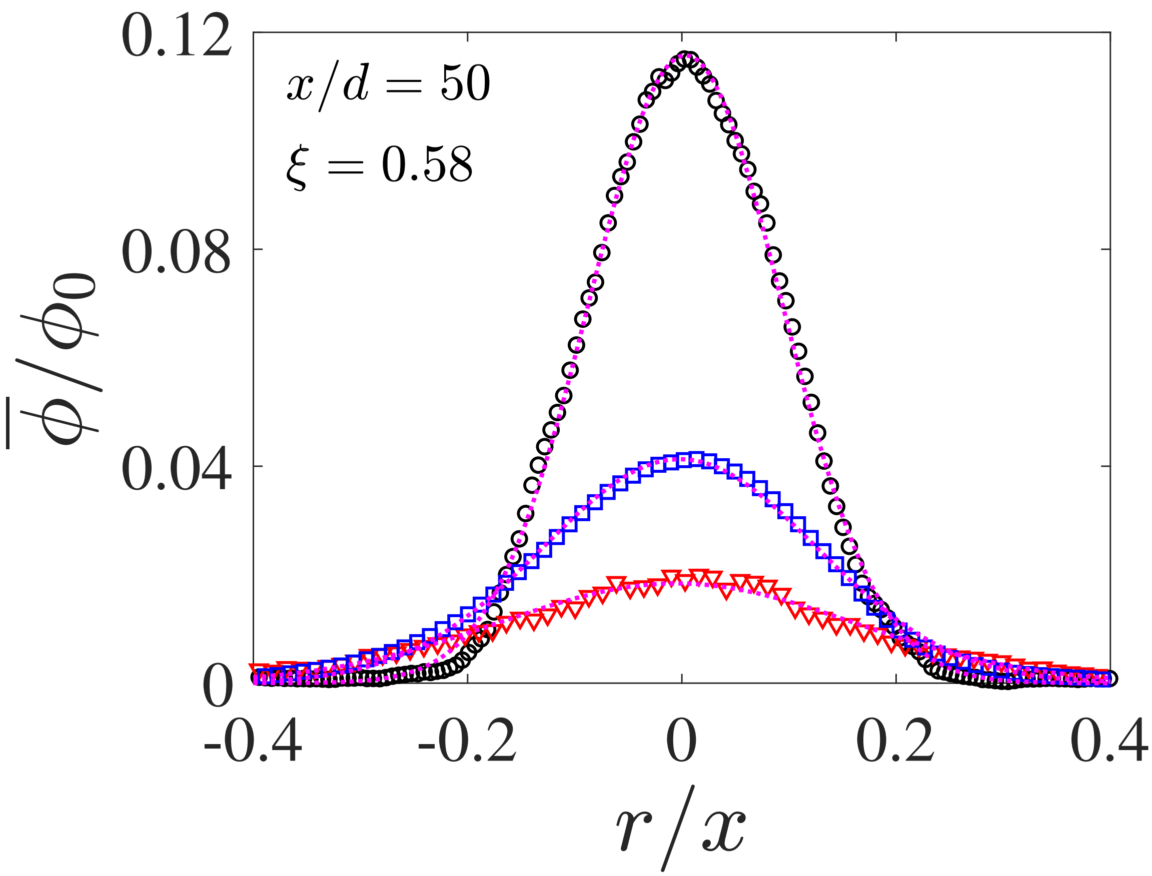
0.12
0.08
0.04
0
$\overline{\phi}/\phi_0$
$x/d = 50$
$\xi = 0.58$
-0.4
-0.2
0
0.2
0.4
r/x

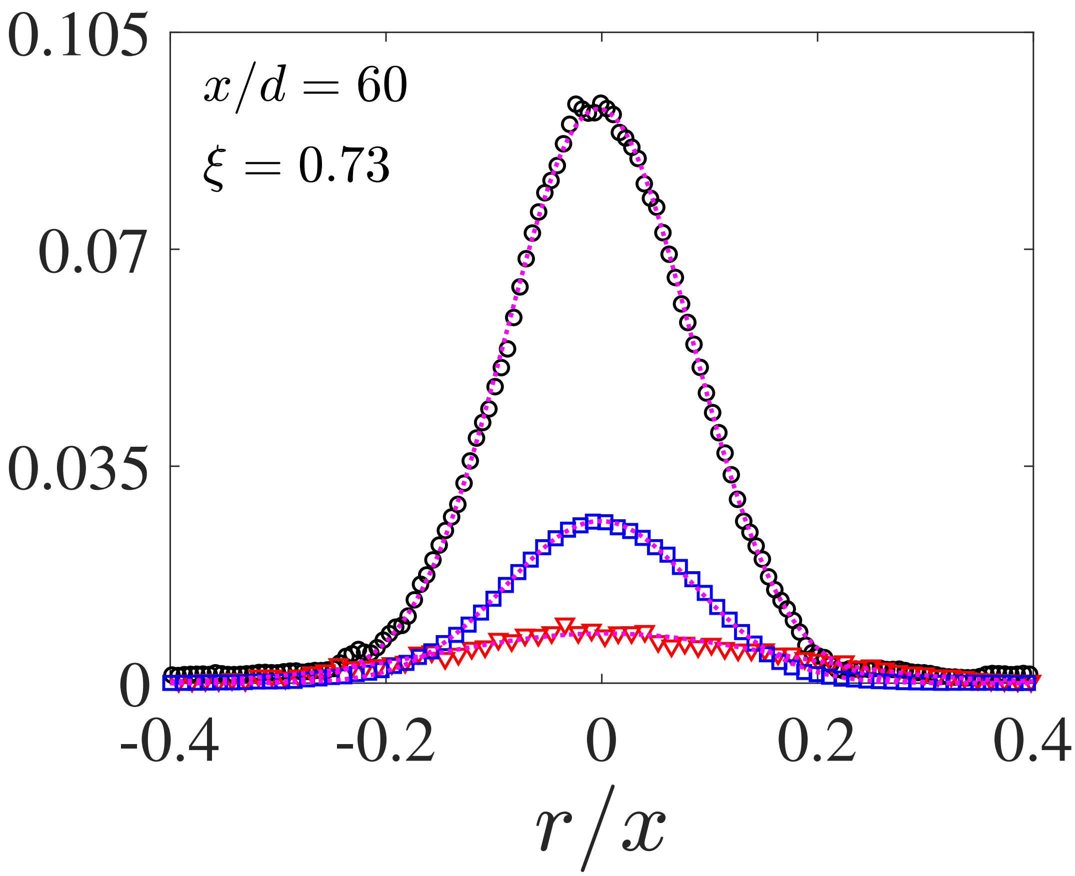
0.105
0.07
0.035
0
$x/d = 60$
$\xi = 0.73$
-0.4
-0.2
0
0.2
0.4
r/x

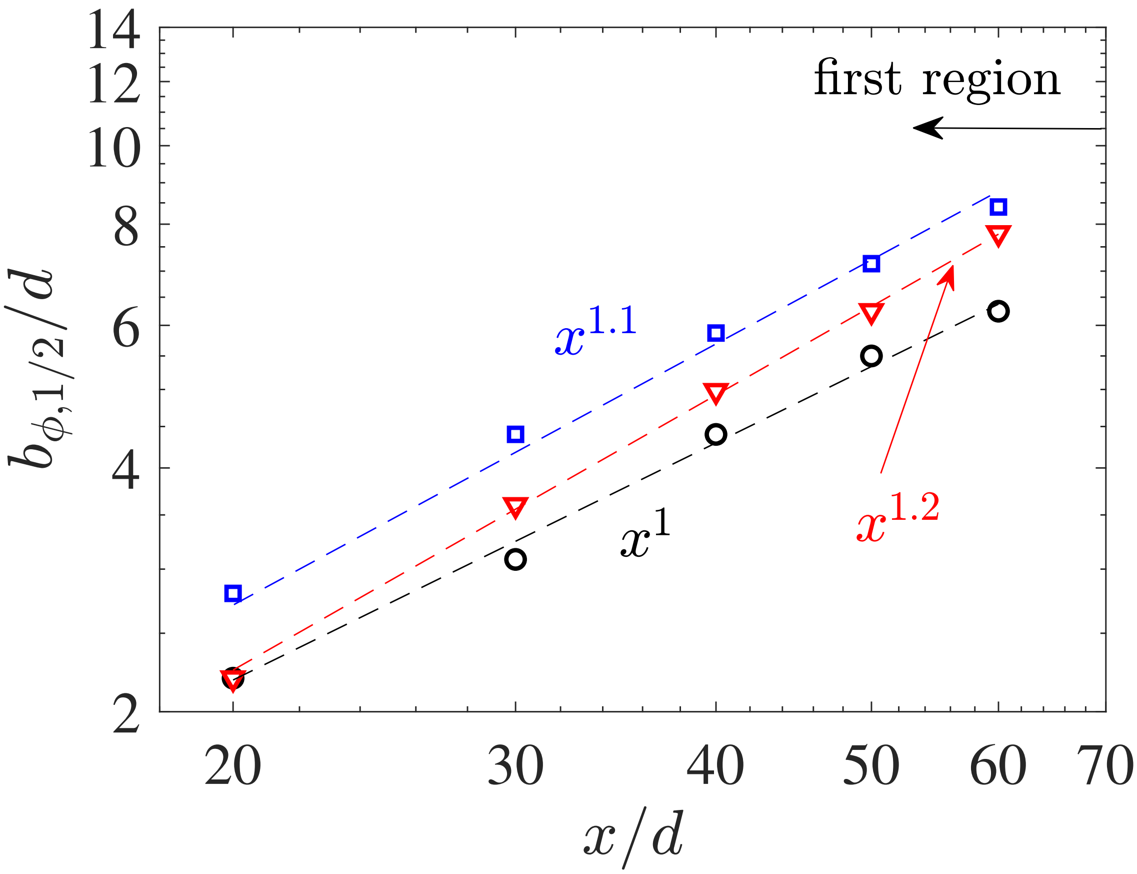
first region
$x^{1.1}$
$x^{1.2}$
x^1
$b_{\phi,1/2}/d$
x/d
14
12
10
8
6
4
2
20
30
40
50
60
70

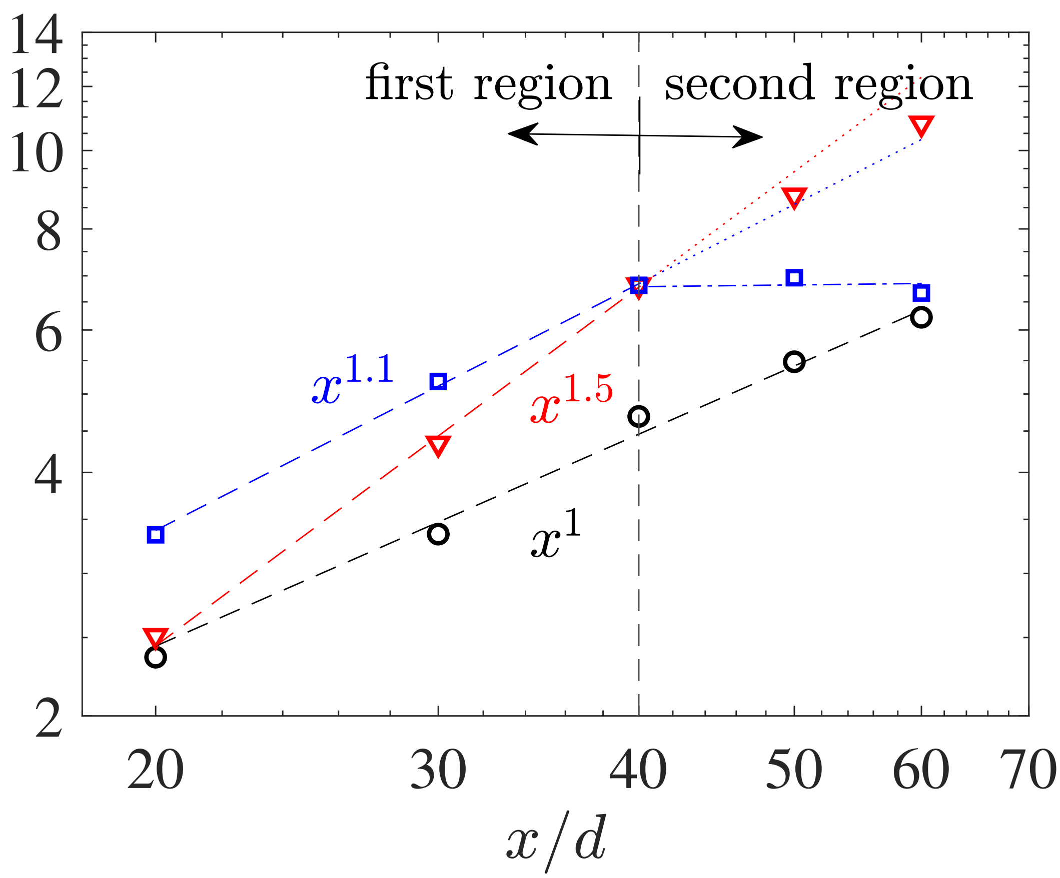
first region
second region
$x^{1.1}$
$x^{1.5}$
x^1
14
12
10
8
6
4
2
20
30
40
50
60
70
x/d

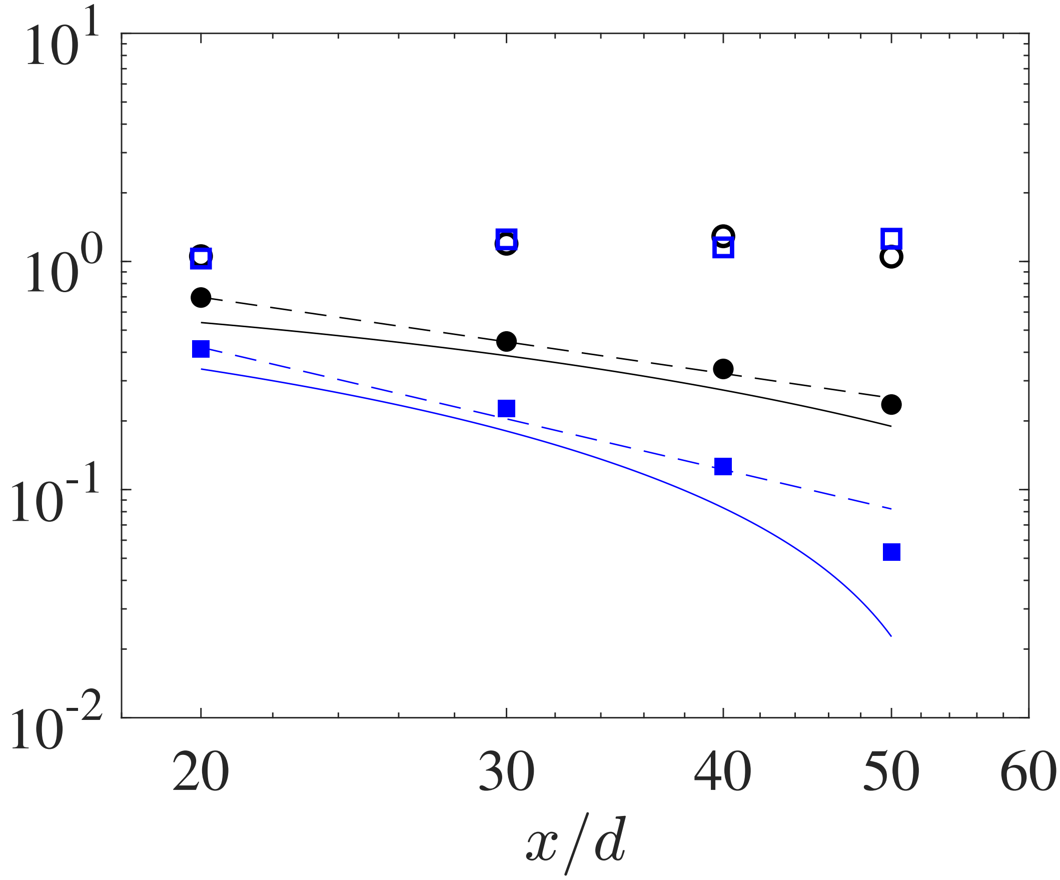
10^1
10^0
10^{-1}
10^{-2}
F/F_0
20
30
40
50
60
x/d

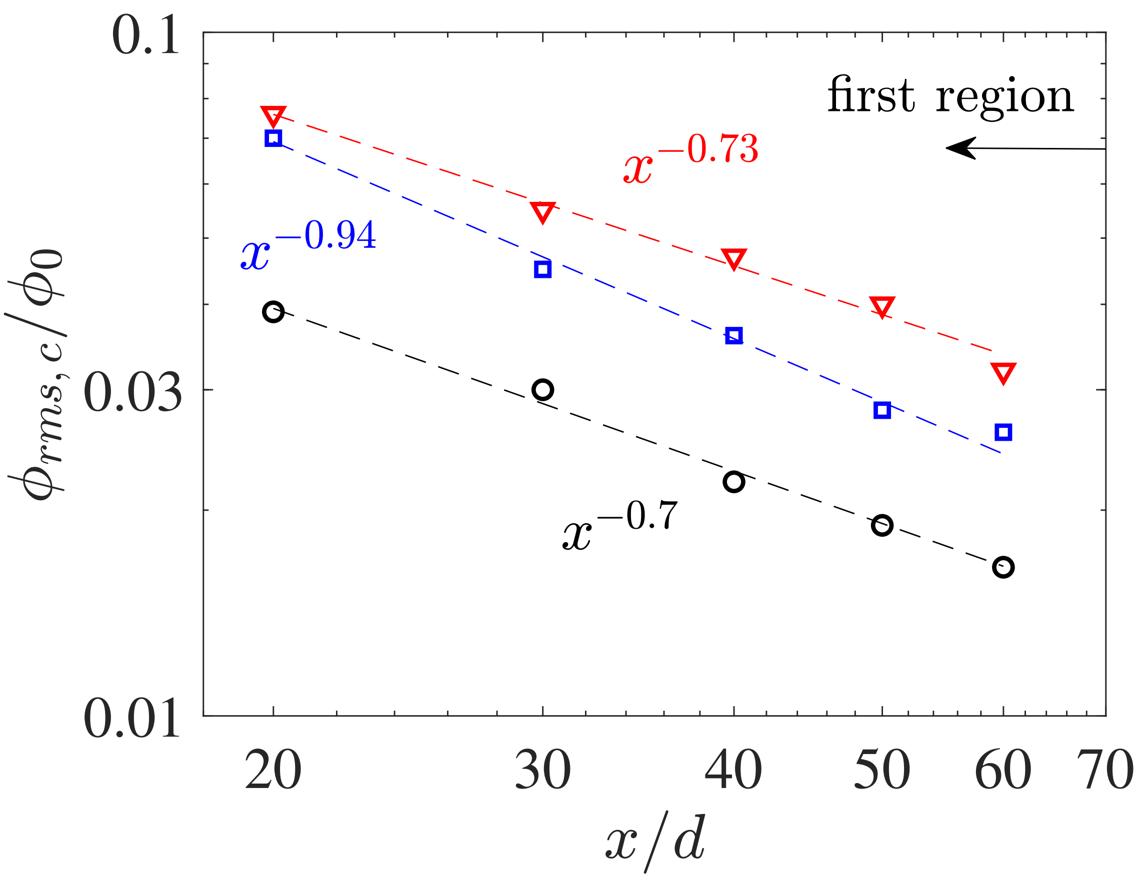
0.1
0.03
0.01
20
30
40
50
60
70
x/d
$\phi_{rms,c}/\phi_0$
first region
$x^{-0.73}$
$x^{-0.94}$
$x^{-0.7}$

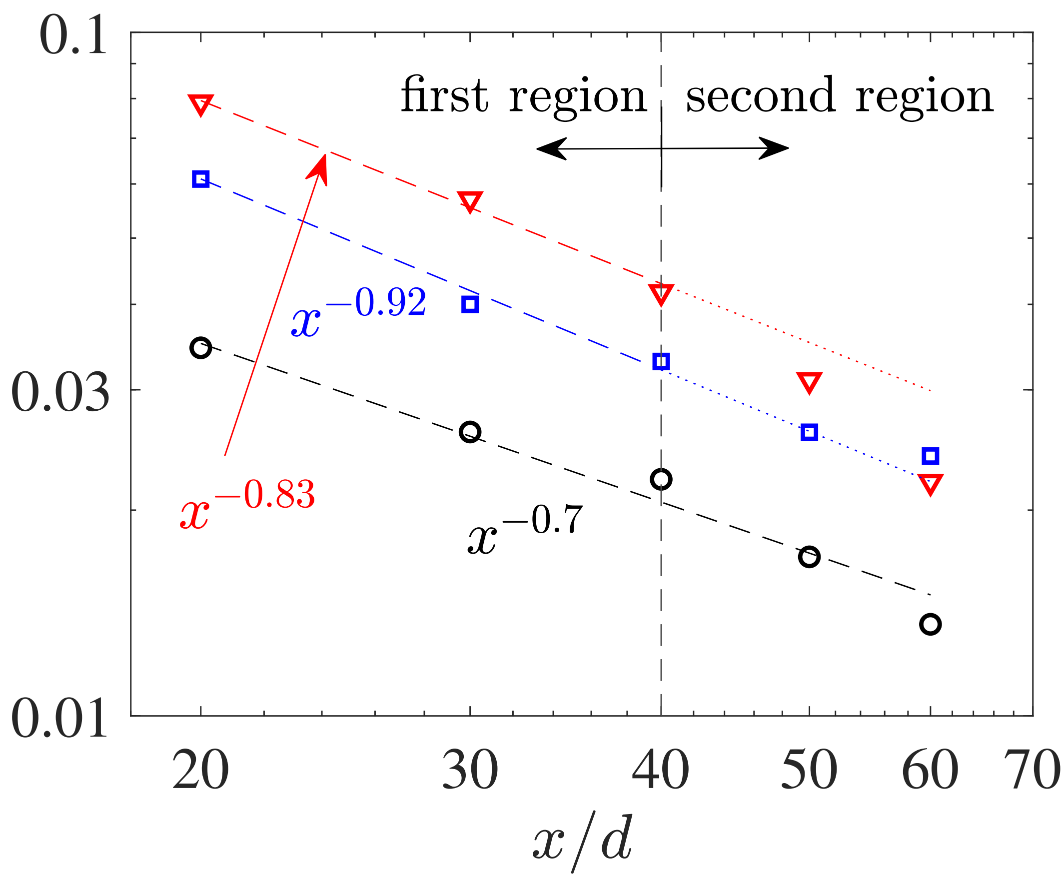
0.1
0.03
0.01
20
30
40
50
60
70
x/d
first region
second region
$x^{-0.92}$
$x^{-0.83}$
$x^{-0.7}$

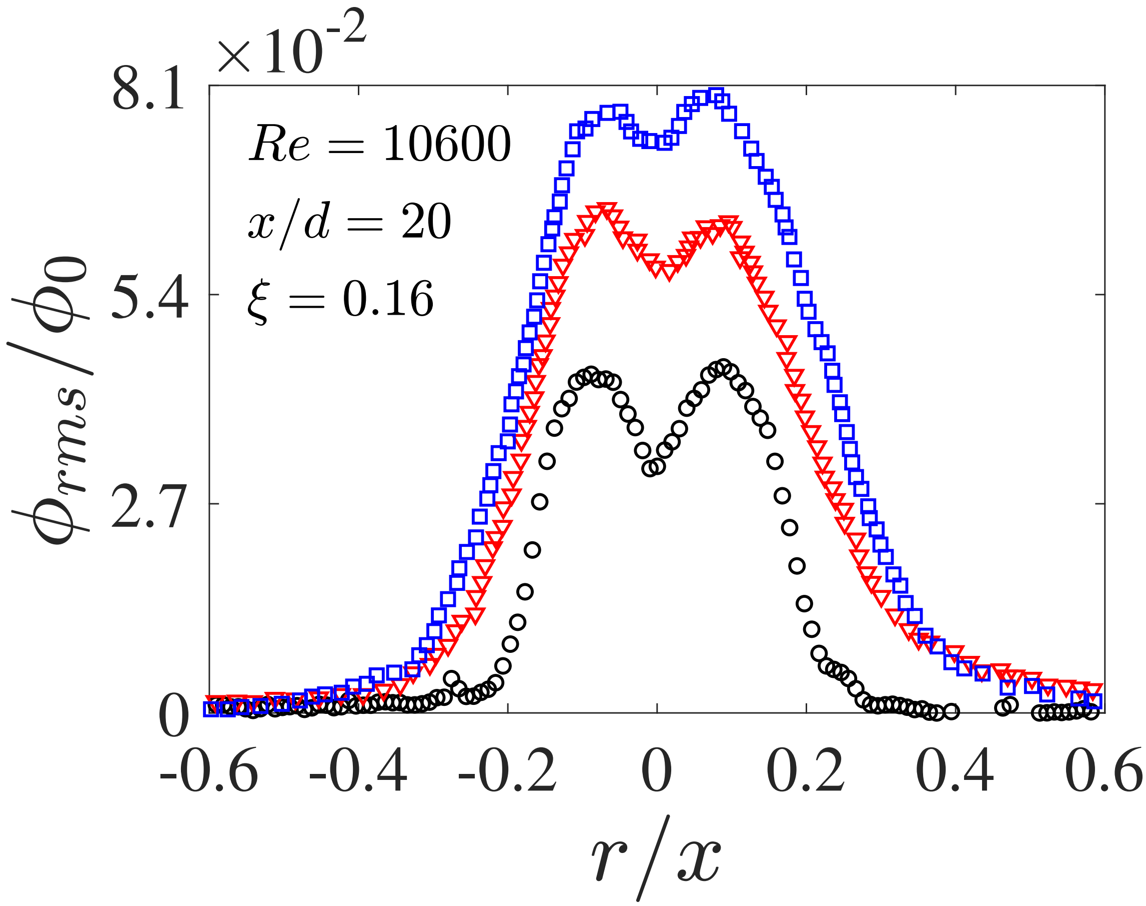
$\times 10^{-2}$
8.1
5.4
2.7
0
ϕ_{rms}/ϕ_0
$Re = 10600$
$x/d = 20$
$\xi = 0.16$
-0.6
-0.4
-0.2
0
0.2
0.4
0.6
r/x

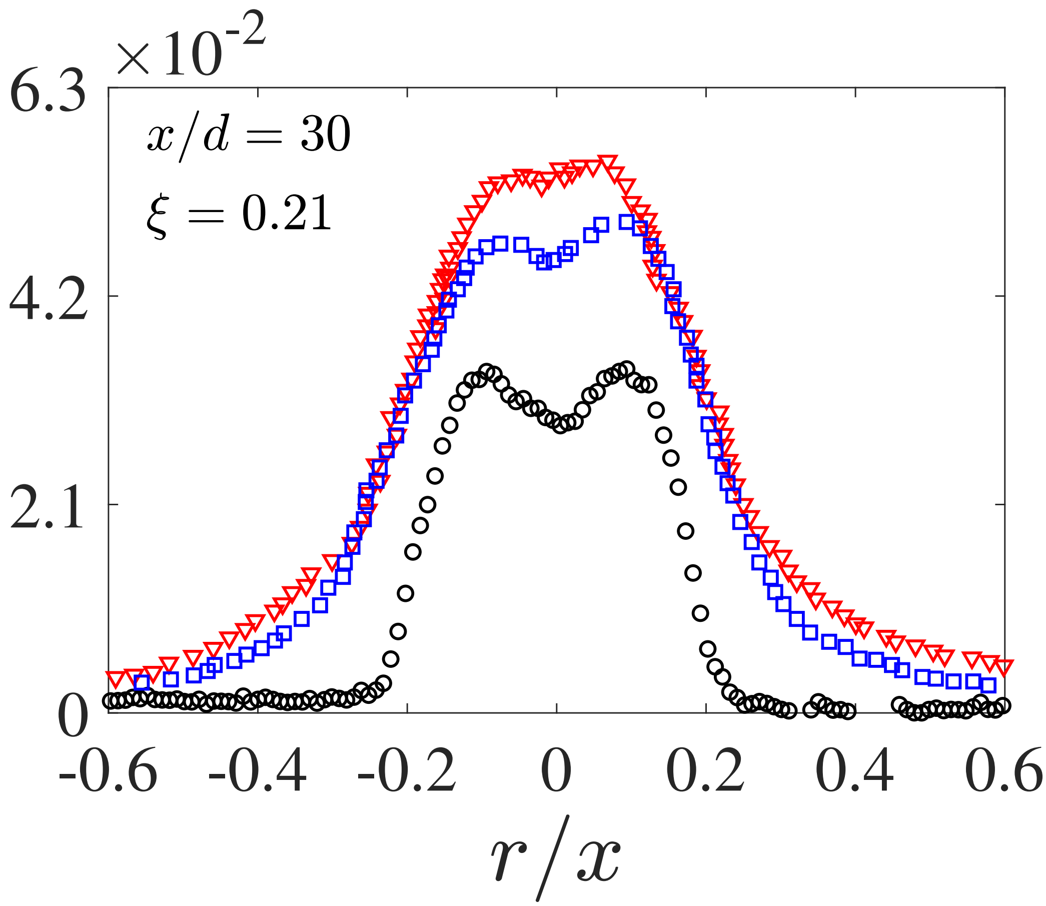
$\times 10^{-2}$
6.3
4.2
2.1
0
$x/d = 30$
$\xi = 0.21$
-0.6
-0.4
-0.2
0
0.2
0.4
0.6
r/x

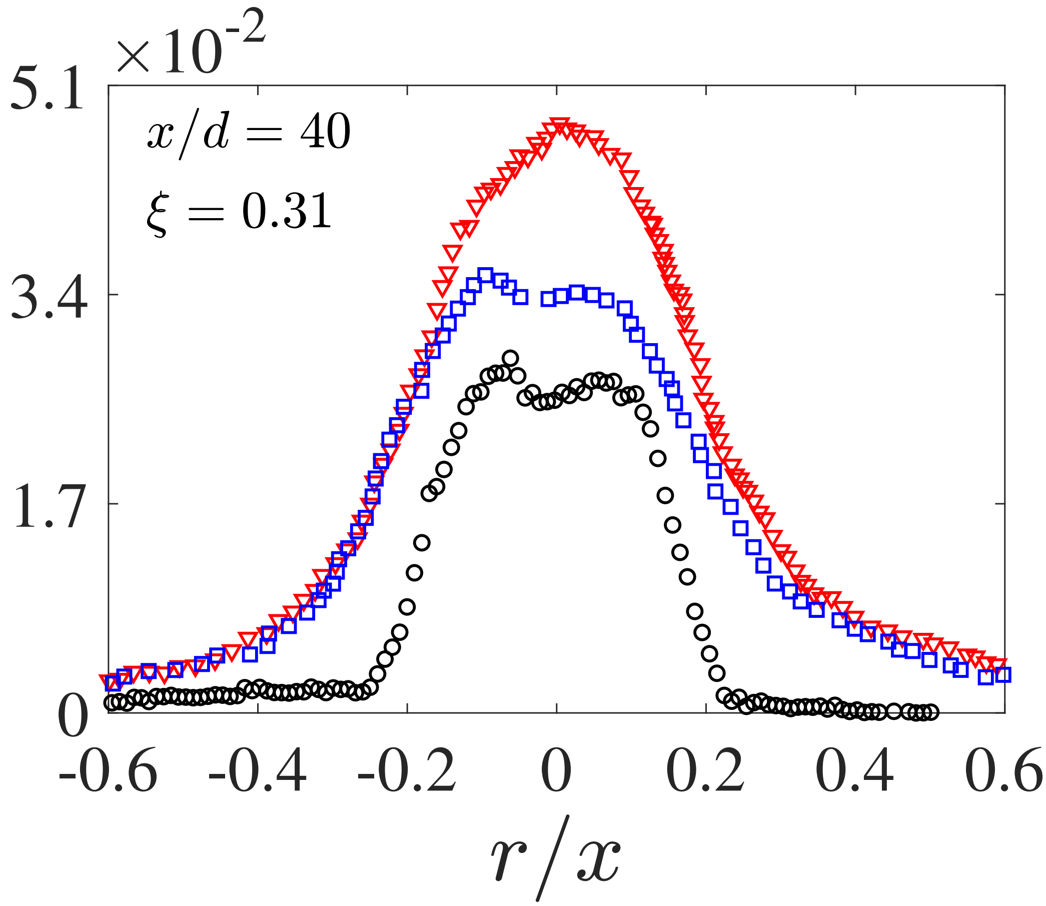
$\times 10^{-2}$
5.1
3.4
1.7
0
$x/d = 40$
$\xi = 0.31$
-0.6
-0.4
-0.2
0
0.2
0.4
0.6
r/x

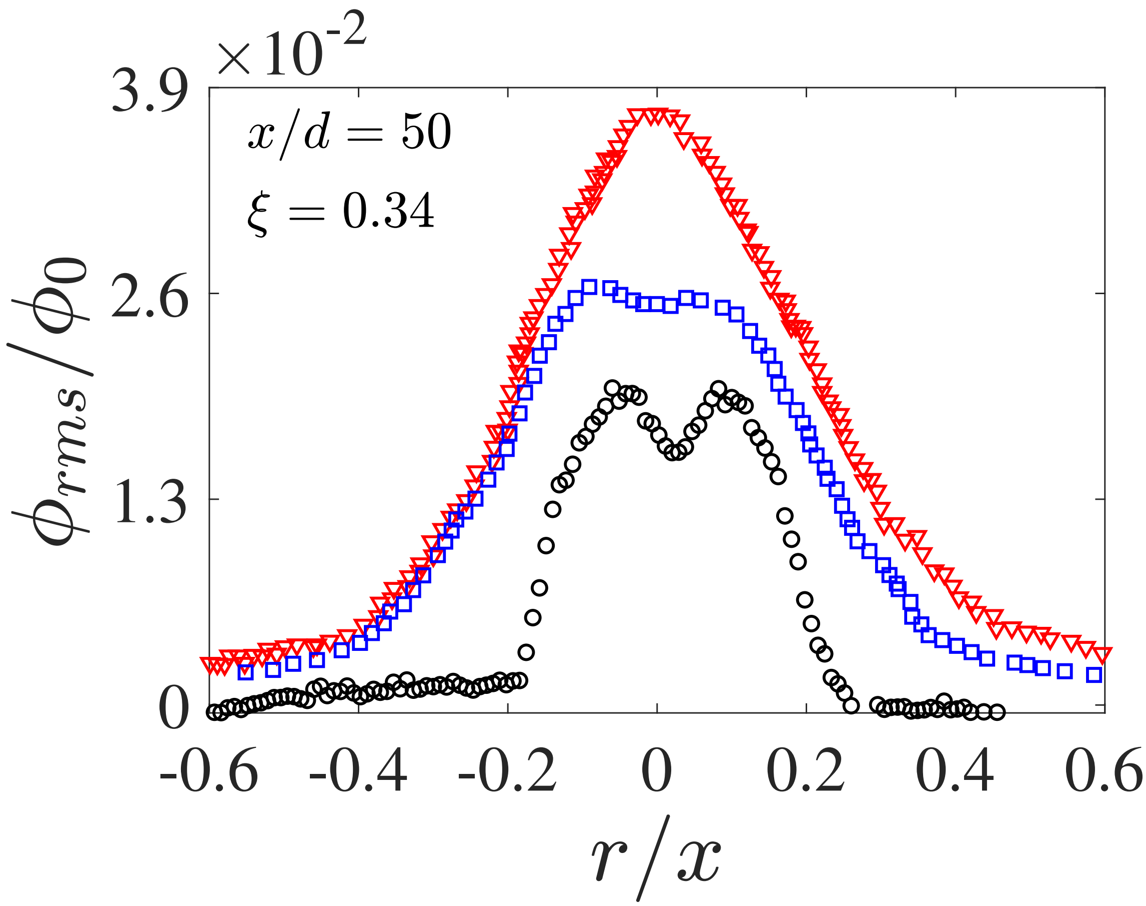
$\times 10^{-2}$
3.9
2.6
1.3
0
$x/d = 50$
$\xi = 0.34$
ϕ_{rms}/ϕ_0
-0.6
-0.4
-0.2
0
0.2
0.4
0.6
r/x

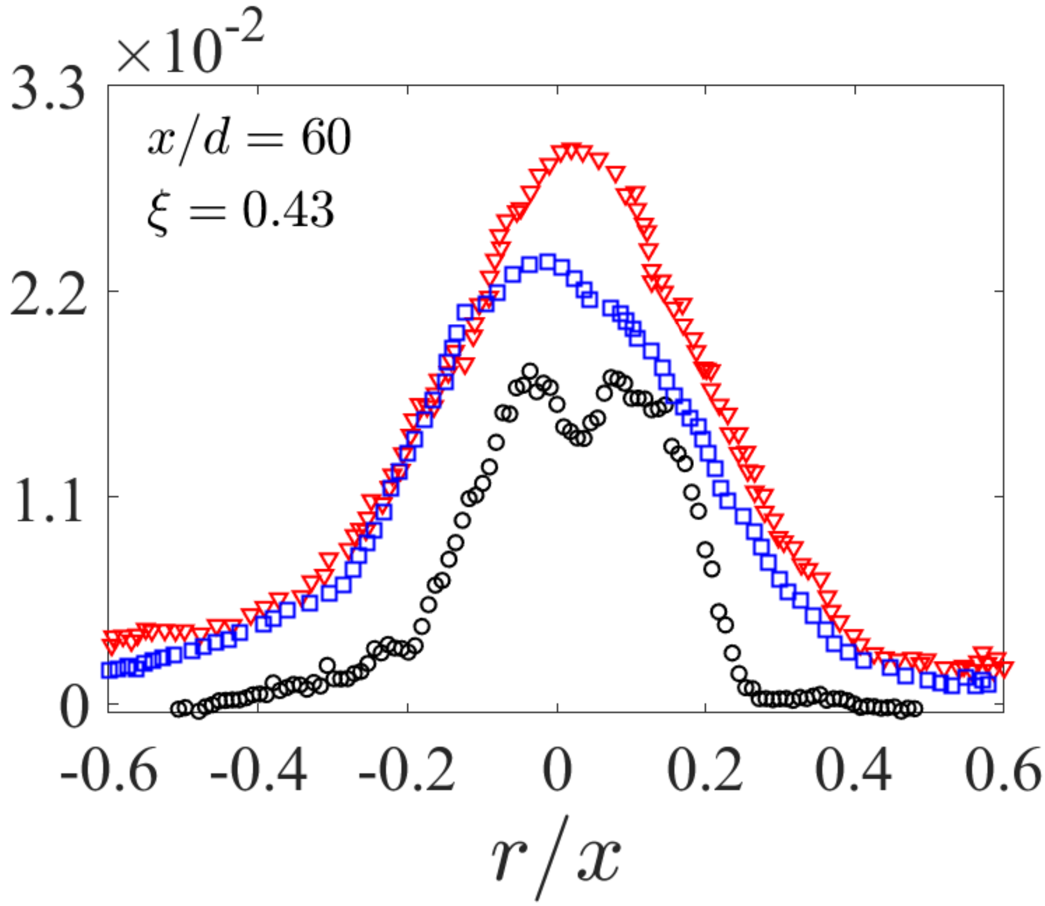
×10-2
3.3
2.2
1.1
0
$x/d = 60$
$\xi = 0.43$
-0.6
-0.4
-0.2
0
0.2
0.4
0.6
r/x

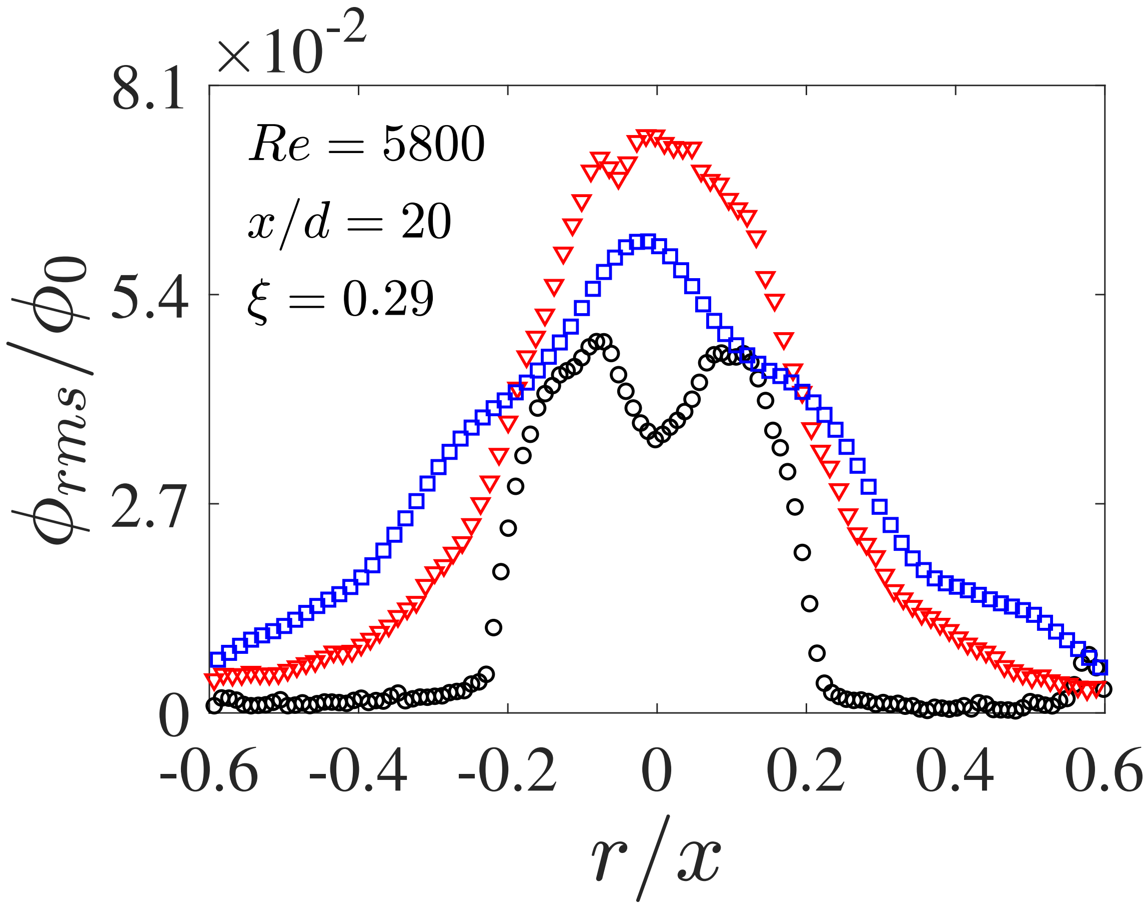

$\times 10^{-2}$
8.1
5.4
2.7
0
ϕ_{rms}/ϕ_0
$Re = 5800$
$x/d = 20$
$\xi = 0.29$
-0.6
-0.4
-0.2
0
0.2
0.4
0.6
r/x

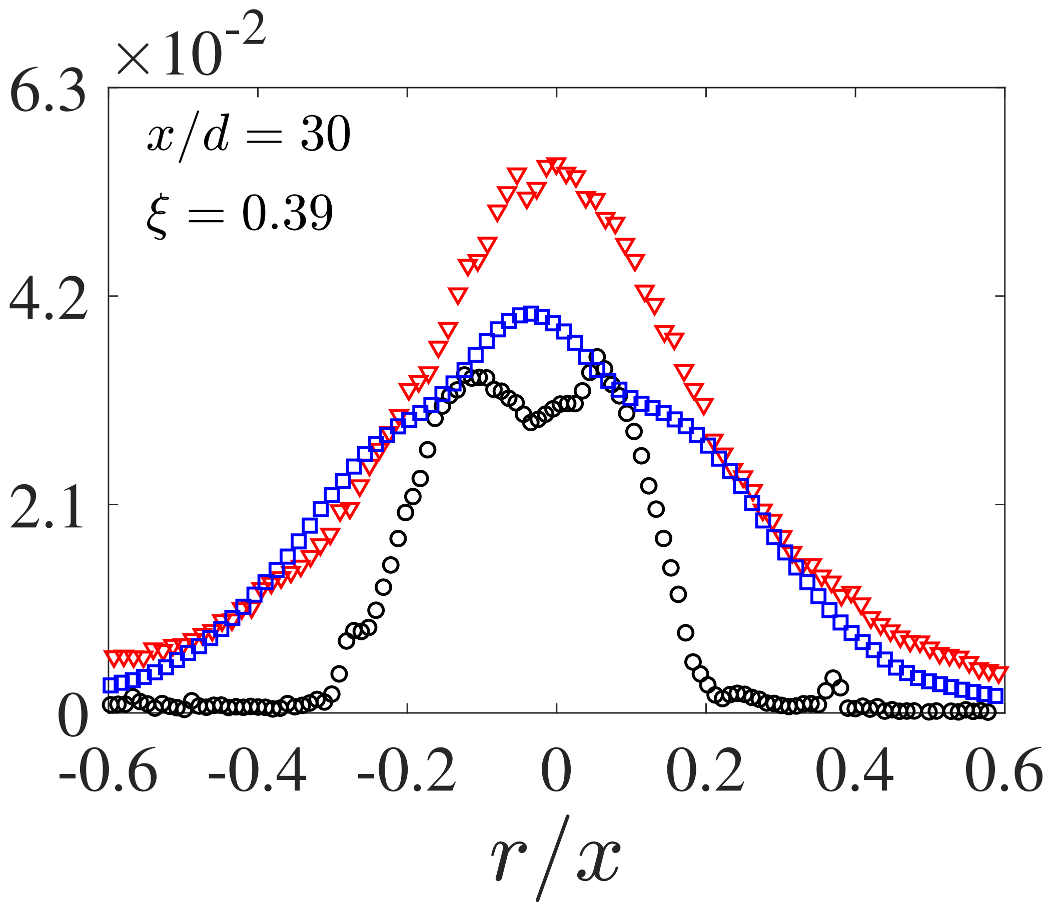
$\times 10^{-2}$
6.3
4.2
2.1
0
$x/d = 30$
$\xi = 0.39$
-0.6
-0.4
-0.2
0
0.2
0.4
0.6
r/x

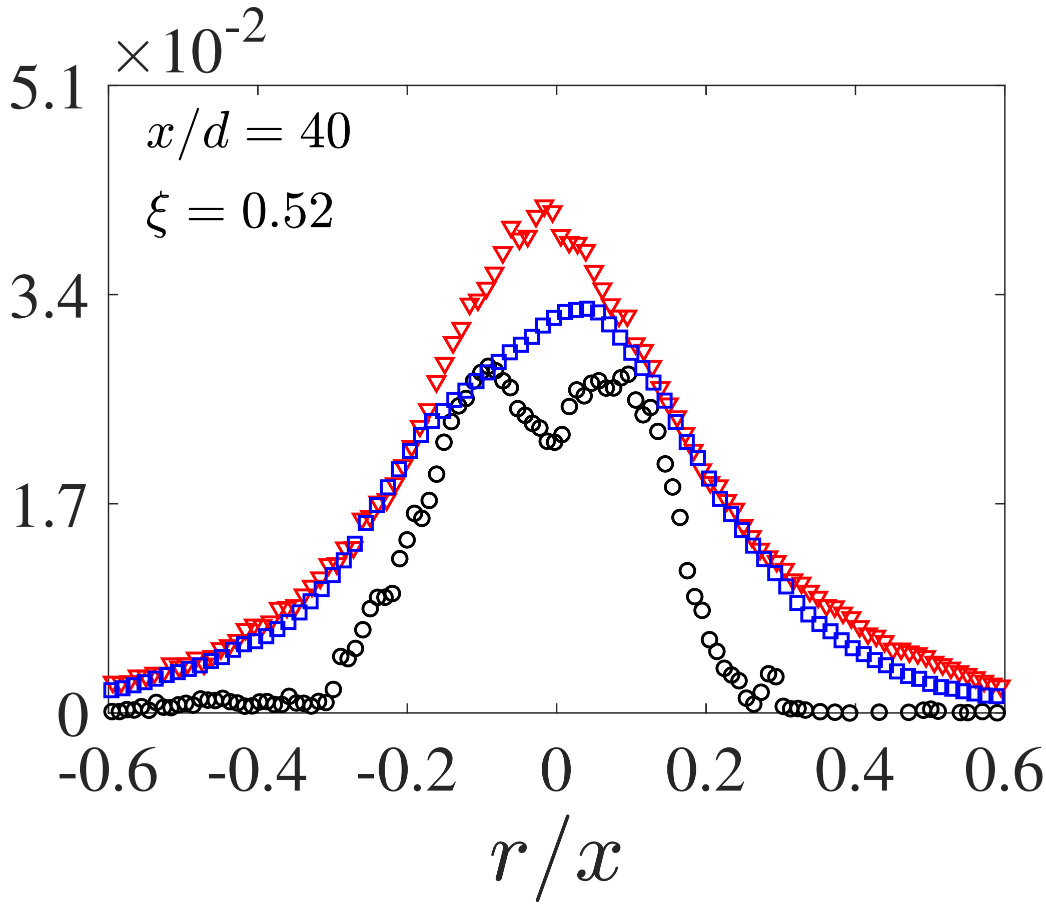
×10^-2
5.1
3.4
1.7
0
x/d = 40
ξ = 0.52
-0.6
-0.4
-0.2
0
0.2
0.4
0.6
r/x

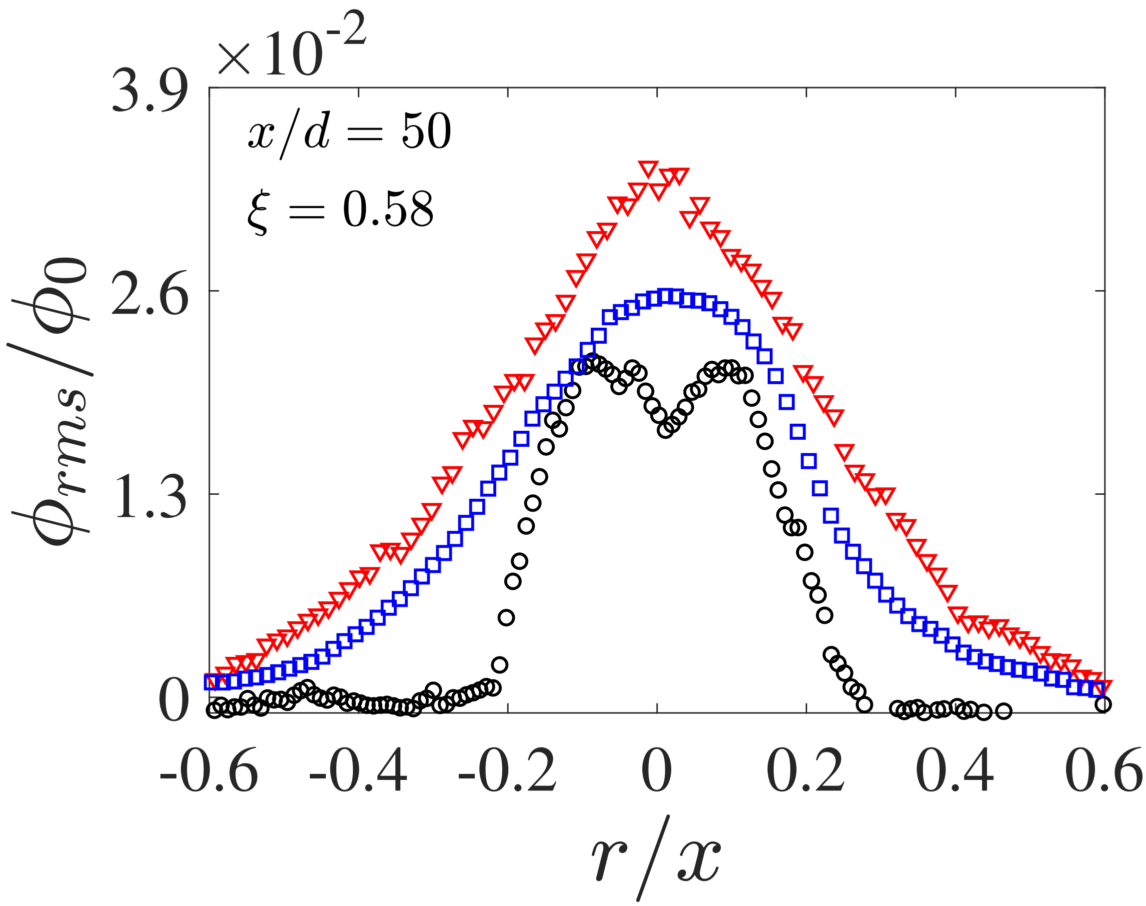
$\times 10^{-2}$
3.9
2.6
1.3
0
$x/d = 50$
$\xi = 0.58$
ϕ_{rms}/ϕ_0
-0.6
-0.4
-0.2
0
0.2
0.4
0.6
r/x

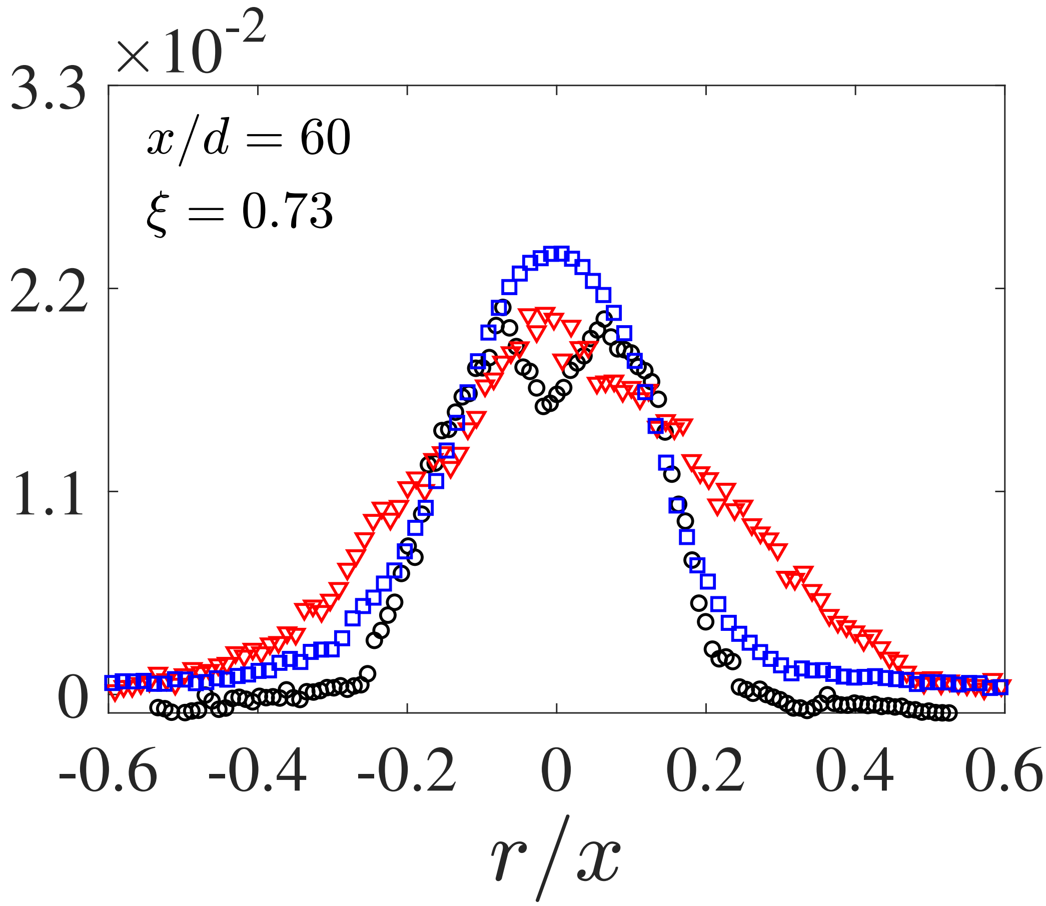
×10^-2
3.3
2.2
1.1
0
x/d = 60
ξ = 0.73
-0.6
-0.4
-0.2
0
0.2
0.4
0.6
r/x

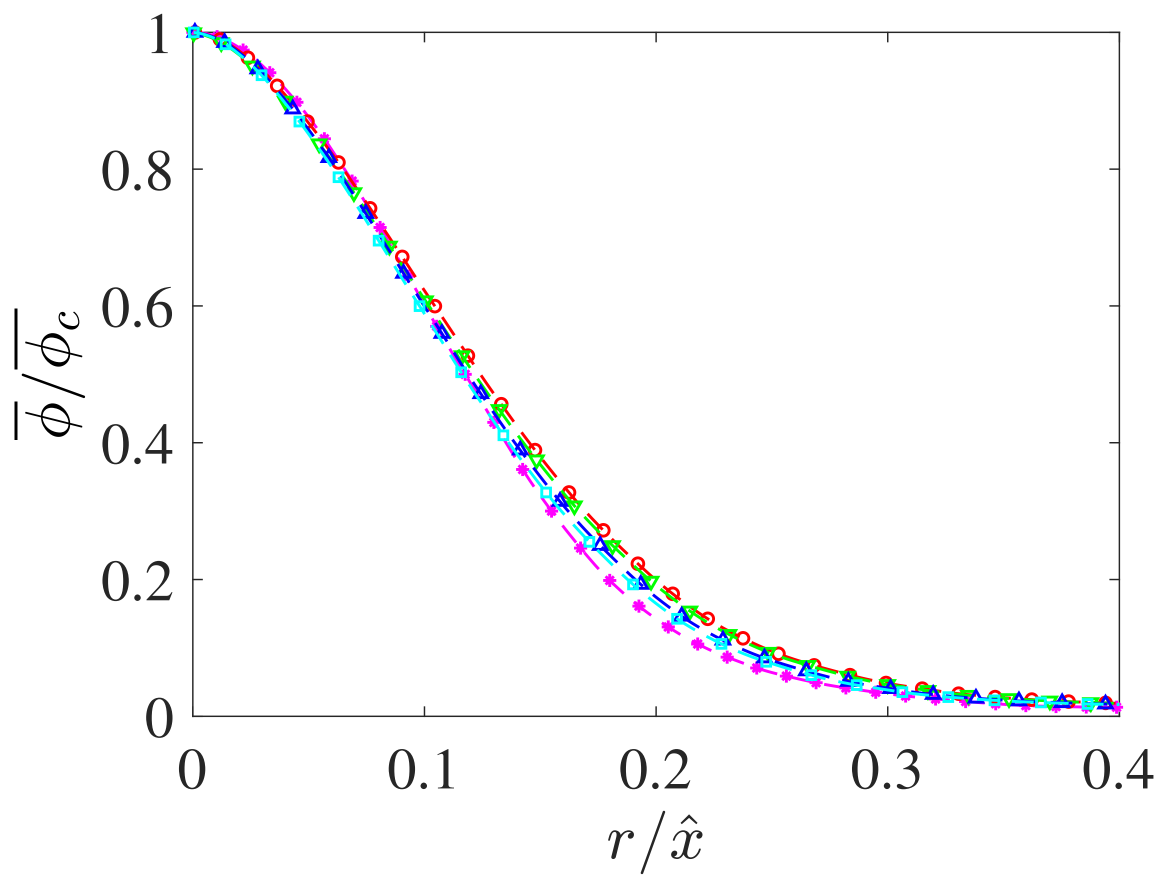
$\overline{\phi}/\overline{\phi_c}$
1
0.8
0.6
0.4
0.2
0
0
0.1
0.2
0.3
0.4
$r/\hat{x}$

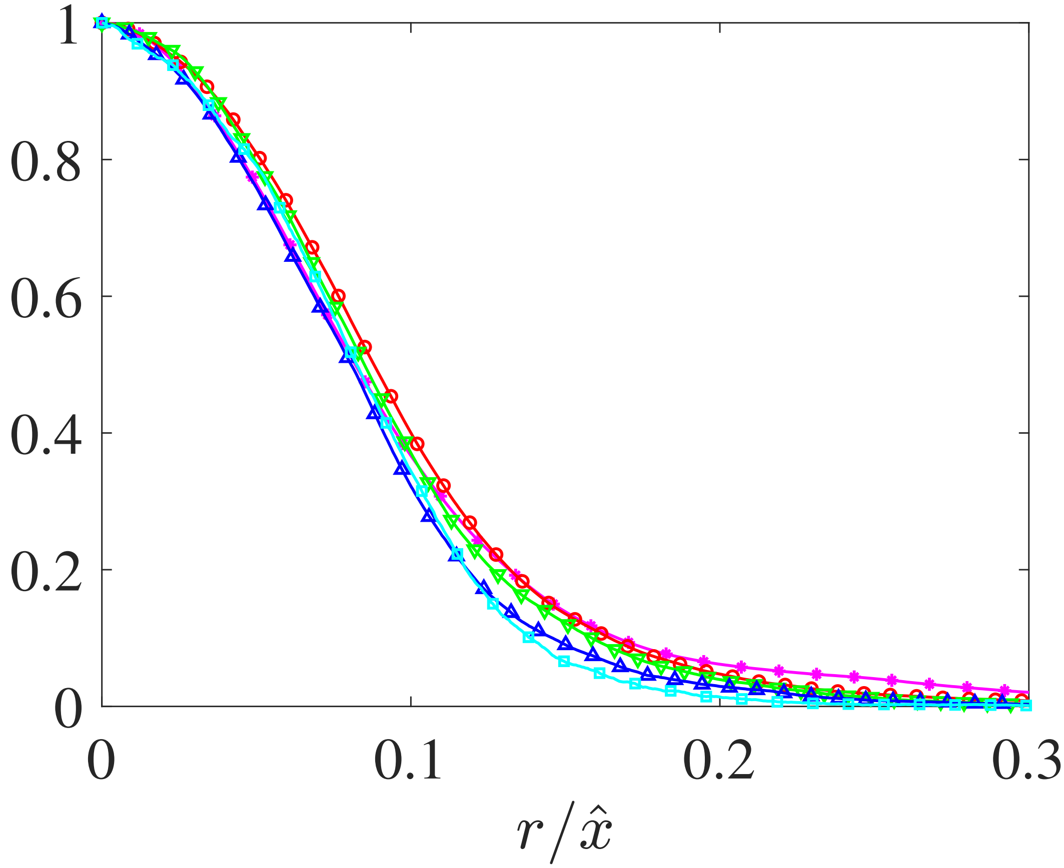
1
0.8
0.6
0.4
0.2
0
0
0.1
0.2
0.3
$r/\hat{x}$

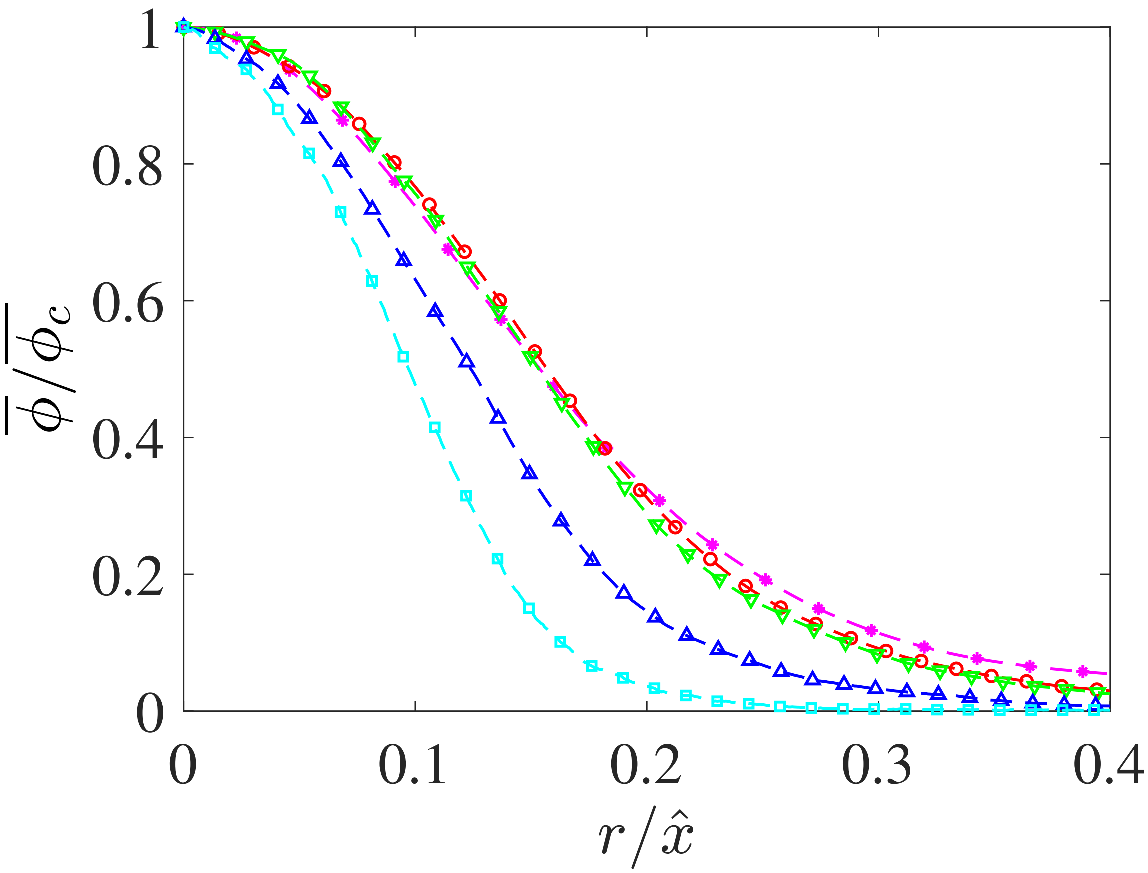
1
0.8
0.6
0.4
0.2
0
$\overline{\phi}/\overline{\phi_c}$
0
0.1
0.2
0.3
0.4
$r/\hat{x}$

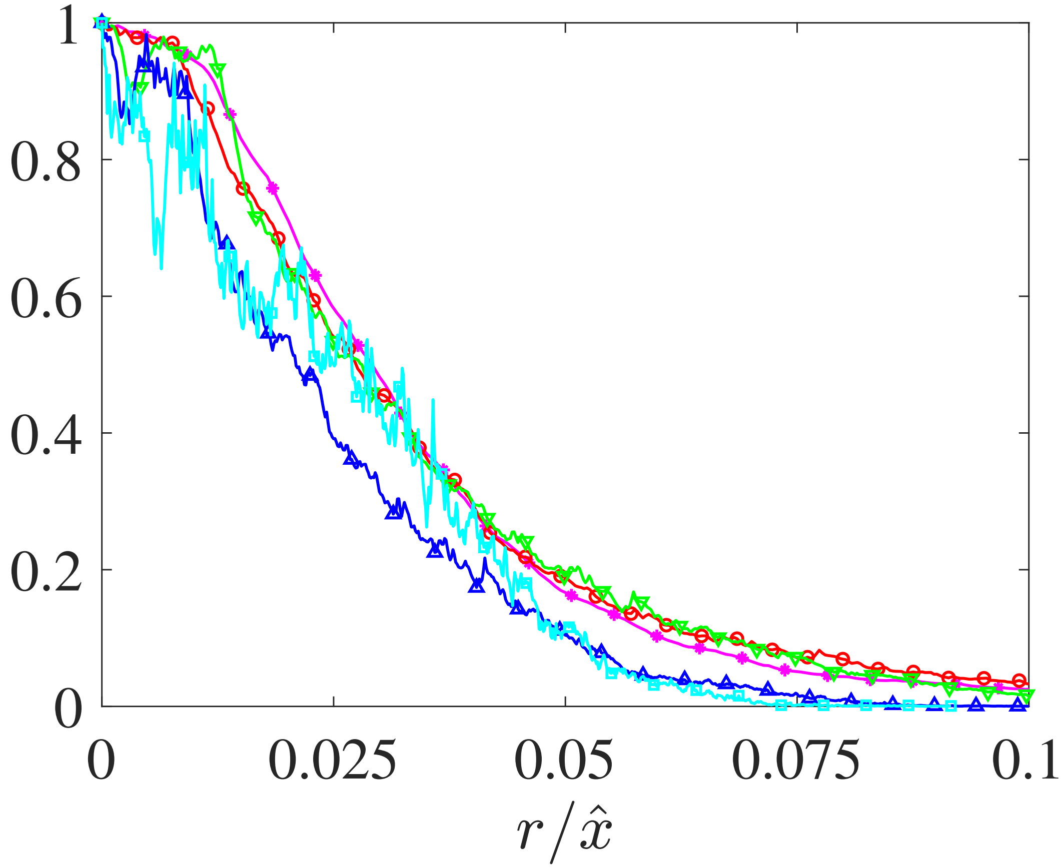
1
0.8
0.6
0.4
0.2
0
0
0.025
0.05
0.075
0.1
$r/\hat{x}$

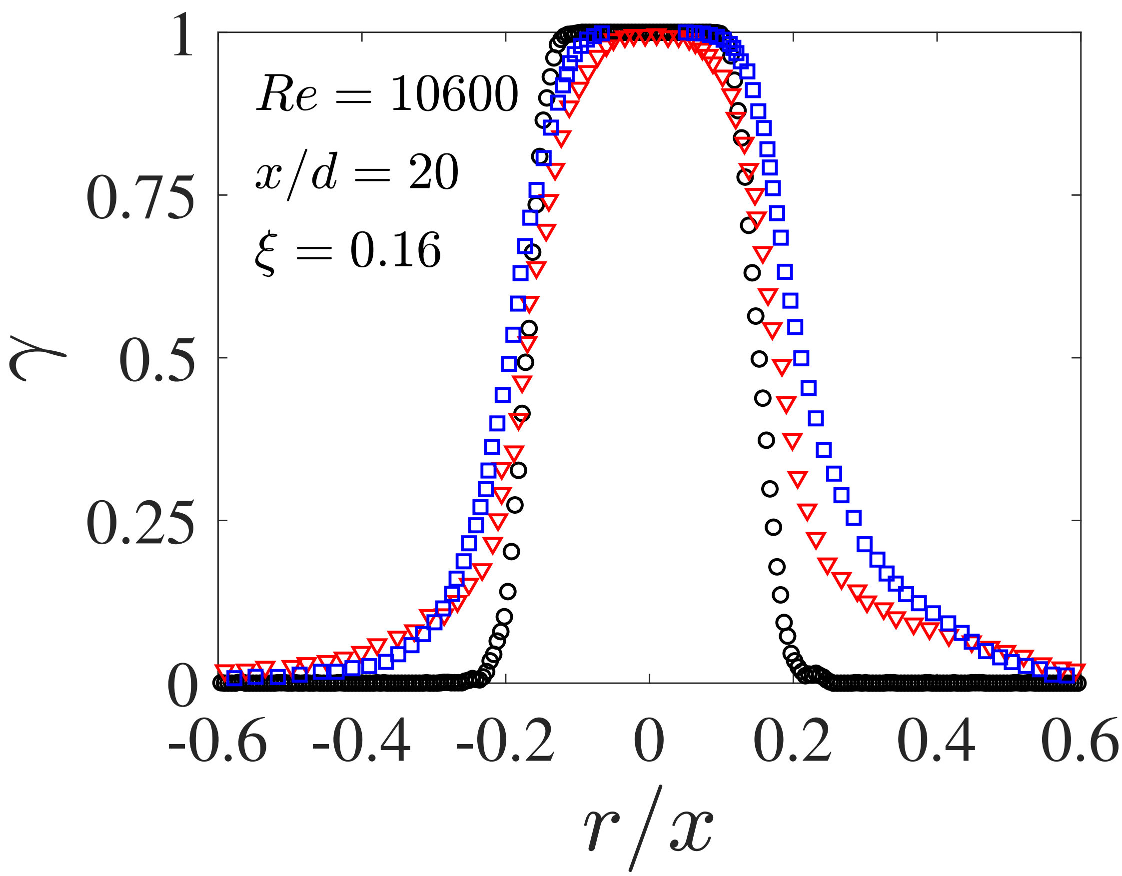
$Re = 10600$
$x/d = 20$
$\xi = 0.16$
γ
1
0.75
0.5
0.25
0
-0.6
-0.4
-0.2
0
0.2
0.4
0.6
r/x

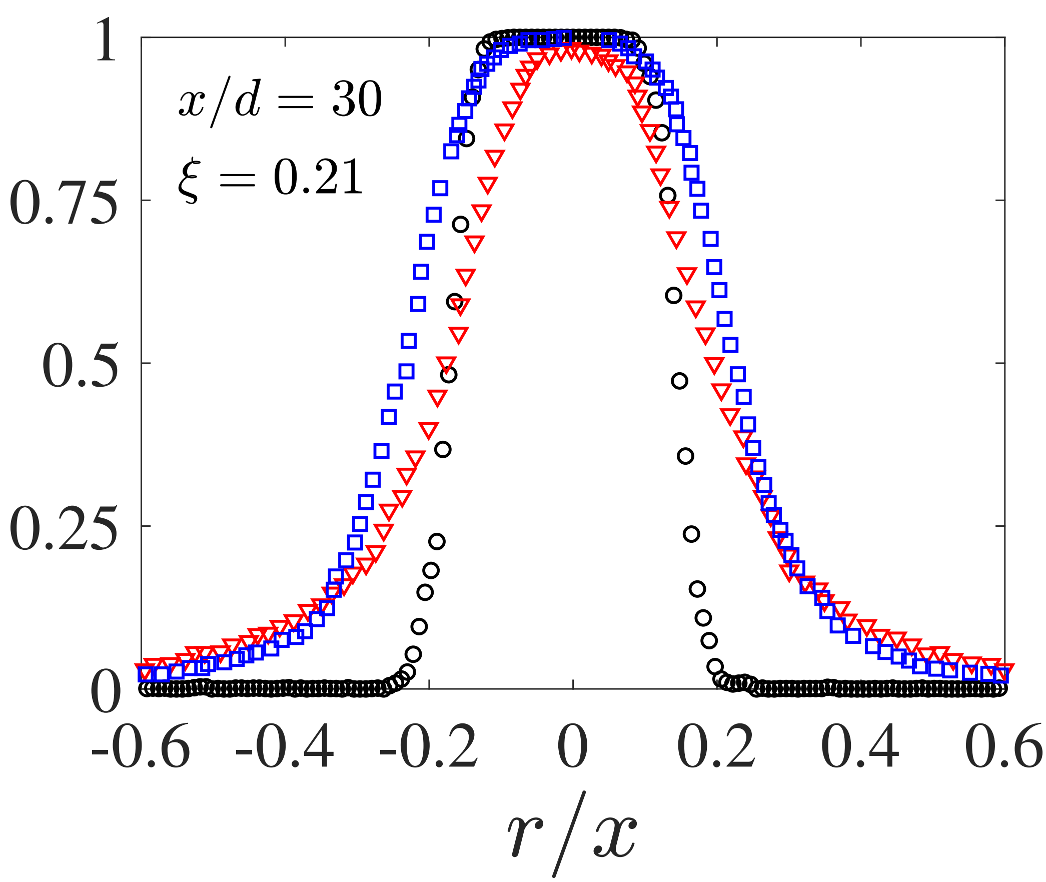
$x/d = 30$
$\xi = 0.21$
1
0.75
0.5
0.25
0
-0.6
-0.4
-0.2
0
0.2
0.4
0.6
r/x

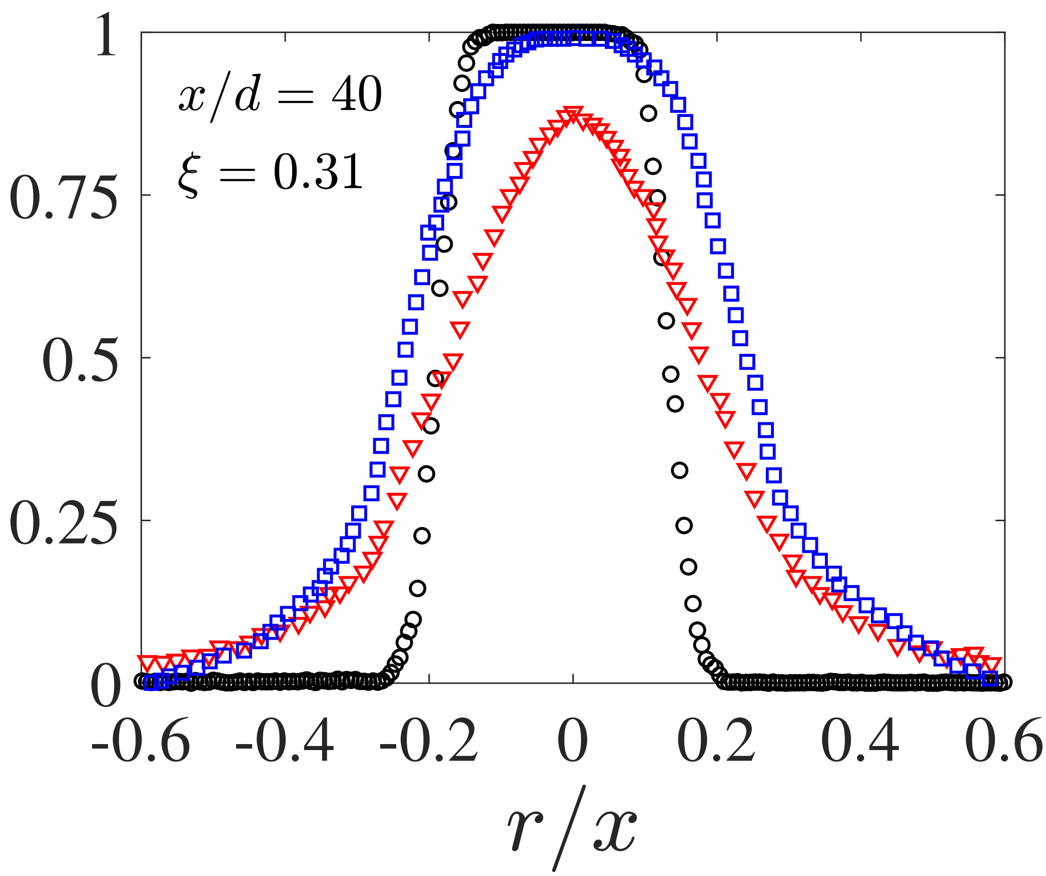
$x/d = 40$
$\xi = 0.31$
1
0.75
0.5
0.25
0
-0.6
-0.4
-0.2
0
0.2
0.4
0.6
r/x

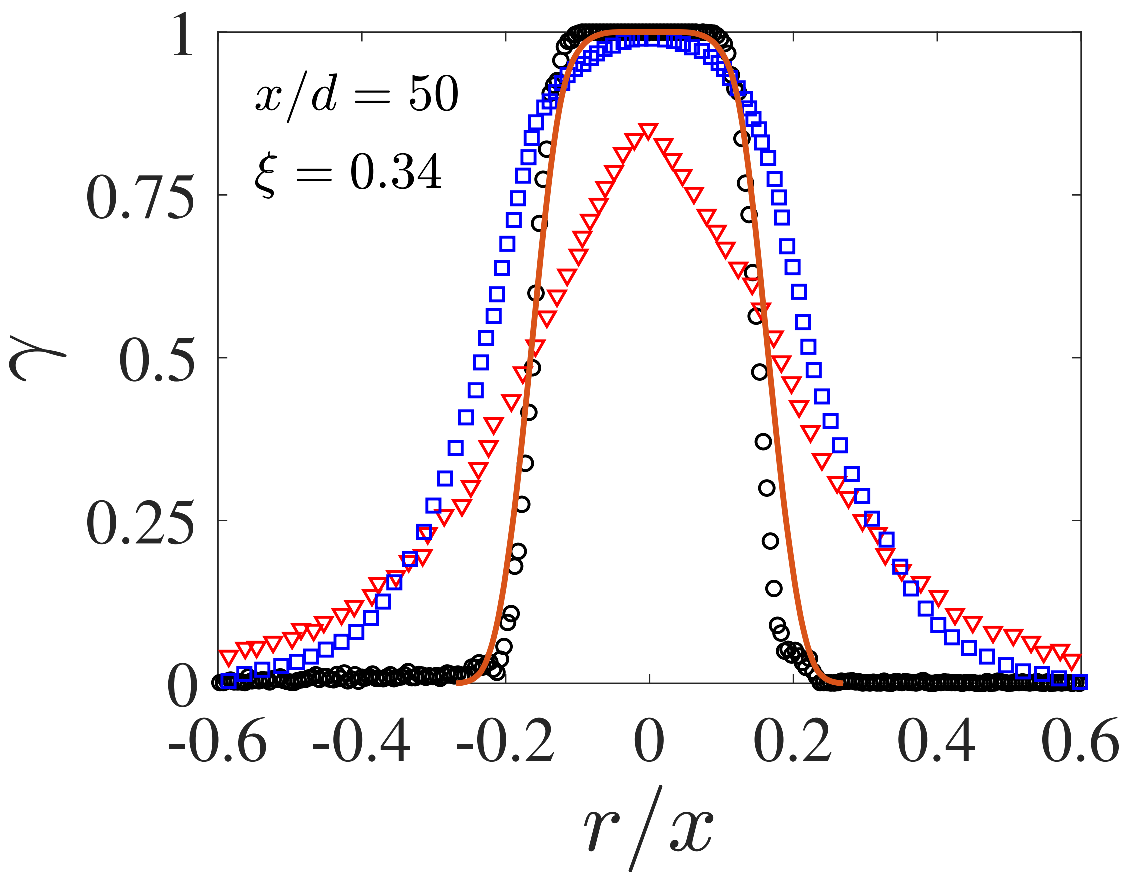
$x/d = 50$
$\xi = 0.34$
γ
r/x
1
0.75
0.5
0.25
0
-0.6
-0.4
-0.2
0
0.2
0.4
0.6

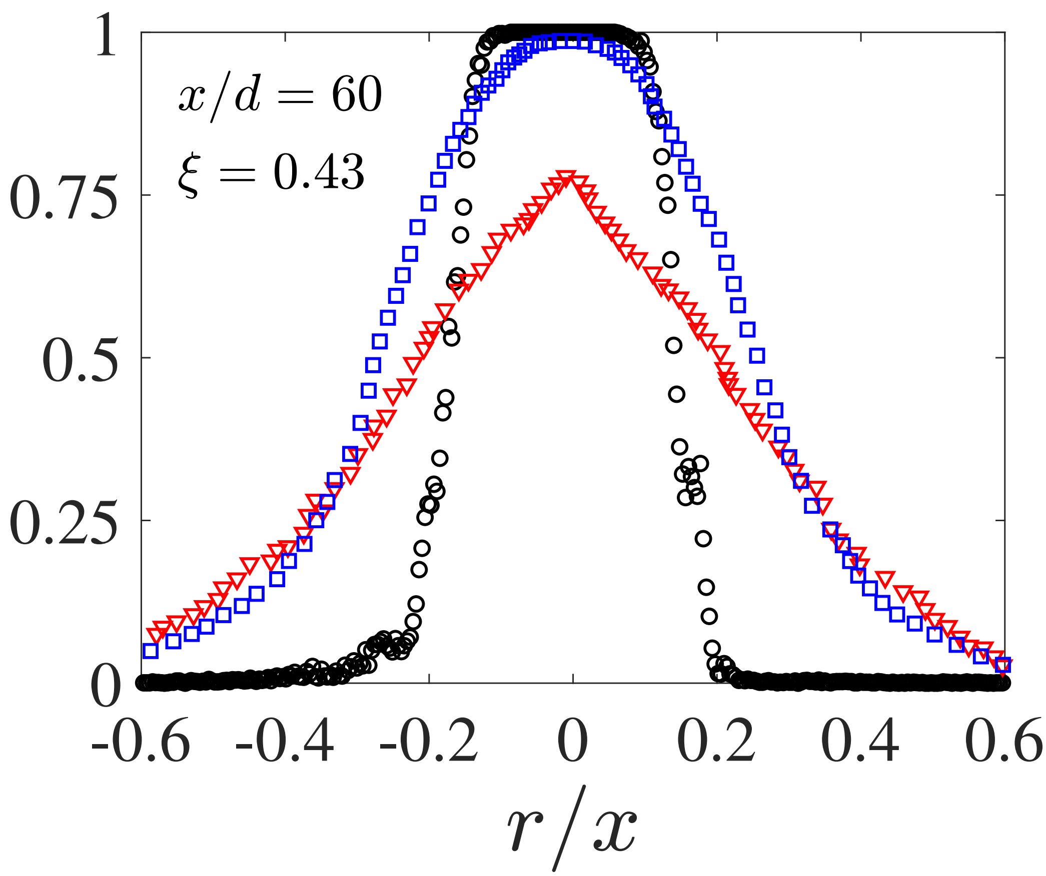
$x/d = 60$
$\xi = 0.43$
1
0.75
0.5
0.25
0
-0.6
-0.4
-0.2
0
0.2
0.4
0.6
r/x

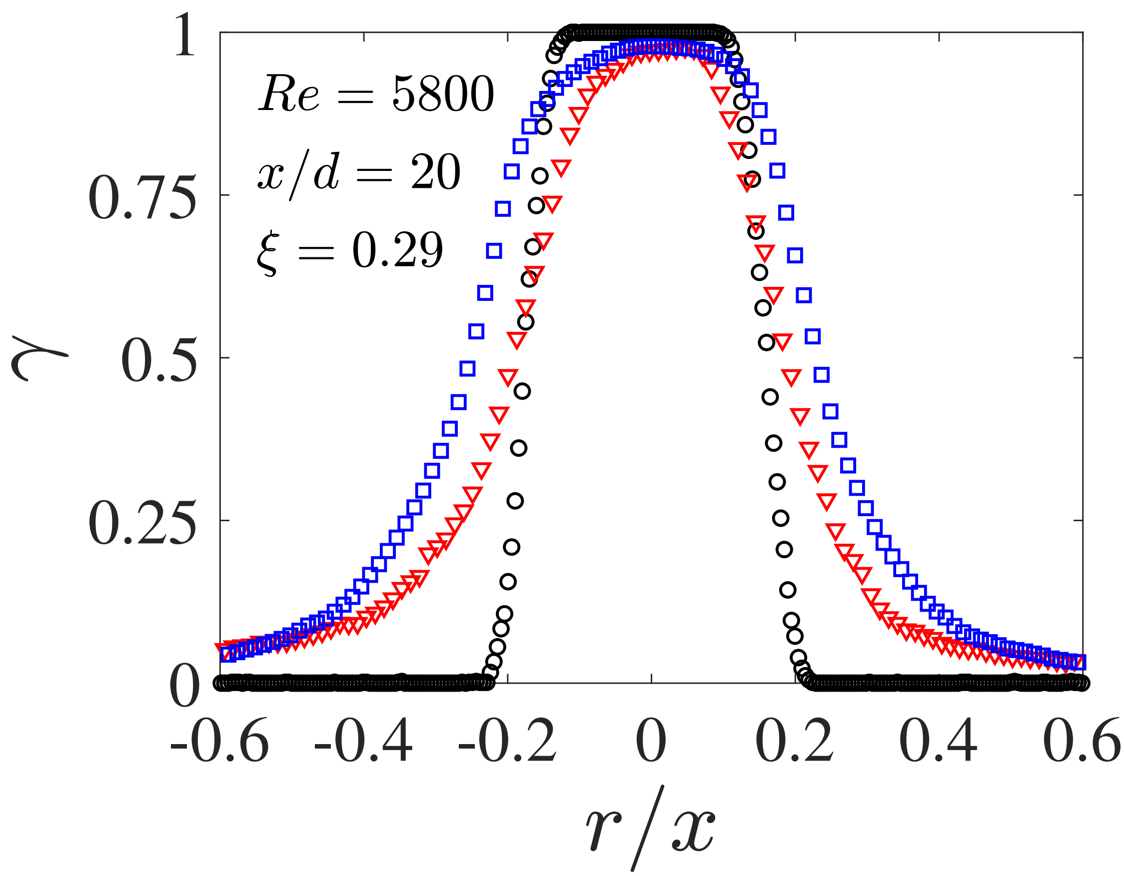
$Re = 5800$
$x/d = 20$
$\xi = 0.29$
γ
1
0.75
0.5
0.25
0
-0.6
-0.4
-0.2
0
0.2
0.4
0.6
r/x

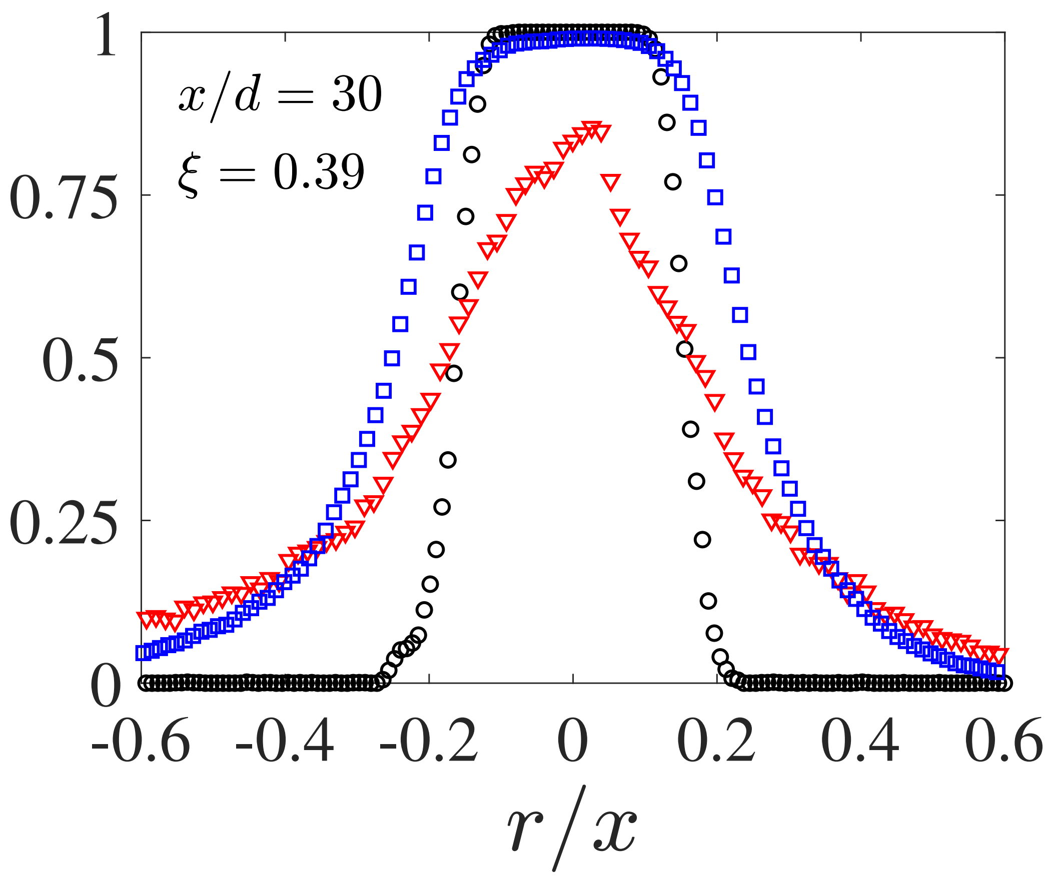

$x/d = 30$
$\xi = 0.39$
1
0.75
0.5
0.25
0
-0.6
-0.4
-0.2
0
0.2
0.4
0.6
r/x

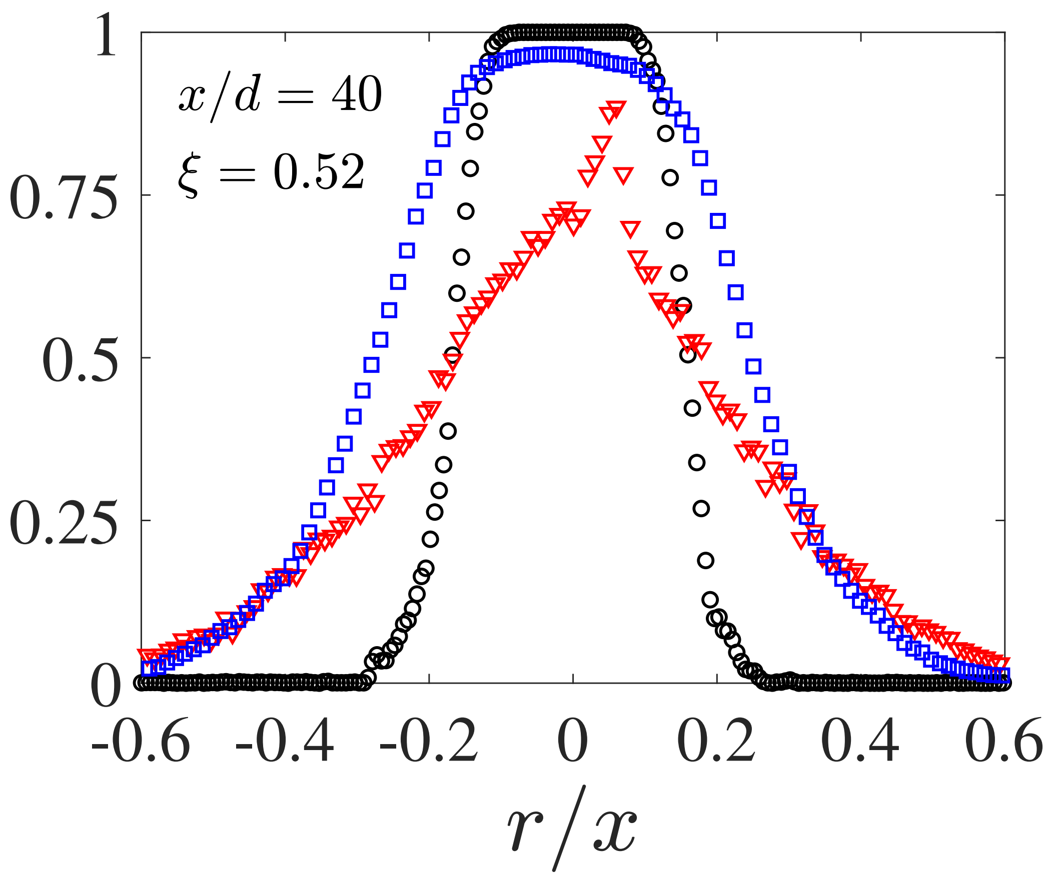
$x/d = 40$
$\xi = 0.52$
1
0.75
0.5
0.25
0
-0.6
-0.4
-0.2
0
0.2
0.4
0.6
r/x

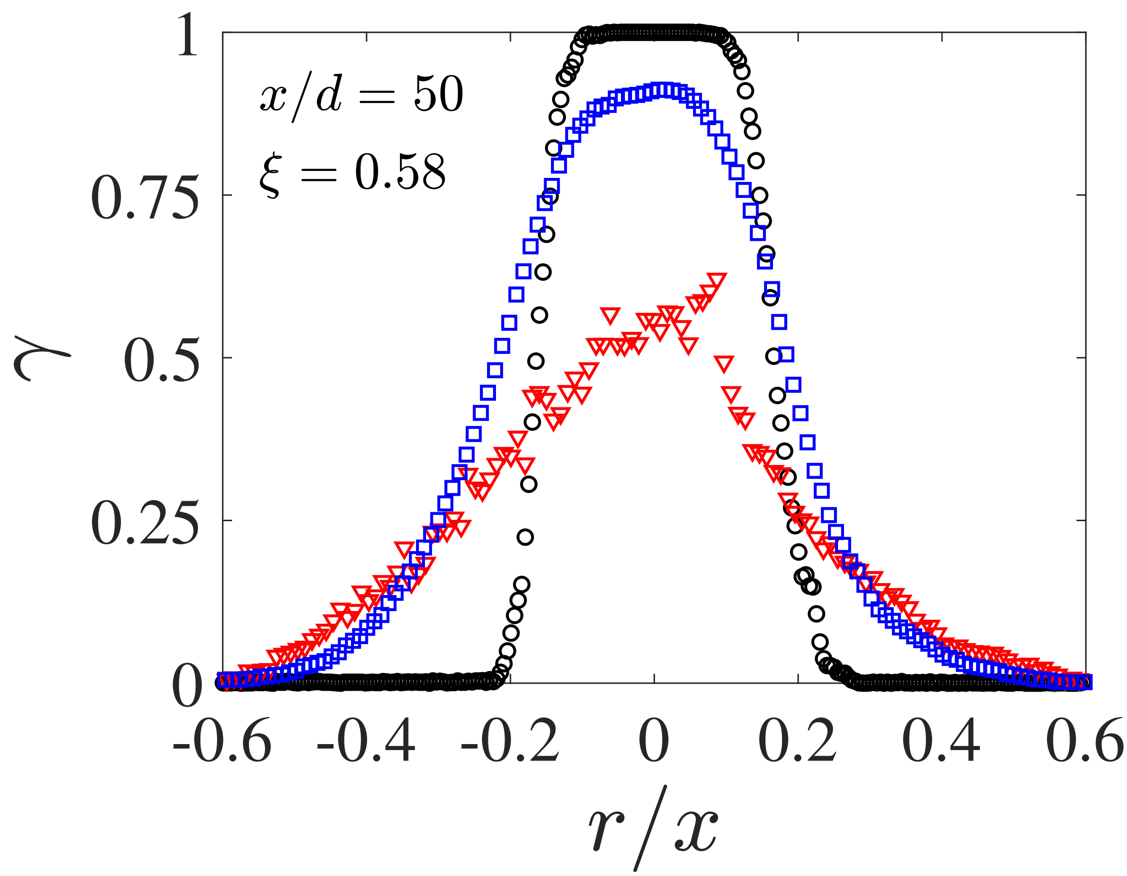
$x/d = 50$
$\xi = 0.58$
1
0.75
0.5
0.25
0
γ
-0.6
-0.4
-0.2
0
0.2
0.4
0.6
r/x

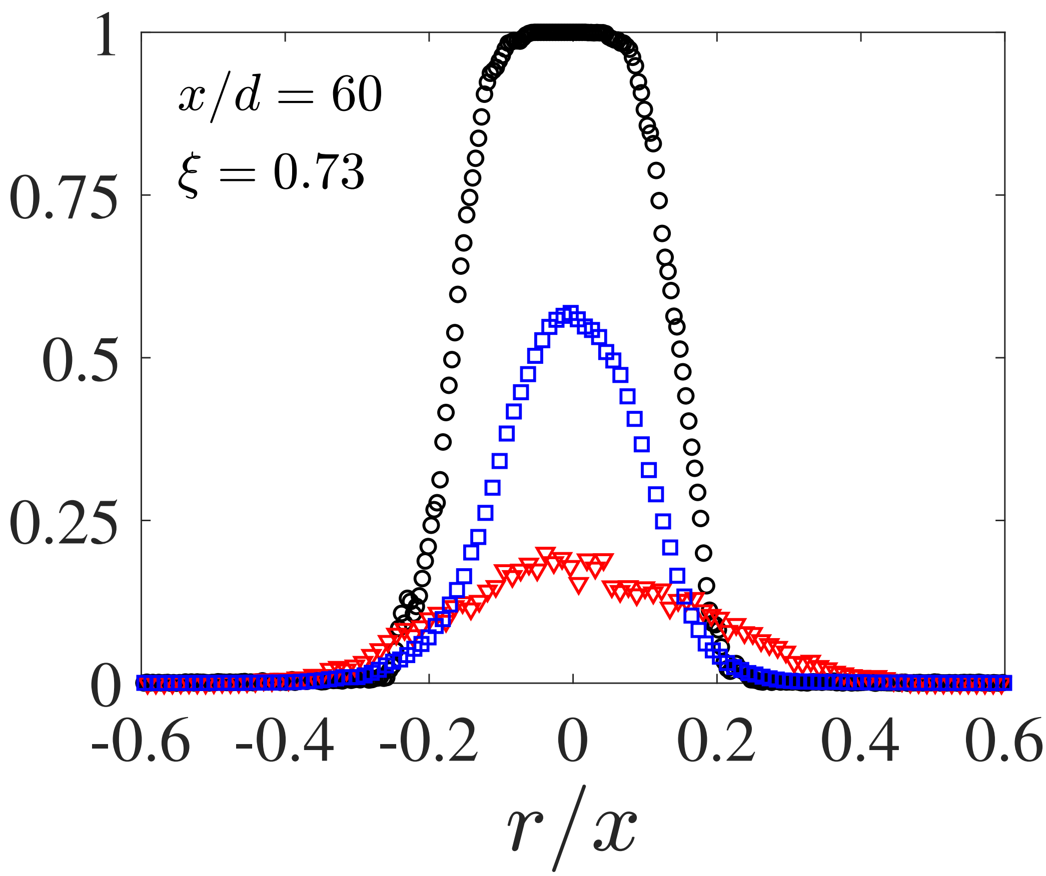
$x/d = 60$
$\xi = 0.73$
1
0.75
0.5
0.25
0
-0.6
-0.4
-0.2
0
0.2
0.4
0.6
r/x

PLEASE CITE THIS ARTICLE AS DOI: 10.1063/5.0071023

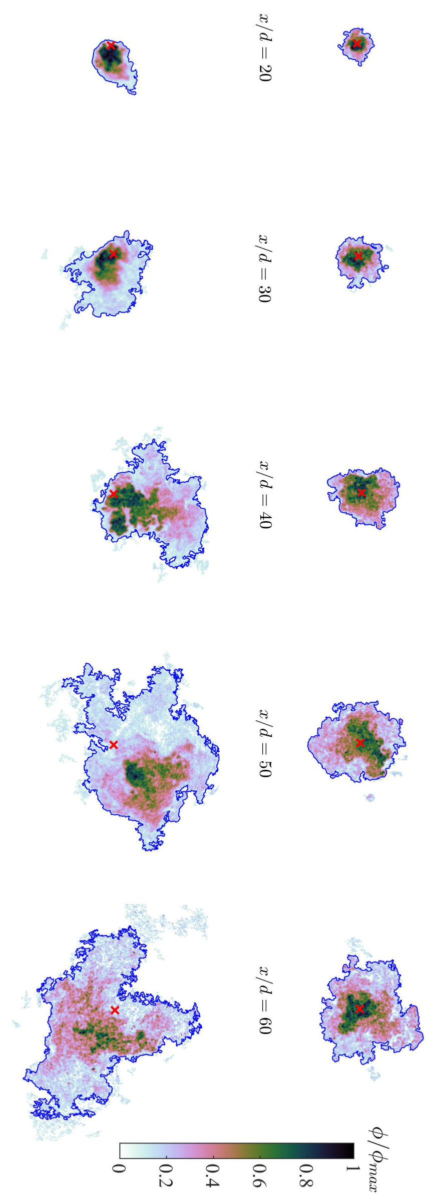

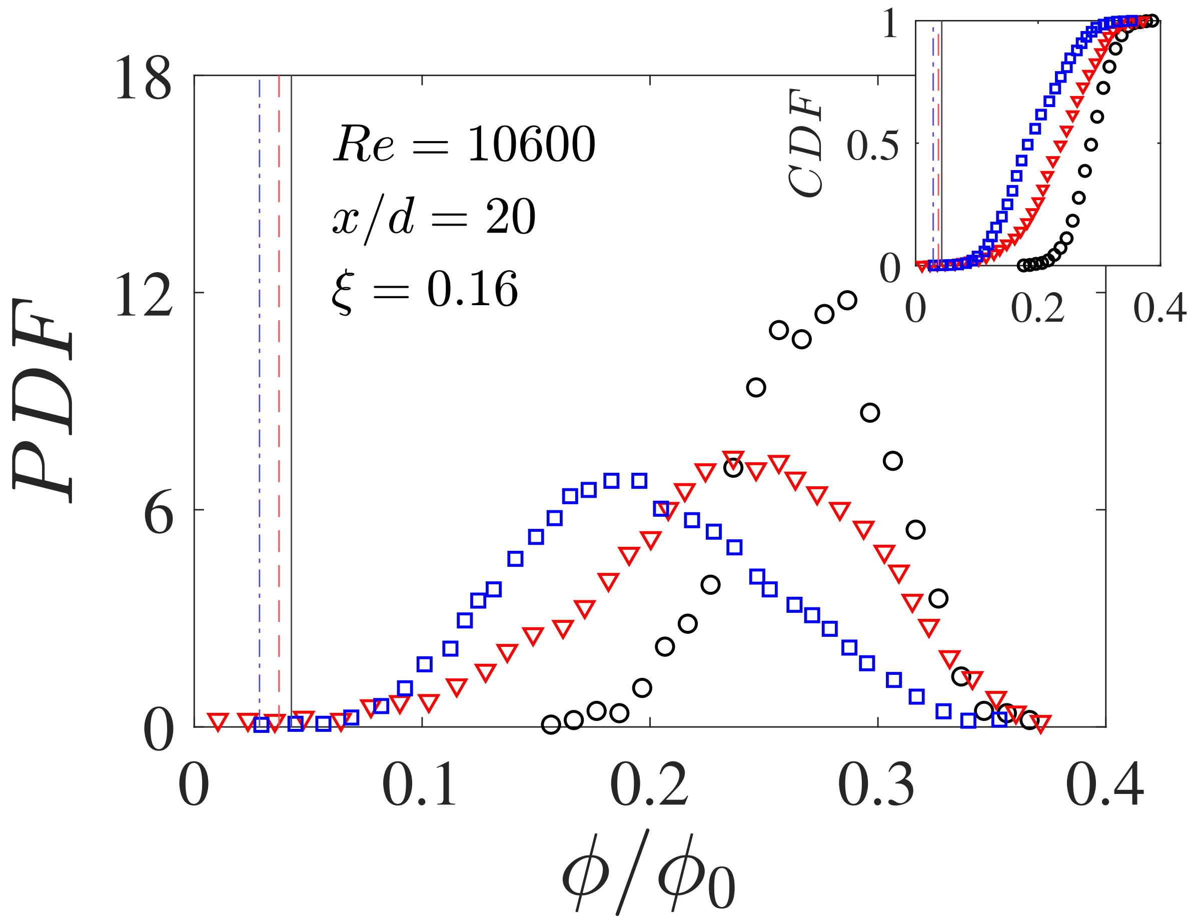
PDF
ϕ/ϕ_0
$Re = 10600$
$x/d = 20$
$\xi = 0.16$
CDF
0
6
12
18
0
0.1
0.2
0.3
0.4
0
0.5
1
0
0.2
0.4

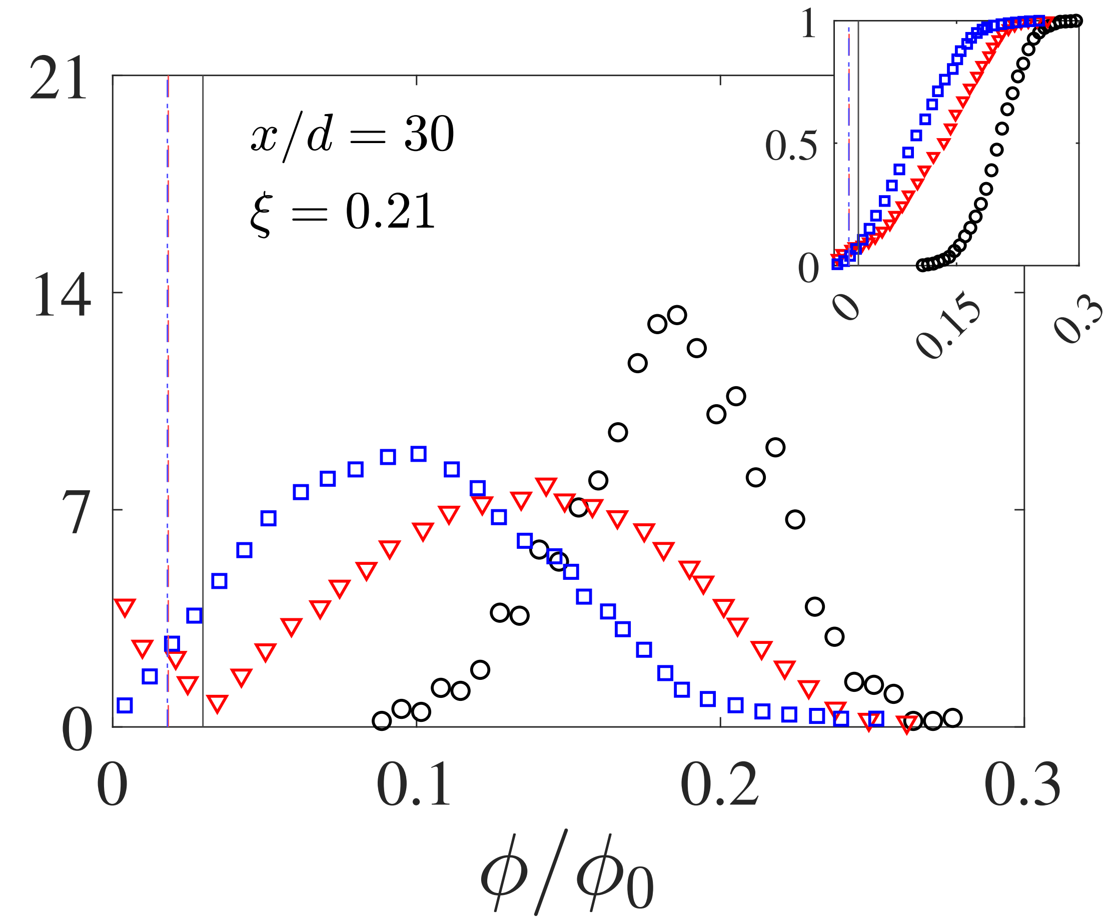
21
14
7
0
0
0.1
0.2
0.3
ϕ/ϕ_0
$x/d = 30$
$\xi = 0.21$
1
0.5
0
0
0.15
0.3

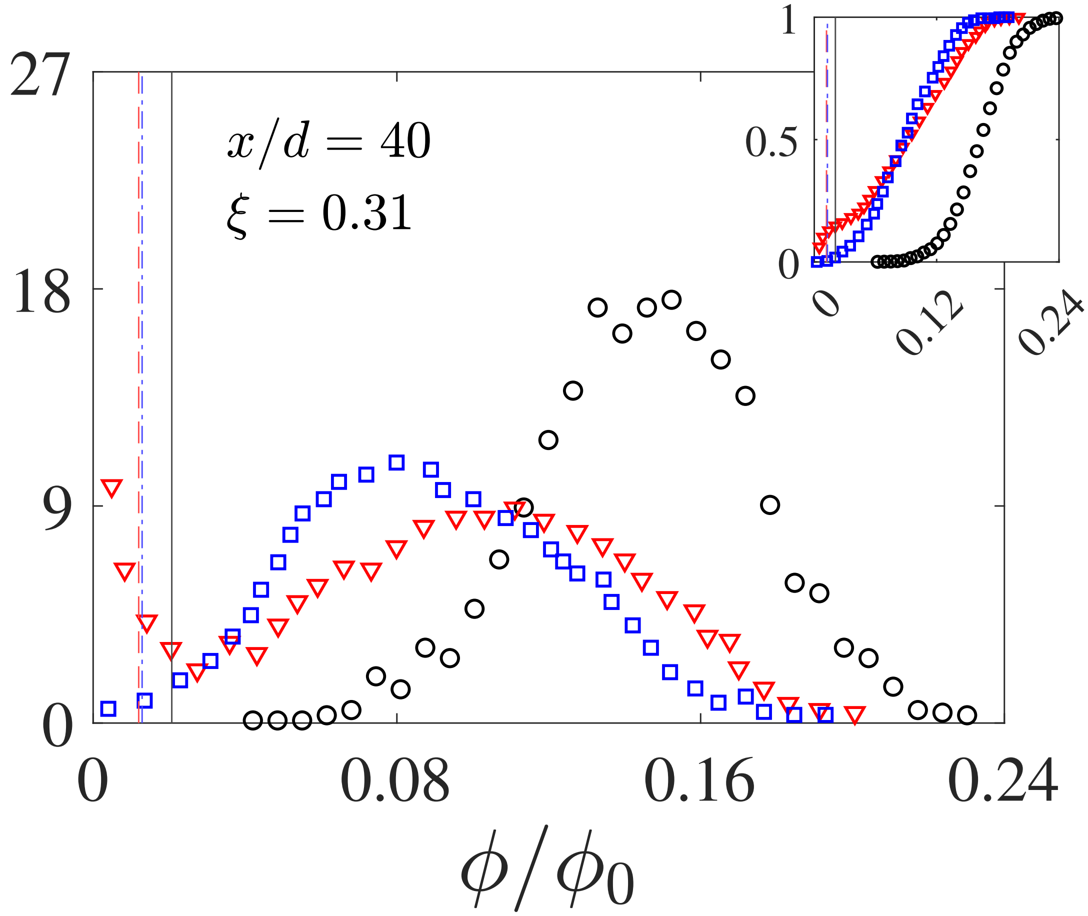
$x/d = 40$
$\xi = 0.31$
27
18
9
0
0
0.08
0.16
0.24
ϕ/ϕ_0
1
0.5
0
0
0.12
0.24

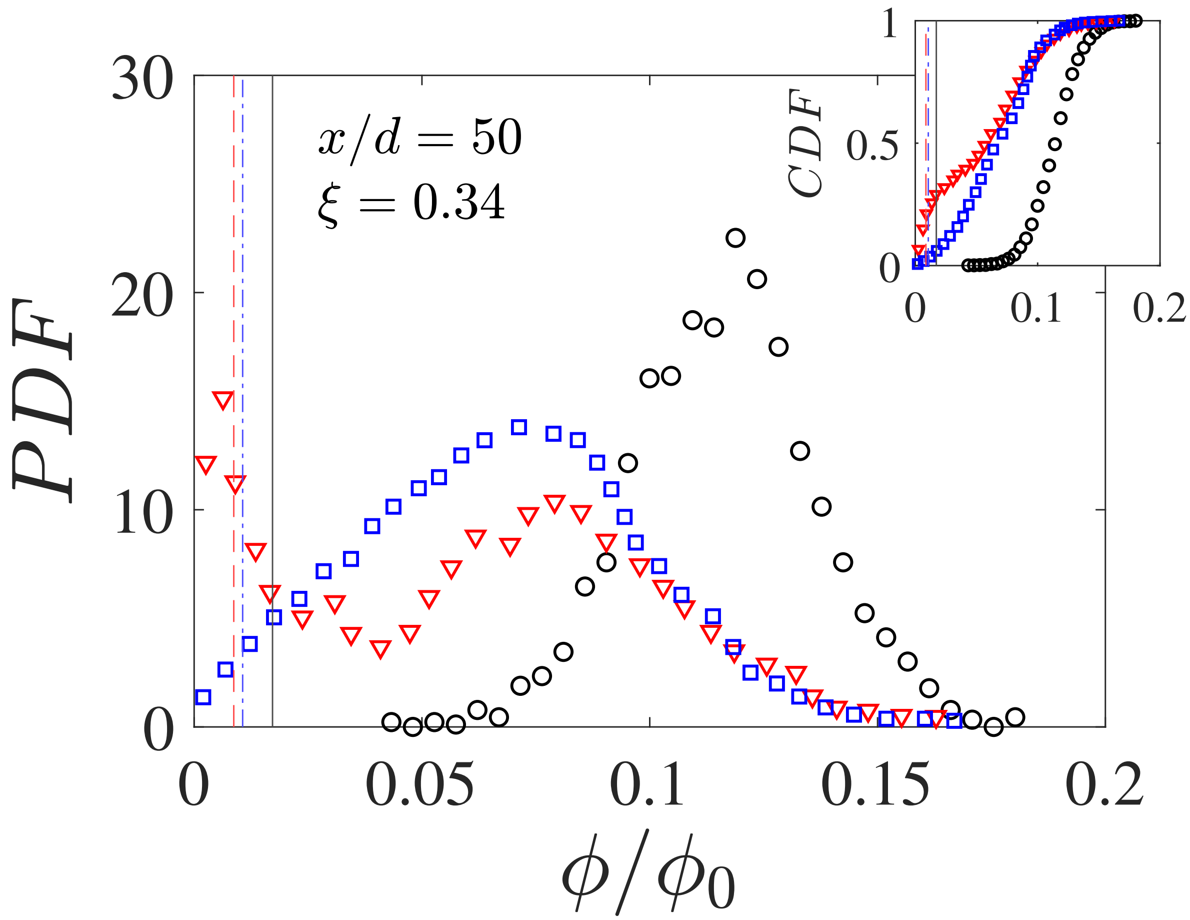
$x/d = 50$
$\xi = 0.34$
PDF
ϕ/ϕ_0
CDF
0
0.05
0.1
0.15
0.2
10
20
30
0.5
1

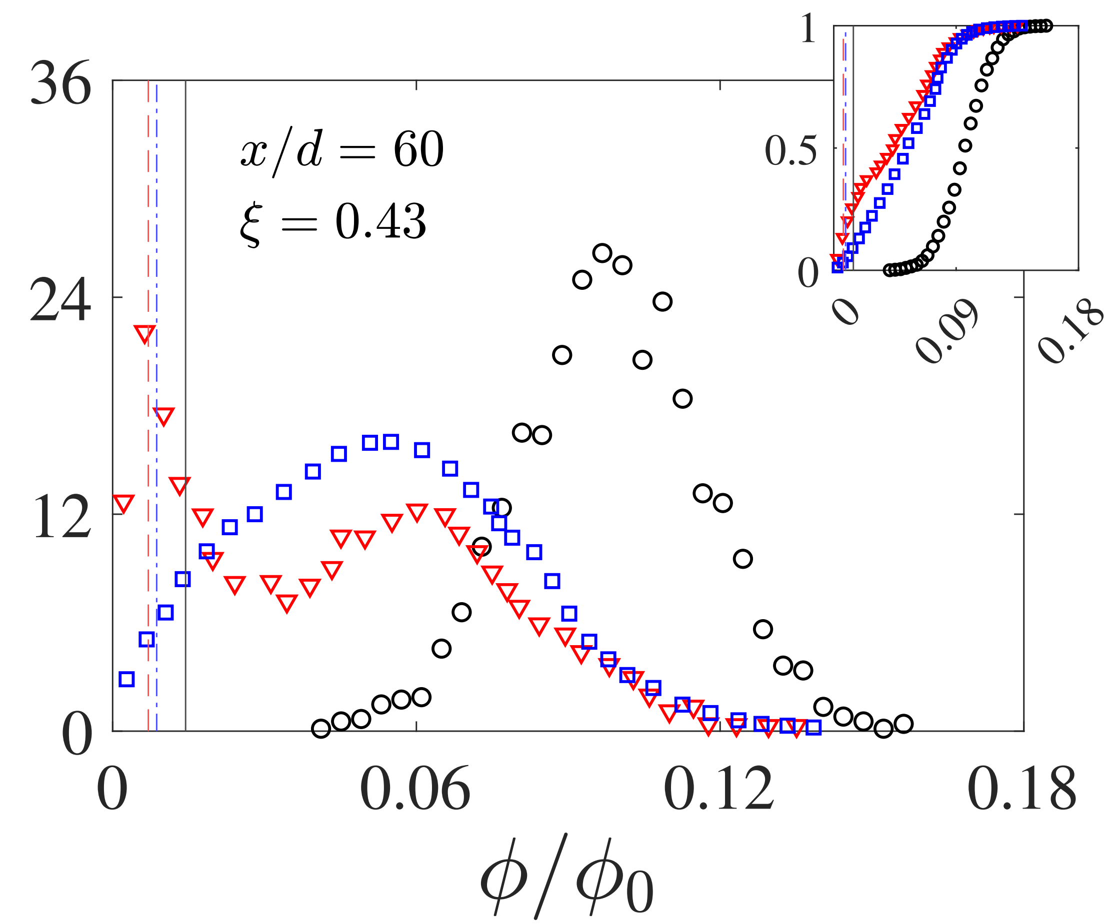
$x/d = 60$
$\xi = 0.43$
36
24
12
0
0
0.06
0.12
0.18
ϕ/ϕ_0
1
0.5
0
0
0.09
0.18

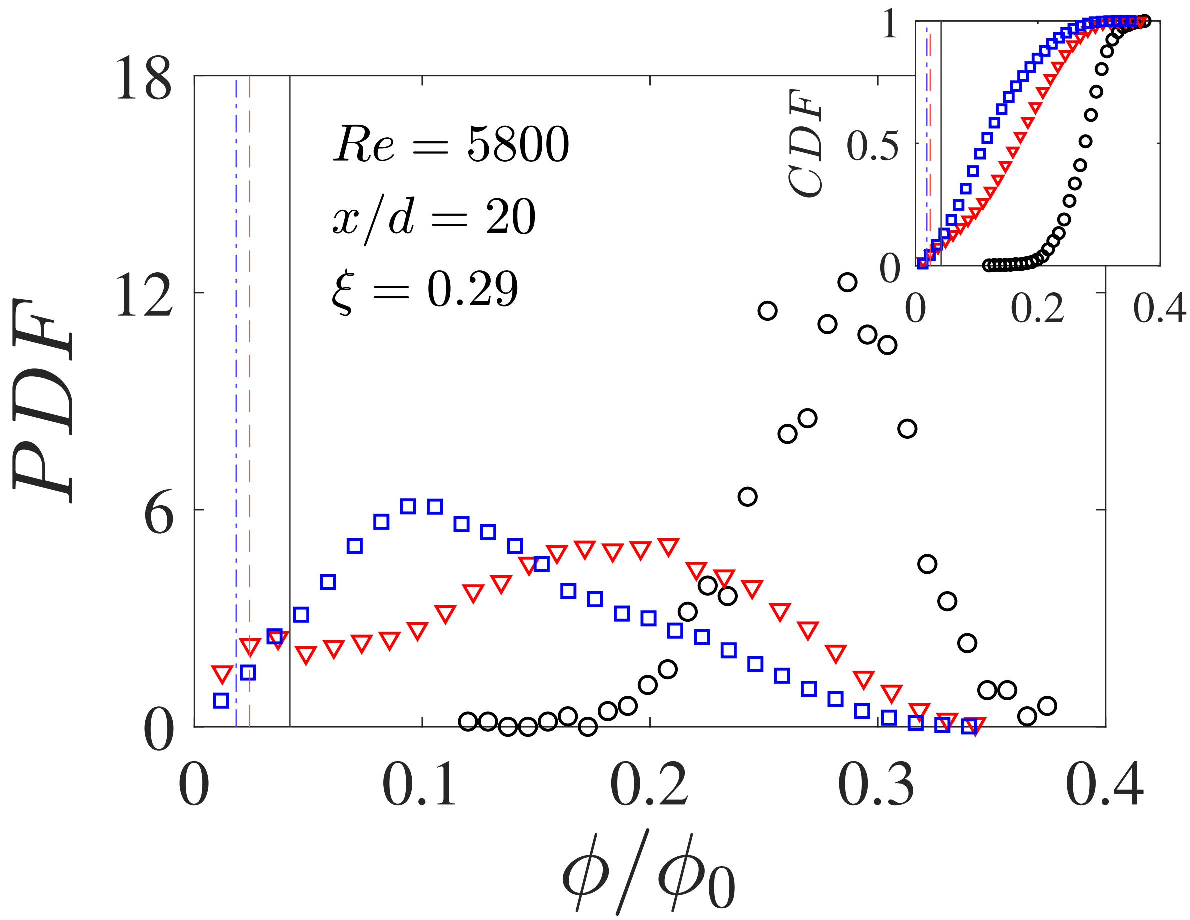
PDF
ϕ/ϕ_0
$Re = 5800$
$x/d = 20$
$\xi = 0.29$
CDF
0
6
12
18
0.1
0.2
0.3
0.4
0.5
1

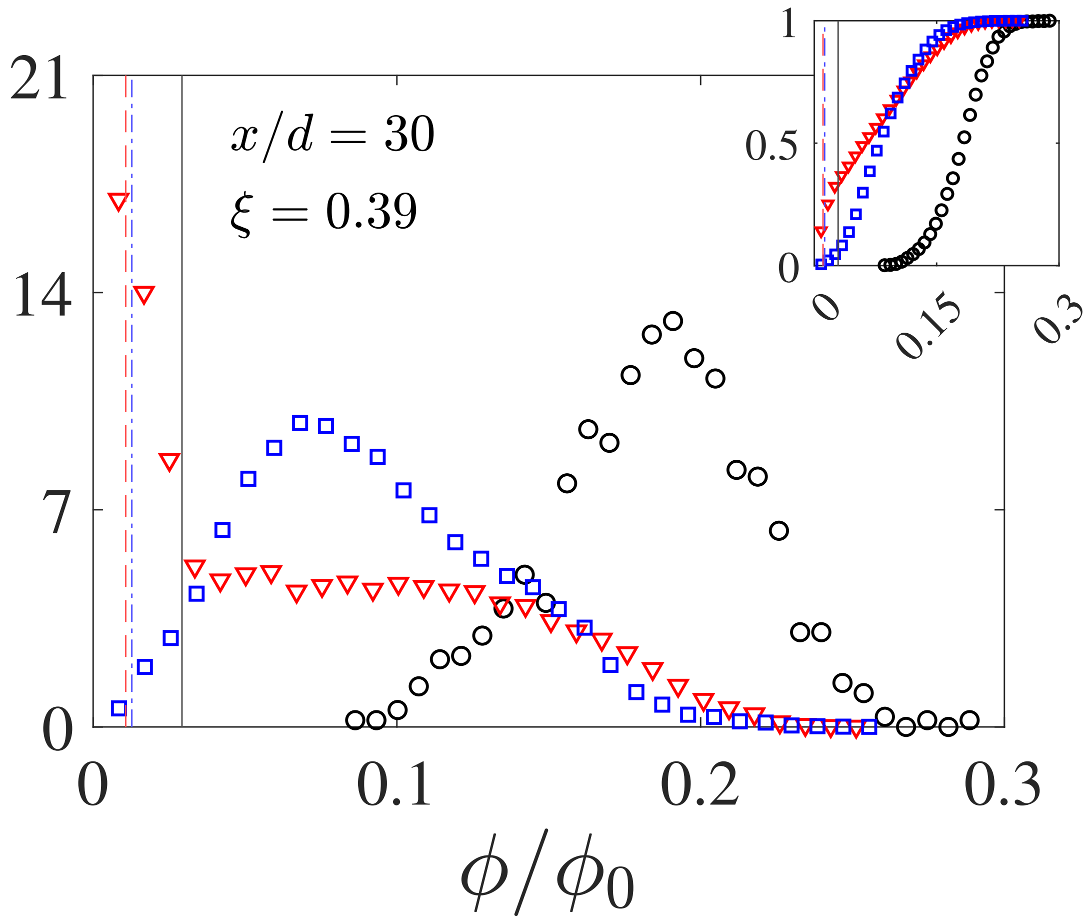
$x/d = 30$
$\xi = 0.39$
21
14
7
0
0
0.1
0.2
0.3
ϕ/ϕ_0
1
0.5
0
0
0.15
0.3

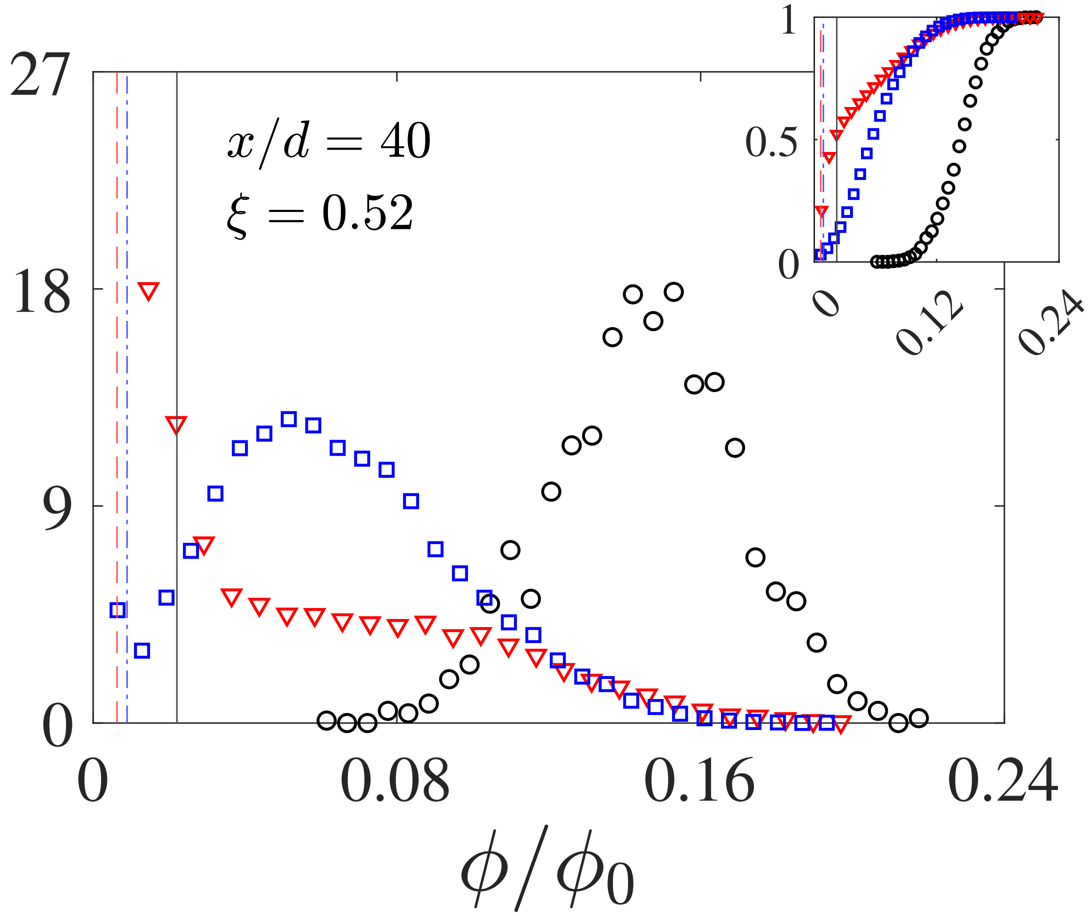
$x/d = 40$
$\xi = 0.52$
27
18
9
0
0
0.08
0.16
0.24
ϕ/ϕ_0
1
0.5
0
0
0.12
0.24

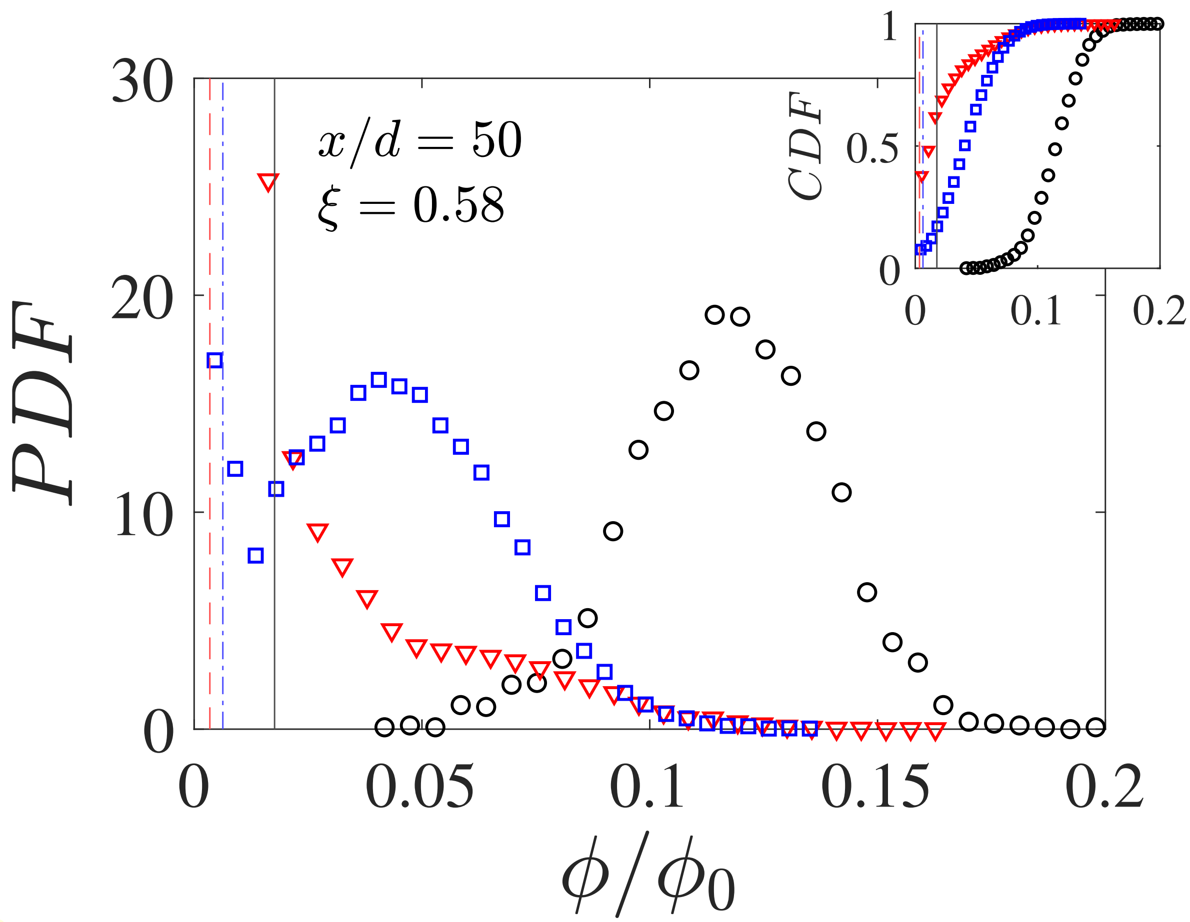
PDF
$x/d = 50$
$\xi = 0.58$
ϕ/ϕ_0
CDF
0
10
20
30
0
0.05
0.1
0.15
0.2
0
0.5
1
0
0.1
0.2

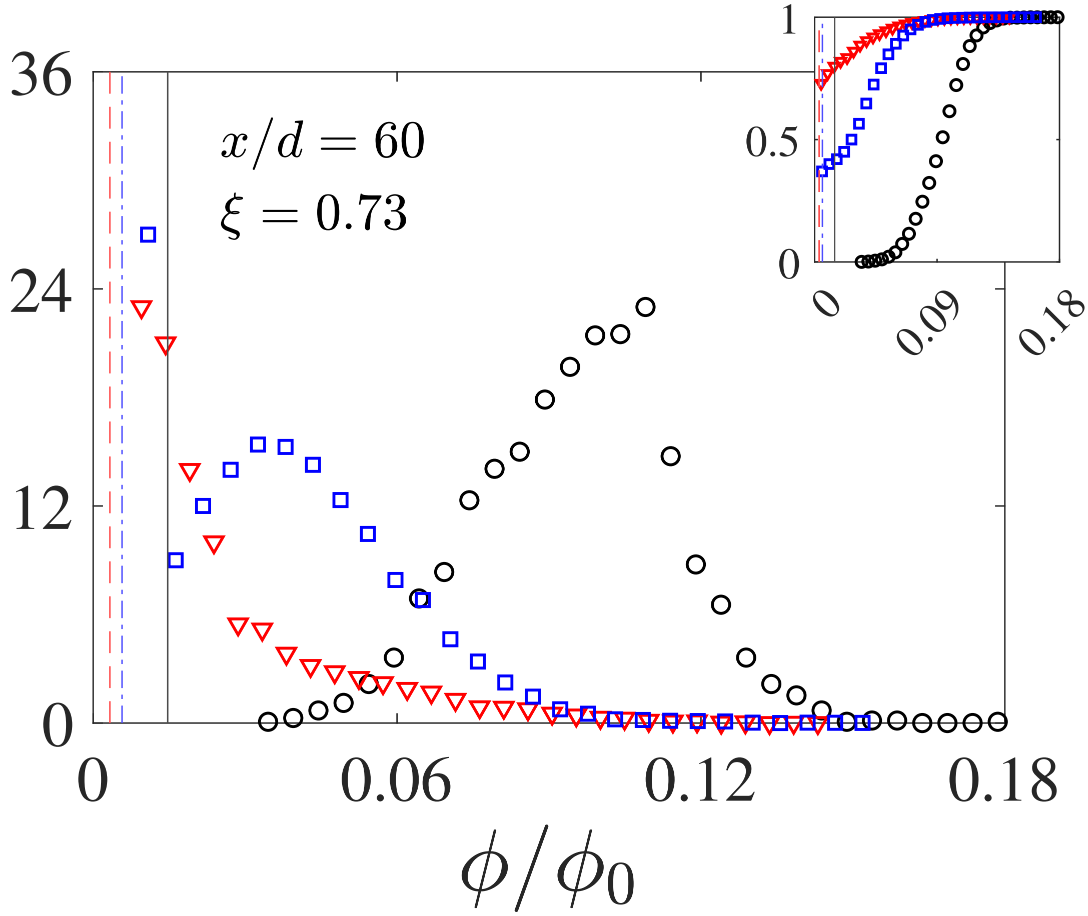
$x/d = 60$
$\xi = 0.73$
36
24
12
0
0
0.06
0.12
0.18
ϕ/ϕ_0
1
0.5
0
0
0.09
0.18

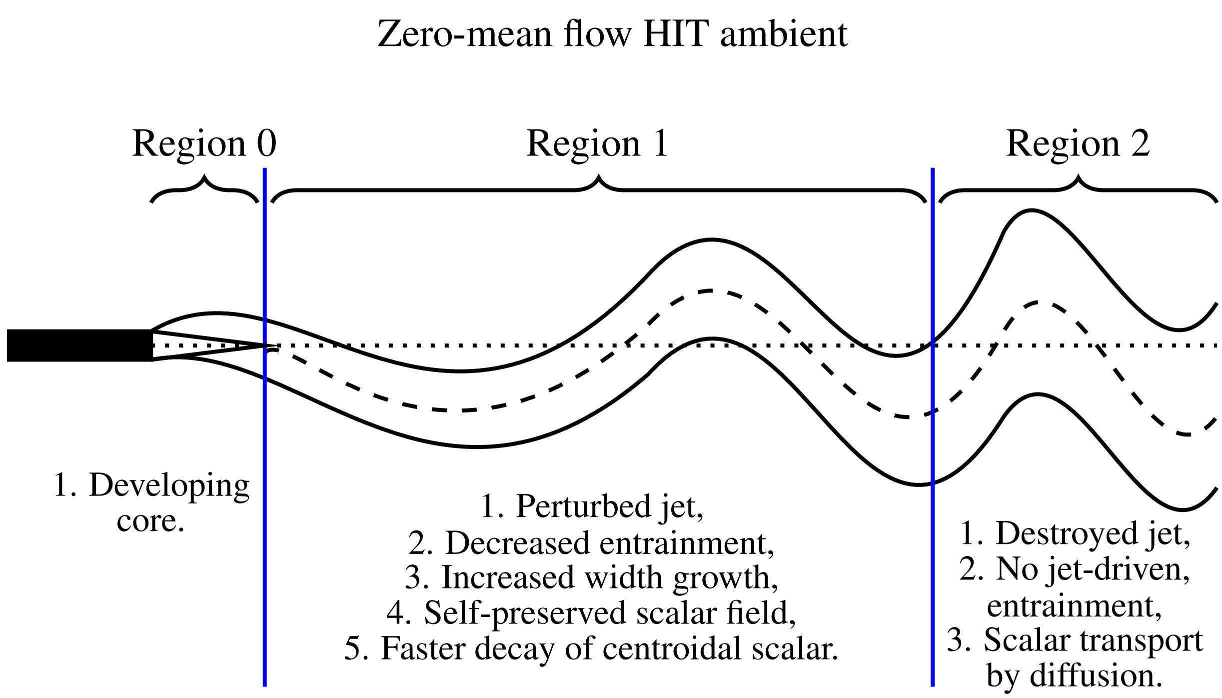
Zero-mean flow HIT ambient
Region 0
Region 1
Region 2
1. Developing core.
1. Perturbed jet,
2. Decreased entrainment,
3. Increased width growth,
4. Self-preserved scalar field,
5. Faster decay of centroidal scalar.
1. Destroyed jet,
2. No jet-driven, entrainment,
3. Scalar transport by diffusion.

PLEASE CITE THIS ARTICLE AS DOI: 10.1063/5.0071023

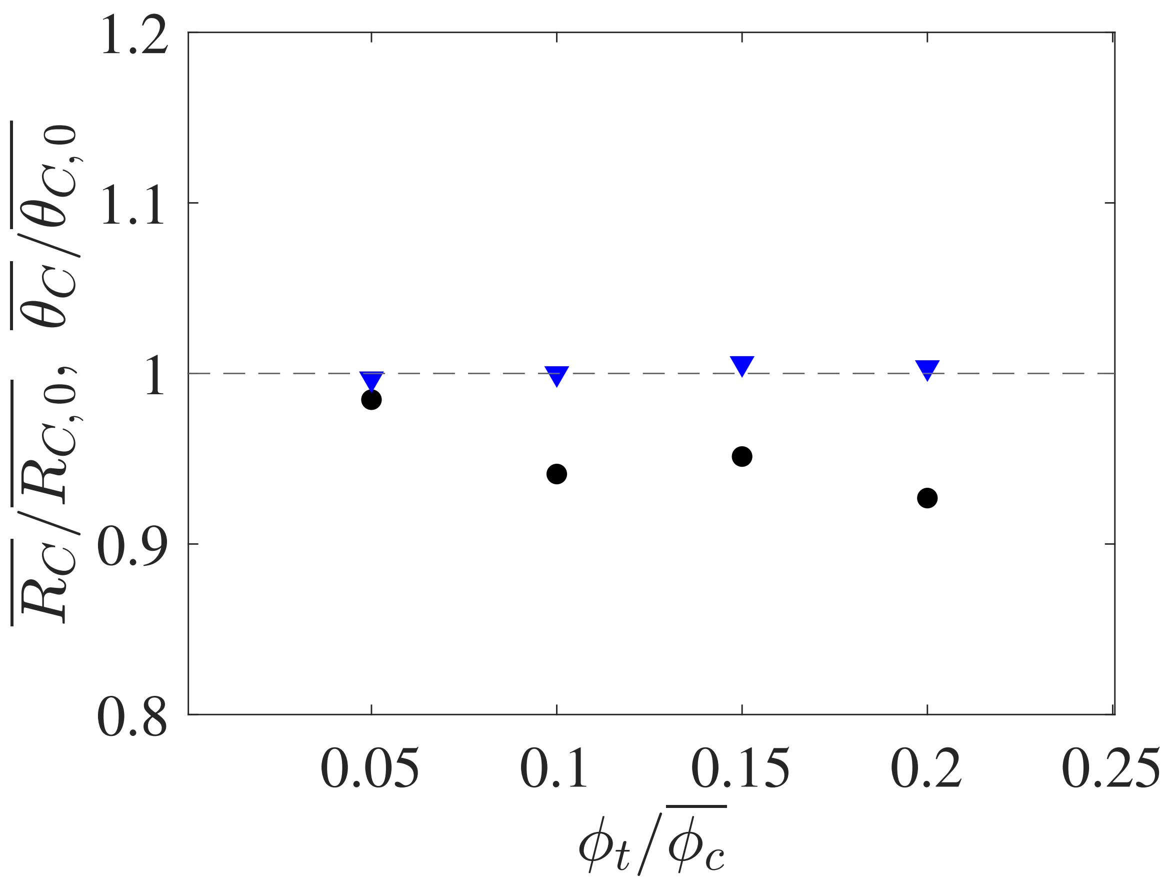

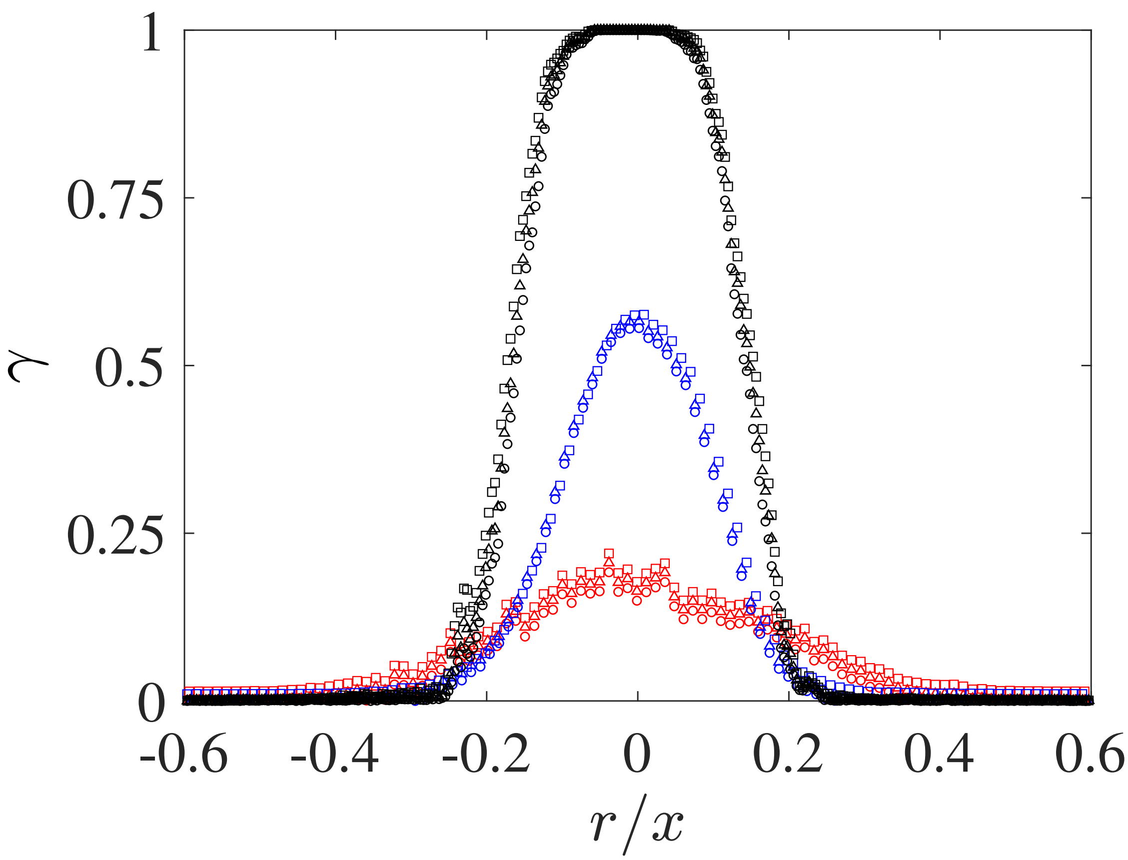
1
0.75
0.5
0.25
0
γ
-0.6
-0.4
-0.2
0
0.2
0.4
0.6
r/x